

MINISTRY OF HIGHER EDUCATION AND SCIENTIFIC RESEARCH
MOHAMED KHIDER UNIVERSITY OF BISKRA
FACULTY OF SCIENCE AND TECHNOLOGY
DEPARTMENT OF ELECTRICAL ENGINEERING



*PHD thesis submitted in partial fulfillment of the requirements for the degree of Doctor
of Electrical Engineering
Option: Energy management*

Control and Energy Management of an Electrical Vehicle

Realised by: **KRAA Okba**

Board of examiners:

Pr. Abdenacer Titaouine	University of Biskra	Chairman
Pr. Abdennacer Aboubou	University of Biskra	Supervisor
Dr. Mohamed Becherif	University of Belfort - France,	Co-supervisor
Pr. Mohamed Boumehrez	University of Biskra	Examiner
Pr. Amar Moussi	University of Biskra	Examiner
Pr. Abdelkrim Allag	University of el Ouad	Examiner

Year: 2014-2015

Abstract

This research focussed on two axes, the first one was the energy management of the electric vehicle's power-train system, and the second one was the control of its drive-train. The first part of study was to address the problem of the control of DC-bus voltage including fuel cell and supercapacitor energy sources. We started by developing a control strategy of a fuel cell stack using a non-isolated DC/DC converter. This control was ensured by hybrid dual loop control, which included a voltage loops with a linear PI controllers and a fast current loops with a non-linear sliding controllers. The implementation of the developed FC's control system was made using an experimental test bench of the studied converter, which was carried out on an experimental bench at reduced power (120 watts) of equipment available in our laboratory MSE. Then, an energy management method based on the flatness strategy and the sliding mode control were suggested and explained to control a hybrid system composed of a fuel cell and a supercapacitor as the main and auxiliary sources. The nonlinear flatness strategy was used to achieve a linearising feedback control law that gives an exponential tracking of the FC and SCs power trajectories. The proposed flatness control allows decoupling the hybrid system into two decoupled sources so as each subsystem has a separated control target expressed in terms of a sliding surface. The role of sliding mode controllers was to ensure the power sharing between the DC-link inverters by controlling the FC and SC currents. The control of the drive-train was to provide an inversion based control and propose an adaptive operation mode of the studied electric vehicle (EV) by using a fuzzy logic to invert the accumulation element. This model-based control was realized by means of formalism called Energy Macroscopic Representation (EMR). Hence, EMR gives in-

sights into the real energy operation of the EV system and allows a deep understanding of its potentials from dynamics point. Also, the EV has been modelled by a linear dynamic model expressed by a state space representation in order to control its velocity by a states feedback controller. The control systems were simulated in Matlab/Simulink and several simulation tests were carried out for the European, the American driving cycles. They were made in order to validate the functionality of the designed control systems.

Key words: Electric Vehicle; Energetic Macroscopic Representation; Maximum Control Structure; State Feedback; Energy Management; Sliding Mode Control; Flatness Control; Hybrid Source; Fuel Cell; Supercapacitor.

Dedicasse

i dedicate this work to

my parents,

my brothers and sisters,

my professors,

and my friends,

Acknowledgment

The research presented in this thesis had been made in LESM (Laboratory of Energy Systems Modelling) at Mohamed Kheider University, Biskra, Algeria. Foremost, I would like to express my sincere gratitude to my advisor Pr. A. Aboubou and my co-advisor Dr. M. Becherif and to Dr. M.Y. Ayad and Pr. Bahri for the continuous support of my Ph.D study and research, for their patience, motivation, enthusiasm, and immense knowledge. They guided me through my research. I could not have imagined having a better advisor and co-advisor and mentor for my Ph.D study.

I also would like to thank my thesis examiners: Pr. Abdenacer Titaouine, Pr. Mohamed Boumehrez, Pr. Amar Moussi, Pr. Djlali Benattous and Pr. Abdelkrim Allag for their insightful comments and corrections.

My sincere thanks to Pr. Kamel Srairi, Dr. Hatem Ghodbane and Dr. Djemai Naimi for the continuous support of my PHD study and research, their guidance helped me the research and writing of this thesis. Also, i thank my fellows at FCLab, and i thank so much S. Aicha, R. Saadi, M. Mehammedi, I. Tagani and all my friends.

Control and Energy Management of an Electric Vehicle

Okba Kraa

April 10, 2015

Contents

- Contents** **I**

- Figures List** **V**

- Tables List** **IX**

- 1 Fundamentals of electric vehicles** **1**
 - 1.1 Introduction 1
 - 1.2 Electrical vehicle history 1
 - 1.3 General description of the vehicle 4
 - 1.3.1 Vehicle resistive forces 6
 - 1.3.1.1 Aerodynamic drag 6
 - 1.3.1.2 Rolling Resistance 7
 - 1.3.1.3 Grading resistance 9
 - 1.4 EV design 10
 - 1.4.1 Traction motor characteristics 10
 - 1.4.2 Maximum speed 11
 - 1.4.3 Gradeability 11
 - 1.4.4 Acceleration 12
 - 1.4.5 The tractive power 13
 - 1.4.6 Energy consumption 14
 - 1.5 Main configurations of EVs 16
 - 1.5.1 Hybrid vehicle 16
 - 1.5.1.1 Series HEV 16

1.5.1.2	Parallel HEV	17
1.5.1.3	Series-parallel combination	18
1.5.2	Pure Electric vehicle	19
1.6	Electric Vehicle Drive-train	22
1.6.1	Mechanical Transmission	22
1.6.2	EV motor drives evaluation	23
1.6.2.1	Direct current motor	24
1.6.2.2	Induction motor drives	25
1.6.2.3	Switched Reluctance Motor Drives	25
1.6.2.4	Permanent Magnet Synchronous Motors	26
1.6.2.5	Comparison between four types of EV motor drives	27
1.7	Conclusion	27
2	Electric Vehicle Supply Sources	29
2.1	Introduction	29
2.2	Electrochemical battery	30
2.2.1	The Lead Acid battery	31
2.2.2	The Nickel based battery	32
2.2.2.1	The Nickel Cadmium (NiCd) battery	32
2.2.3	The Nickel-Metal Hydride (NiMH) battery	32
2.2.4	The Lithium based battery	33
2.2.4.1	The Lithium Polymer battery	34
2.2.4.2	Lithium-Ion (Li-Ion) Battery	34
2.2.5	Electric model of battery	37
2.2.5.1	Specific power	38
2.2.5.2	Energy efficiency	38
2.2.5.3	Battery state of charge	39
2.3	Supercapacitors	39
2.3.1	Basic principles of supercapacitors	40
2.3.2	Electric model of supercapacitor	41
2.3.2.1	Supercapacitor's state of charge	41
2.4	Fuel cell vehicle	42
2.4.1	Fuel cell history	42

2.4.2	Basic principle of the fuel cell	43
2.4.3	Fuel cell advantages and disadvantages	44
2.4.4	Fuel cell modelling	45
2.4.5	Fuel cell static model	46
2.5	Different hybrid sources of an electrical vehicle	48
2.5.1	FC-battery vs FC-subercapacitors	48
2.5.2	Battery vs Supercapacitor	49
2.6	Conclusion	51
3	Energy management of hybrid sources	52
3.1	Introduction	52
3.2	Fuel cell control	53
3.2.1	Modelling of the studied system	53
3.2.2	Sliding mode based closed-loop control of the studied converter	55
3.2.3	Stability	58
3.2.4	Simulation results	58
3.2.5	Experimental results	62
3.3	Hybridization of energy storages	64
3.4	Modelling of studied FC-SC hybrid source	65
3.4.1	Modelling of the FC-SCs DC bus voltage	66
3.5	Flatness-sliding mode control of the DC-bus energies	67
3.5.1	Differential flatness principle	68
3.5.2	Flatness control of FC-SC hybrid source	69
3.5.3	Trajectory planning	71
3.6	Sliding Mode controller	72
3.6.1	Stability of the flatness control system	74
3.7	Simulation results	74
3.8	conclusion	81
4	Control of an electric vehicle	83
4.1	Introduction	83
4.2	Energetic macroscopic representation	84
4.2.1	Action reaction principle	84

4.2.2	Integral causality	84
4.2.3	EMR elements	85
4.2.4	Inversion based control of an EMR	85
4.3	Modelling of the electric vehicle	86
4.3.1	Architecture of the studied EV	86
4.3.2	EMR of the electric vehicle	87
4.3.2.1	The EV supply source	87
4.3.2.2	Chopper	87
4.3.2.3	Motor drive	87
4.3.3	Modelling of the mechanical coupling	88
4.3.3.1	Mechanical differential	88
4.3.3.2	Left and right wheels	88
4.3.3.3	Chassis	89
4.3.3.4	Environment	89
4.4	Inversion of EMR simulator	89
4.4.1	Inversion of standard elements	89
4.4.2	Inversion of accumulation elements	90
4.4.2.1	Inversion of chassis	90
4.4.3	Inversion of Armature	91
4.5	Development of fuzzy logic-based control	91
4.5.1	Adaptive fuzzy logic control design	91
4.5.2	Basic concepts of fuzzy logic	92
4.5.2.1	Fuzzification interface	92
4.5.2.2	Rule base system	93
4.6	Simulation results	93
4.7	State-space model of the electric vehicle	100
4.8	Formulation of the control problem	101
4.8.1	State Feedback Controller using poles placement	101
4.8.2	Reconstruction of the state model	101
4.9	Linear quadratic regulator	103
4.10	Simulation results	103
4.11	Conclusions	108

Figures List

1.1	Electroboat [Ber05]	2
1.2	La Jamais contente in 1899 [Ber05]	3
1.3	World Electrified Vehicle Sales [Zac]	5
1.4	Forces acting on a vehicle	6
1.5	Aerodynamic drag acting on a vehicle	7
1.6	Tire deflection and rolling resistance on a hard road surface	8
1.7	Vehicle climbing a grade	9
1.8	Typical variable-speed electric motor characteristics	11
1.9	Tractive effort vs. vehicle speed (with a traction motor of $s_r = 6$ and single-gear transmission)	12
1.10	Acceleration time and distance vs. final speed	13
1.11	Typical electric motor efficiency characteristics [YWWS13]	15
1.12	Series hybrid vehicle	17
1.13	Parallel hybrid vehicle	18
1.14	Serie-Parallel hybrid vehicle	19
1.15	Pure electric vehicle	20
1.16	Modern electric vehicle	21
1.17	Possible EV configurations [Hus11], (C: Clutch,D: Differential, FG: Fixed gearing, GB: Gearbox, WM: Wheel Electric motor)	22
2.1	An electrochemical battery cell	30
2.2	The battery's equivalent circuit	38
2.3	Typical battery charge and discharge efficiency [EGE09].	39
2.4	Principle construction of a supercapacitor	40

2.5	Supercapacitor equivalent circuit [ABH11]	41
2.6	Typical supercapacitor's SOC [EGE09]	42
2.7	Basic operation of a fuel cell	44
2.8	Fuel cell system.	46
2.9	A fuel cell equivalent electric circuit [Mat]	47
2.10	A PEMFC typical polarization curve	48
2.11	Energetic comparison between capacitors, SCs, batteries and FCs.	50
3.1	Circuit of the studied FC converter [SBA+14]	53
3.2	Open-loop of each converter stage.	55
3.3	The closed-loop structure of the IBC phases.	55
3.4	The closed-loop structure of the IDDBC phases.	55
3.5	Control of system	56
3.6	SISO design task	56
3.7	Load cycle.	60
3.8	IDDBC Output voltage V_s .	60
3.9	IBC output voltage V_1 .	60
3.10	Inductors current of IDDBC stage and its reference.	61
3.11	Inductors current of IBC stage and its reference.	61
3.12	Experimental setup of the studied converter.	62
3.13	Experimental results of the closed-loop control law: (a) load current cycle; (b) IBC and IDDBC voltages.	63
3.14	Experimental results: IBC and IDDBC currents.	63
3.15	The IBC and IDDBC's voltages while the V_s 's (a) increasing and (b) decreasing.	63
3.16	Concept of hybrid energy storage operation modes.	65
3.17	Studied structure of the FC-SCs hybrid power source of an EV,	66
3.18	The studied hybrid power source	70
3.19	Structure of flatness and sliding mode based control of a FC-SCs DC bus.	73
3.20	The DC link voltage (a) transient behaviour;(b) steady behaviour.	76
3.21	Energy of DC link voltage and its reference	76
3.22	The power reference of load	77
3.23	The FC's voltage	77

3.24	The FC's current and its reference	77
3.25	The SC's voltage	78
3.26	The SC's current and its reference	78
3.27	Load, FC and SC power responses	78
3.28	SC's voltage and current	79
3.29	SC's voltage and current in discharging mode	79
3.30	SC's voltage and current in charging mode	79
3.31	DC-bus's voltage and its reference	80
3.32	FC's voltage and current with its reference	80
3.33	SC's voltage and current with its reference	80
3.34	Response of system powers	81
4.1	Causality principle	84
4.2	The studied electric vehicle structure	86
4.3	EMR simulator of the studied EV in Matlab/simulink	90
4.4	EMR and MCS simulator of the studied EV in Matlab/simulink	91
4.5	(a) A typical structure of the developped AFLC.	92
4.6	(a) FLC's MF for the input ξ ; (b) FLC's MF for the output $F_{t_{ref}}$	94
4.7	(a) FS's MF for the input; (b) FS's MF for the output $F_{t_{ref}}$'s range.	94
4.8	Reference and vehicle velocities with (a) EOM (b) DOM.	96
4.9	(a)Reference and measured EV speeds with the AOM SOC%=78%;(b)Left and right vehicle velocities.	97
4.10	EV speeds with the AOM (a)SOC(0)=100% (b)SOC(0)=60%.	98
4.11	SOCs (SOC(0)=100%), Comparison of EV with AOM and classic DOM.	99
4.12	Bloc diagram of the EV.	100
4.13	Structure of state feedback control of studied EV	101
4.14	Structure of the studied control system	104
4.15	Reference and vehicle speed applying FTP-75.	104
4.16	Reference and vehicle speed applying HWFET.	105
4.17	Reference and vehicle speed applying NEDC.	105
4.18	(a) Reference and vehicle's velocities; (b) Armature's current.	106
4.19	wheels's velocities while vehicle makes a turn.	106

4.20 (a) Reference and vehicle speed with double FTP-75 (b) Energy consumption of EV 107

Tables List

- 1.1 Indicative drag coefficients for different body shapes [Hir05] 8
- 1.2 Comparisons of four motors [XCC08] 27
- 2.1 Advantages and disadvantages of Lead Acid battery 31
- 2.2 Advantages and disadvantages of NiCd 32
- 2.3 Advantages and disadvantages of NiMH 33
- 2.4 Advantages and disadvantages of Lithium Polymer battery 34
- 2.5 Advantages and disadvantages of Lithium-Ion battery 35
- 2.6 Different chemical battery technologies[Red11] (E_s : specific energy wh/kg) 36
- 2.7 Used batteries technologies in EV's manufacturers [YWWS13] 37
- 2.8 Fuel cell types characteristics [Hus11] 45
- 2.9 Measured Li-battery and simulated SC (650 F) efficiencies [MT10] 50
- 3.1 Parameters of the FC-converter system. 59
- 3.2 Parameters of the FC-SC hybrid source. 75
- 4.1 Energetic macroscopic representation blocks 85
- 4.2 The rule base system of FLC. 92
- 4.3 The rule base of FLS. 93
- 4.4 Parameters of the EV system. 95

Introduction

The consumption increasing of fossil fuels accompanied by excessive concentration of greenhouse gases in the atmosphere and the inevitable exhaustion of fossil resources expected by the end of this century are the basis of orientation towards the use of Electric Vehicles (EVs) in transportation. The electrical solution meets the requirements doubling of urban traffic and the scarcity of fossil fuels. Currently, the EVs are developing fast during this decade due to the drastic issues of protecting the environment and the depletion of fossil resources. While commercial hybrid cars have been rapidly exposed in the market, EVs appeared to be an interesting alternative to conventional internal combustion engine (ICE) vehicles. However, EVs still have serious limitations, if EVs do not have issues with increasing oil prices or pollution problems (at least around the vehicle), but they face the constraints of high cost, reliable batteries and travel range limitation. A smooth hybridization of many kinds of electric sources e.g. Fuel Cell (FC), battery and SuperCapacitor (SCs) could be a significant step to improve the autonomy and dynamic behaviour of the EV supply source [Hus11]. Extensive research efforts and investments have been given to the advanced battery technologies that are suitable for EVs all over the world. The U.S. government has been strongly supporting its Research and Development (R&D) activities in advanced batteries through the Department Of Energy (DOE): about 2 billion grants are focussed to accelerate the manufacturing and development of the next generation of U.S. batteries and EVs [Hus11]. European Commission and governmental organizations in Europe and Japanese Ministry of Economy, Trade and Industry (METI) have also been continuously supporting the R&D activities in advanced batteries. Lishen, and Chunlan have obtained strong subsidy supports from the Chinese government for their research and manufacturing of advanced batteries and electric vehicles.

The advantages brought by the use of the electric motor give intense interests in a wide range of applications. Control laws are constructed starting from the key feature of the electric motor. One is the fact that the torque transmitted at the wheel can be measured, depending on the current that passes through the motor. The second is its response time, the independent control as well as the fact that it can produce negative torques in generator mode to help to decelerate the vehicle and to store energy at the same time.

In other hand, to answer the constraints of the study of complex electromechanical systems such as the EV where it consists of many components, e.g. the electronic sources, the power electronics, the electric machine, the transmission and the wheels, an Energetic Macroscopic Representation (EMR) was proposed. The EMR has been first developed by L2EP laboratory (Lille, France) [Fra05] and has been applied to energetic and multi-physic systems by Femto-ST CNRS Lab (Belfort, France). It does not have the role to replace the traditional representations, but rather to supplement them by a more energetic actions-reaction description. Maximum Control Structure (MCS) results directly from an inversion of the considered EMR model. The recent researches have shown the interest of using fuzzy logic control in different engineering applications such as the control strategy of EV. Since fuzzy control is simple, easy to realize, no need for modelling and has strong robustness, it is suitable for nonlinear control where parameters and/or model are unknown or variable.

The electric vehicles still face many issues :

- How to maximally extend the driving-range?
- How to satisfy the energy requirements of the EVs both in steady and dynamic states?
- Ways of improving the regenerative braking energy?

Aiming at resolving the aforementioned challenges, a hybrid power source system is a significant solution to extend the driving-range and satisfy the energy requirements of the EVs both in steady and dynamic states. It is based on the combination of two or more energy sources. So, the drawbacks of each one can be compensated by advantages of others.

The problem of the energy management of a hybrid system (or multi-sources system), is to find the best distribution of power between the different energy sources. This distribution must satisfy the power demands of the load and observe the operating constraints (e.g. power of the fuel cell terminals of the supercapacitors charge status). In this work, we were interested of the energy management strategies based on the DC voltage regulation focus on the management of transient power peaks and regenerative braking by regulating the DC voltage using the energy stored in the energy storage sources.

There are many works on the energy management based on the DC voltage regulation of a hybrid system included multi-power sources, for example, Dawei Gaon [GJL08] studied a fuel cell hybrid bus equipped with a fuel cell system and two energy storage devices(battery and an ultracapacitor). He employed a fuzzy logic strategy to manage the power flow of this hybrid system. Thounthong et al. studied a regulated DC-bus voltage FC/supercapacitor hybrid sources based on basic linear controller by setting controller parameters depending on defined operating point [TRD07]. Then, he studied a regulated DC-bus voltage FC/battery/supercapacitor hybrid source by applying the same control method [TRD09]. Becherif in [ABH+10] studied FC/SC hybrid power sources using fuel cell as main source, a DC link and supercapacitors as transient power source. The energy management is reached using passivity-based control. The energy management of hybrid power sources using a flatness or a sliding mode controls has been already studied recently, by Thounthong , [TTD14], Sikkabu [SFP+13] and Payman [?] who worked on an regulated voltage FC/battery/SC hybrid sources by developping a flatness based energy management controller to manage the powers flow, and a Pulse-Width Modulation (PWM) with PI regulators to control the converters. By Ayad [ABH11], who studied the control of an DC-link voltage battery/SC hybrid sources using sliding mode strategy. Nevertheless, there are still some points about the control methods to be studied, particularly in the area of robustness, stability and efficiency of the converters control.

Our contribution in the EV's energy management is based on a new combination of the sliding and flatness controllers to manage and control a hybrid FC/SCs DC link voltage for EV or HEV applications. Basically, its principle is the generation of the desired reference trajectory of the DC link energy by using a flatness control. The sliding mode controllers were used to ensure the power sharing between the DC-bus inverters, they ensure that

the the SC and FC currents track their references, these last are calculated from the SC and FC powers.

The novelty of the present work was a specific Adaptive Fuzzy Logic Control (AFLC) based on Maximum Control Structure (MCS). This structure was designed to control EV speed. The speed control parameters and the EV operation mode were also adapted online according to the battery state of charge (SOC) and the distance between the EV and the nearest charging station. The goal was to reduce the energy used by EV and meet the requested autonomy. EV operation mode had to be economic, Dynamic or Eco-Dynamic (EOM, DOM or EDOM) where the EOM (less dynamic) were imposed in order to safe consumption and to obtain an economic (and not dynamic) vehicle. EDOM corresponds to a medium vehicle speed and the DOM corresponds to a dynamic vehicle in which the speed response must be fast (sport vehicle).

The outline of the thesis is structured in four main chapters, organized as follows:

Chapter 1: in this chapter, we introduced and described the EV's drive train's sizing and the different EV's motors. Tractive performance of an EV power-train system was also studied at each gear ratio of transmission. The analysis of the applied forces on an EV on the road allows obtaining the tractive power and determining the driving performances including maximum speed, acceleration and energy consumption.

Chapter 2: the fundamentals and comparison of EV battery, SCs and FC technologies, were suggested and explained in order to find an answer to the following question "**Which energy source is best for EV's road transport in the future?**". There are several types of energy storage that had been proposed and used for EVs and HEV applications. These energy storage devices, mainly include chemical batteries and supercapacitors. Also, we presented the principle of different sources and specific requirements of the EV's supply source.

Chapter 3: in this chapter, We presented a control strategy of a fuel cell stack using a non-isolated DC/DC converter. This control is ensured by hybrid dual loop control, which includes a voltage loops with a linear PI controllers and a fast current loops with a non-linear sliding controllers. flatness and sliding mode control strategies, have been developed for the energy management of an EV DC-bus hybrid source. It includes a FC to supply the mean power to the load (primary source), and a SC storage device that is used as an auxiliary power source, its role is to manage the load power peaks during the

dynamic transient variations and to recover the energy through regenerative braking.

Chapter 4: in this chapter, the energy macroscopic representation has been used to give insights into the energy operation of EV system and to allow a deep understanding of its potentialities from dynamic point. Then a specific Adaptive Fuzzy Logic regulator (AFL) was integrated in MCS to control the EV's velocity. The speed control parameters and the EV operation mode are also adapted on-line according to the battery state of charge to reduce the energy used by EV and meet the requested autonomy. In other hand, states space model was developed in this chapter for modelling the electromechanical behaviour of an EV. This dynamic model is useful to develop a control strategy based on states feedback. The states feedback control had been used to control the EV speed, by using two types of methods to determine the values of the controller parameters, the first one is pole placement and the second one is Linear Quadratic Regulator (LQR)

Fundamentals of electric vehicles

1.1 Introduction

Recently the development of the new generation vehicle, which is more efficient and less air polluting is accomplished actively. This vehicle's generation development can be divided to two kinds, one is the EV and the other one is the Hybrid Electric Vehicle (HEV). Nowadays, EVs are particularly well suited to urban applications and commuter-town cars. To use EVs as a practical solution, it is necessary to have technical feasibility and commercial viability that meets the user's needs and affordability. The EV must first be safe, reliable and cost effective with good performance and effective travel range, with consistency of the battery system being the key to determine the usefulness as vehicle. In this chapter, general description of EVs design and used motors in EV drive has been discussed. Tractive performance of an EV powertrain system is also studied at each gear ratio of transmission. Through analysis of the EV dynamic behavior on the road: rolling resistance and tractive performance; and the driving performance such as maximum speed, acceleration and energy consumption of the vehicle, are obtained and they will be used for the supply sources sizing.

1.2 Electrical vehicle history

The first electric vehicle was built by Thomas Davenport from Brandon, UK in 1834, he built a battery to supply an electric motor and he used it to drive a small vehicle that managed to go a short ride on rail. In 1881, Frenchman Gustave built EV includes

a DC motor that fed by lead-acid batteries, the whole vehicle and its driver weighed approximately 160 kg [Hus11]. Two years later, a vehicle similar to this was built by two British professors. These early realizations did not attract much attention from the public because the technology was not mature enough to compete with horse carriages. Speeds of 15 km/h and a range of 16 km were not exciting for potential customers.

The following 20 years were an era during which electric vehicles competed with their gasoline counterparts. This was particularly true in America, where there were not many paved roads outside few cities [Put12]. The limited range of electric vehicles was not a problem. However, in Europe, the rapidly increasing number of paved roads called for extended ranges, thus favoring gasoline vehicles.

In 1894, the first commercial electric vehicle was Morris and Salom's Electroboat shown in the Fig. 1.1. This vehicle was operated as a taxi in New York City by its inventors company. The Electroboat proved to be more profitable than horse cabs despite a higher purchase price (around 3000 vs. 1200\$ in that era). It could be used for three shifts of 4 h with 90-min recharging periods in between. It was powered by two 1.5 hp motors that allowed a maximum speed of 32 km/h and a 40-km range [Put12].



Figure 1.1: Electroboat [Ber05]

The most significant technical advance of that era was the invention of regenerative braking by Frenchman M.A. Darracq on his 1897 coupe. This method allows recuperating the vehicle's kinetic energy while braking and recharging the batteries, which greatly enhances the driving range. It is one of the most significant contributions to electric and hybrid electric vehicle technology as it contributes to energy efficiency more than anything else in urban driving. In addition, among the most significant electric vehicles of that era

was the first vehicle ever to reach 100 km/h. It was "La Jamais Contente (Fig. 1.2)" built by Frenchman Camille Jenatton in 1899 [Put12]. Electric vehicles started to disappear. Their high cost did not help, but it is their limited driving range and performance that really impaired them unlike their gasoline counterparts, which became more powerful, more flexible, and above all, easier to handle. The last commercially significant electric vehicles were released around 1905 [Put12]. During nearly 60 years, the only electric vehicles sold were common golf carts and delivery vehicles.



Figure 1.2: La Jamais contente in 1899 [Ber05]

In 1945, the innovation of the transistor and thyristor allowed switching high currents at high voltages. This made it possible to regulate the power fed to an electric motor without the very inefficient rheostats, and allowed the running of AC motors at variable frequency. During the 1960s and 1980s, about the environment triggered some researches on electric vehicles and many carmakers produced prototypes and small series of electric vehicles designed especially for specific markets [Cor10]. However, despite advances in battery technology and power electronics, their range and performance were still an obstacle.

The modern electric vehicle era culminated during the 1980s and early 1990s with the release of a few realistic vehicles by firms such as GM with the EV1 and PSA with the 106 Electric. Although these vehicles represented a real achievement, especially when compared with early realizations, it became clear during the early 1990s that electric automobiles could never compete with gasoline automobiles for range and performance.

The reason is in batteries, the energy is stored in the metal of electrodes, which weigh far more than gasoline for the same energy content. The automotive industry abandoned the electric vehicle to conduct research on hybrid electric vehicles. After a few years of development, these are far closer to the assembly line for mass production than electric vehicles have ever been.

In recent years, (exactly starting from 2000), the appearance prototype replacing part of the battery by a fuel cell generator pack, made the advanced vehicle technology research turned to the energy management of EV hybrid sources as well as fuel cell-SC or battery [Ber05], Hybridization of the fuel cell system with a peaking power source is an effective technology to overcome the disadvantages of the fuel cell alone-powered vehicles. In the context of the EV development, it is the battery technology that is the weakest, blocking the way of electric vehicles to market. Great effort and investment have been put into battery research, with the intention of improving performance to meet the electric vehicle's requirement. Unfortunately, progress has been very limited. Performance is far behind the requirement, especially energy storage capacity per unit weight and volume. This poor energy storage capability of batteries limits electric vehicles only to some specific applications, such as at airports and rail-road stations, on mail delivery routes, and on golf-courses, etc. In fact, basic study shows that electric vehicles will never be able to challenge liquid fuelled vehicles even with the optimistic value of battery energy capacity. However, the automobile industry has been a major driving force in research. because EVs, now seen as the vehicles of future and as a possible solution to reduce the greenhouse gas emission in environment. Today all major car manufacturers produce EVs, many of them are available for sale or public location, many prototypes such as , Toyota PRUIS, Nissan MIEV, Peugeot 205 and hydrogen fuel cell electric London taxis are available today (Fig1.3. These EVs include induction motors, DCM or PMSM.

1.3 General description of the vehicle

Figure. 1.4 shows the forces acting on a vehicle moving up a grade. The tractive effort F_t in the contact area between tires of the driven wheels and the road surface propels the vehicle forward. It is produced by the power plant torque and is transferred through



Figure 1.3: World Electrified Vehicle Sales [Zac]

transmission and final drive to the drive wheels. While the vehicle is moving, there is resistance that tries to stop its movement. The resistance usually includes tire rolling resistance, aerodynamic drag, and uphill resistance. According to Newton's second law, vehicle acceleration can be written as

$$\frac{dV}{dt} = \frac{\sum F_t - \sum F_{tr}}{\delta M_v} \quad (1.1)$$

where V is vehicle speed, $\sum F_t$ and $\sum F_{tr}$ are the total vehicle tractive effort and resistance forces. M_v is the total vehicle mass and δ is the mass factor, which is an effect of rotating components in the powertrain.

The vehicle tangential velocity is v_x . The gravitational force in the normal direction is balanced by the road reaction force, and hence, there will be no motion in the y normal direction. In other words, the tire always remains in contact with the road. Therefore, the normal velocity $v_y = 0$. These justified simplifications allow using a one-directional analysis for vehicle propulsion in the x direction. It is shown in the following that the vehicle tractive force and the opposing forces are all in the x direction. Hence, for simplicity, the "x" will not be used in the symbols.

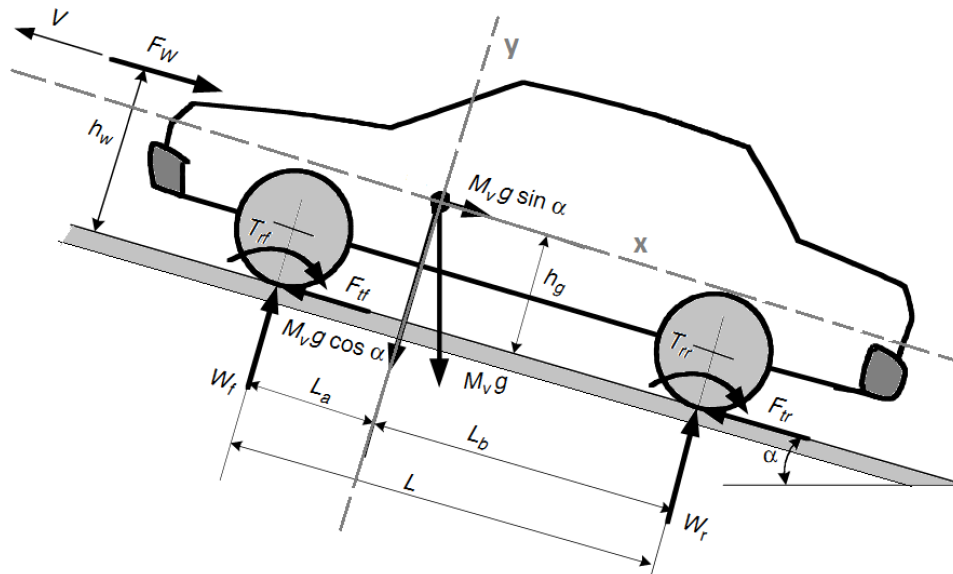


Figure 1.4: Forces acting on a vehicle

1.3.1 Vehicle resistive forces

The vehicle resistance opposing its movement includes rolling resistance of the tires, appearing in Fig. 1.4 as aerodynamic drag F_w , rolling resistance torque T_{rf} , and grading resistance (the term $M_v g \sin \alpha$ in Fig. 1.4). All of the resistances will be discussed in detail in the following sections.

1.3.1.1 Aerodynamic drag

The aerodynamic drag is a resistive force that opposes the direction of thrust of a vehicle as shown Fig. 1.5. Given a set of vehicle conditions, the drag force can be calculated by a function of the vehicle frontal area, the air density, the coefficient of vehicle drag, and the vehicle speed squared as it is shown in (1.2) [Hir05]. The fact that the vehicle speed has a cubic relation to the force of drag reveals that a small change in the speed of the car can require an enormous amount of engine power to overcome the forces of drag. In addition, the relation between drag and speed shows that aerodynamics of vehicles do not matter so much at lower speeds; they have a much more profound effect at highway speeds [Hir05]. Aerodynamic drag is expressed as

$$F_w = \frac{1}{2} \rho A_f c_d (V_{veh} + V_w)^2 \quad (1.2)$$

Where c_d is the aerodynamic drag coefficient that characterizes the shape of the vehicle and V_w is the component of wind speed on the vehicle's moving direction, which has a positive sign when this component is opposite to the vehicle speed and a negative sign when it is in the same direction as vehicle speed. The aerodynamic drag coefficients for a few types of vehicle body shapes are shown in Table. 1.1.

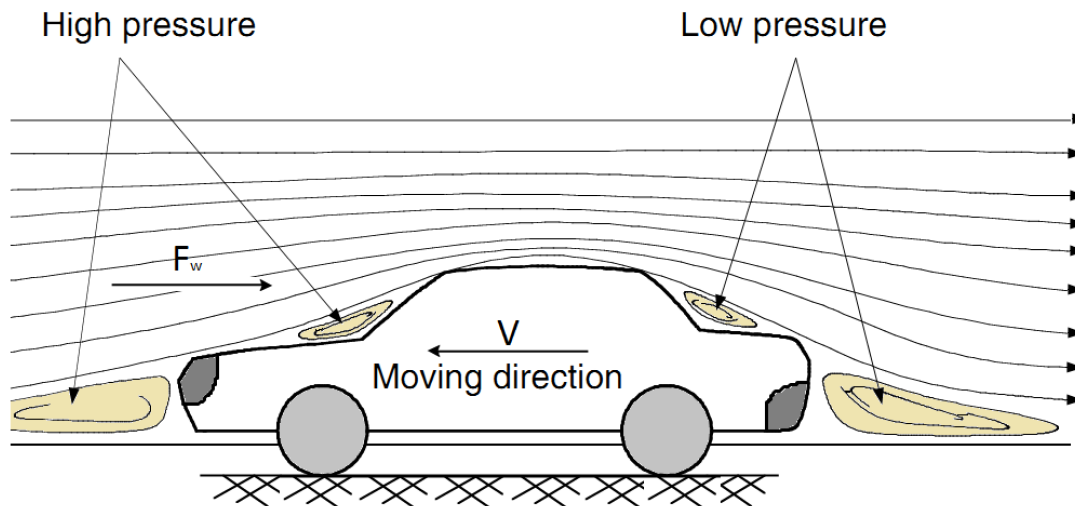


Figure 1.5: Aerodynamic drag acting on a vehicle

1.3.1.2 Rolling Resistance

Tire rolling resistance is defined as the force required maintaining the forward movement of a loaded pneumatic tire in a straight line at a constant speed. It is primarily caused by hysteresis in the tire materials. This is due to the deflection of the carcass while the tire is rolling. This phenomenon results in the ground reaction force shifting forward. This forwardly shifted ground reaction force, with the normal load acting on the wheel center, creates a moment that opposes the rolling of the wheel as shown in Fig. 1.6. The moment is called the rolling resistant moment, and can be expressed as [EGE09]

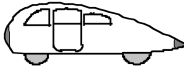



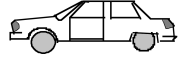
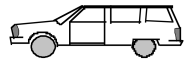
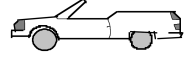
$$T_r = a.P \quad (1.3)$$

To keep the wheel rolling, a force F , acting on the center of the wheels, is required to balance this rolling resistant moment. This force is expressed as

$$F = \frac{T_r}{r_d} = \frac{aP}{r_d} \quad (1.4)$$

Where r_d is the effective radius of the tire and $f_r = a/r_d$ is called the rolling resistance

Table 1.1: Indicative drag coefficients for different body shapes [Hir05]

Vehicle Type	Aerodynamic Coefficient
	0.15-0.20
	0.23
	0.2-0.25
	0.3-0.4
	0.4-0.55
	0.5-0.7
	0.5-0.7
Streamlined buses	0.3-0.4
Motorcycles	0.6-0.7
Buses	0.6-0.7
Trucks, road trains	0.8-1.5

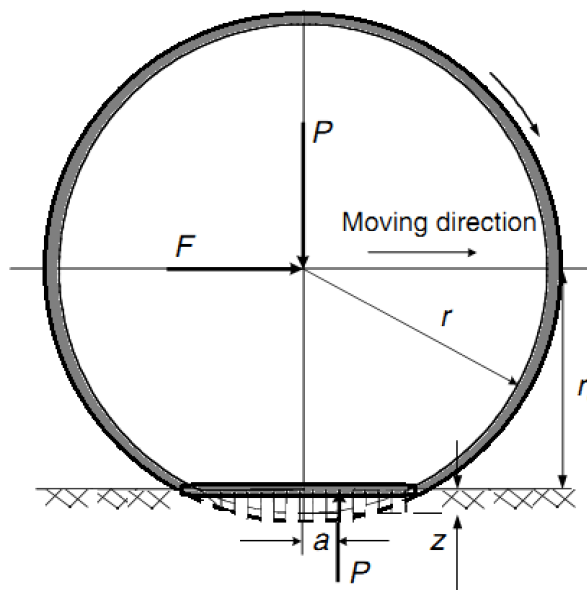


Figure 1.6: Tire deflection and rolling resistance on a hard road surface

coefficient. In this way, the rolling resistant moment can be replaced equivalently by horizontal force acting on the wheel center in the opposite direction of the movement of the wheel. This equivalent force is called rolling resistance with a magnitude as shown

$$F_r = f_r P \quad (1.5)$$

Where P is the normal load, acting on the center of the rolling wheel. When a vehicle is operated on a slope road, the normal load, P , should be replaced by the component, which is perpendicular to the road surface. That is

$$F_r = f_r P \cos(\alpha) \quad (1.6)$$

1.3.1.3 Grading resistance

When a vehicle goes up or down a slope, its weight produces a component, which is always directed to the downward direction, as shown in Fig. 1.7. This component either opposes the forward motion (grade climbing) or helps the forward motion (grade descending). In vehicle performance analysis, only uphill operation is considered. This grading force is usually called grading resistance (F_g) [EGE09], [Ber05]. From that figure, F_g can be expressed as

$$F_g = M_v g \sin(\alpha) \quad (1.7)$$

To simplify the calculation, the road angle, α , is usually replaced by grade value when

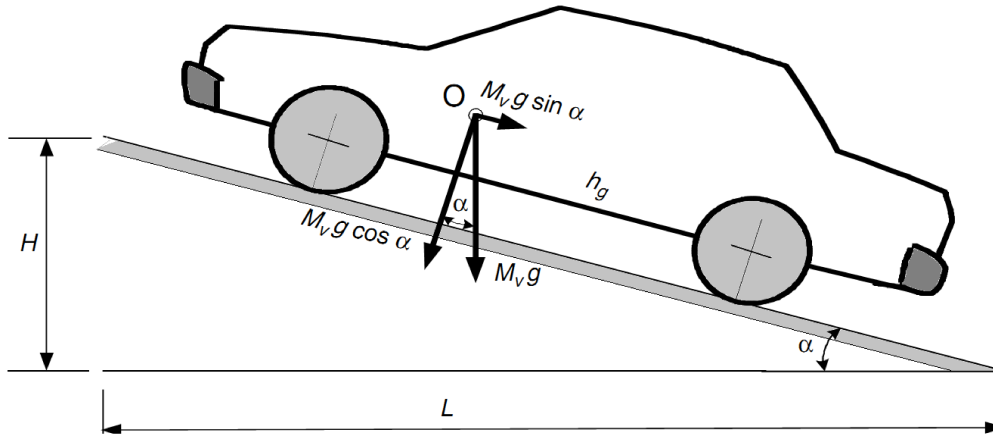


Figure 1.7: Vehicle climbing a grade

the road angle is small. As shown in Fig. 1.7, the grade is defined by

$$l = \frac{H}{L} = \tan(\alpha) = \sin(\alpha) \quad (1.8)$$

In some literatures [EGE09], [Ber05], the tire rolling resistance and grading resistance together are called road resistance (F_{rd}), which is expressed as

$$F_{rd} = F_r + F_g = M_v g (\cos(\alpha) + l) \quad (1.9)$$

1.4 EV design

The vehicle design depends mostly on the speed-power (torque) characteristics of the traction motor. Its driving performance is usually evaluated by its acceleration time, maximum speed, and gradeability. In EV drive train design, proper motor power rating and transmission parameters are the primary considerations to meet the performance specification [MH94].

1.4.1 Traction motor characteristics

Variable speed of an electric motor drives usually have the characteristics shown in Fig 1.8. At the low speed region (less than the base speed), the motor has a constant torque. In the high-speed region (higher than the base speed), the motor has a constant power. This characteristic is usually represented by a speed ratio s_r , defined as the ratio of its maximum speed to its base speed. In low-speed operations, voltage supply to the motor increases with the increase of the speed through the electronic converter while the flux is kept constant. At the point of base speed, the voltage of the motor reaches the source voltage. After the base speed, the motor voltage is kept constant and the flux is weakened, dropping hyperbolically with increasing speed. Hence, its torque also drops hyperbolically with increasing speed [Ber05].

The figure. 1.9 shows the torque speed profiles of a 60 kW motor with different speed ratios s_r ($s_r = 2, 4, \text{ and } 6$). It is clear that with a long constant power region, the maximum torque of the motor can be significantly increased, and hence vehicle acceleration and gradeability performance can be improved and the transmission can be simplified. However, each type of motor inherently has its limited maximum speed ratio. For example, a permanent magnet motor has a small $s_r = 2$ because of the difficulty of field weakening due to the presence of the permanent magnet. Switched reluctance motors may achieve $s_r = 6$ and induction motors about $s_t = 4, 3, 2$ [EGE09].

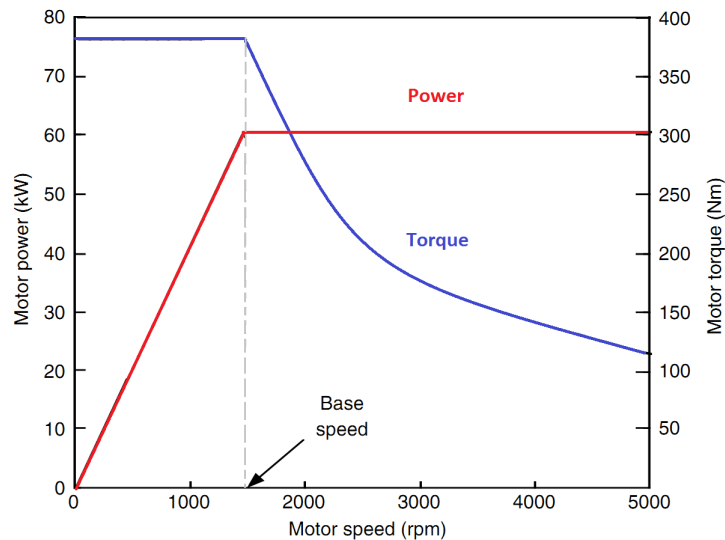


Figure 1.8: Typical variable-speed electric motor characteristics

1.4.2 Maximum speed

Basic vehicle performance includes maximum cruising speed, gradeability, and acceleration. The maximum speed of a vehicle can be easily found by the intersection point of the tractive effort curve with the resistance curve (rolling resistance plus aerodynamic drag), in the tractive effort vs. vehicle speed diagram shown in Fig. 1.9 and 1.10. It should be noted that such an intersection point does not exist in some designs, which usually use a larger traction motor or a large gear ratio. In this case, the maximum vehicle speed is determined by the maximum speed of the traction motor as [EGE09]

$$V_{max} = \frac{\pi W_{m_{max}} r_d}{30 i_{g_{min}} i_0} \quad (1.10)$$

Where $W_{m_{max}}$ is the motor speed in rpm, $i_{g_{min}}$ is the minimum gear ratio of the transmission (highest gear), i_0 is the gear ratio of final drive and r_d is the radius of the drive wheels.

1.4.3 Gradeability

Gradeability is determined by the net tractive effort of the vehicle $F_{t_{net}}$ ($F_{t_{net}} = F_t - F_r - F_w$), as shown in Fig. 1.9. At mid and high speeds, the gradeability is smaller than the gradeability at low speeds. The maximum grade that the vehicle can overcome at the given speed can be calculated by [Ber05]

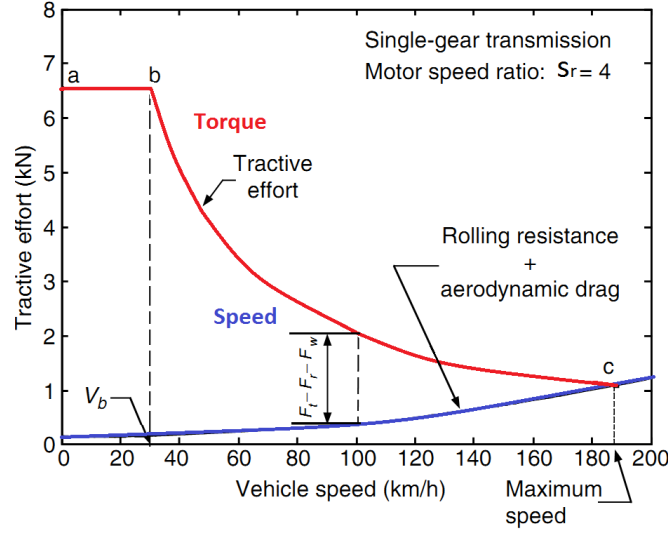


Figure 1.9: Tractive effort vs. vehicle speed (with a traction motor of $s_r = 6$ and single-gear transmission)

$$l = \frac{F_{t_{net}}}{M_v g} = \frac{F_t - (F_r + F_w)}{M_v g} \quad (1.11)$$

1.4.4 Acceleration

The vehicle acceleration performance is evaluated by the time used to accelerate the vehicle from a low-speed V_1 (usually zero) to a higher speed 100 km/h for passenger cars). Using Newton's second law (1.1), the acceleration of the vehicle can be written as [Ber05], [Hus11]

$$a = \frac{dV}{dt} = \frac{F_t - (F_r + F_w)}{M_v \delta} \quad (1.12)$$

where δ is called "mass factor", it is defined by

$$\delta = 1 + \frac{i_w}{M_v r_d^2} \quad (1.13)$$

i_w is the total angular moment of wheels. From (1.12), the acceleration time, t_a , and distance, S_a , from low speed V_1 to high speed V_2 can be written, respectively, as

$$t_a = \int_{V_1}^{V_2} \frac{M_v \delta V}{(P_t/V) - M_v g f_r - (1/2) \rho c_d A_f V^2} dV \quad (1.14)$$

and

$$S_a = \int_{V_1}^{V_2} \frac{M_v \delta}{(T_p i_g i_0 \eta_t / r_d) - M_v g f_r - (1/2) \rho c_d A_f V^2} dV \quad (1.15)$$

It is difficult to obtain the analytical solution from (1.14), therefore, numeral methods are usually used. Fig. 1.10 shows the acceleration time and distance along with vehicle speed

for an electric machine-powered electric vehicle. For initial evaluation of the acceleration time vs. the tractive power P_t , one can ignore the rolling resistance and the aerodynamic drag and obtain [EGE09]

$$t_a = \frac{\delta M_v}{2P_t} (V_2^2 + V_1^2) \quad (1.16)$$

where the vehicle mass factor (δ) is a constant.

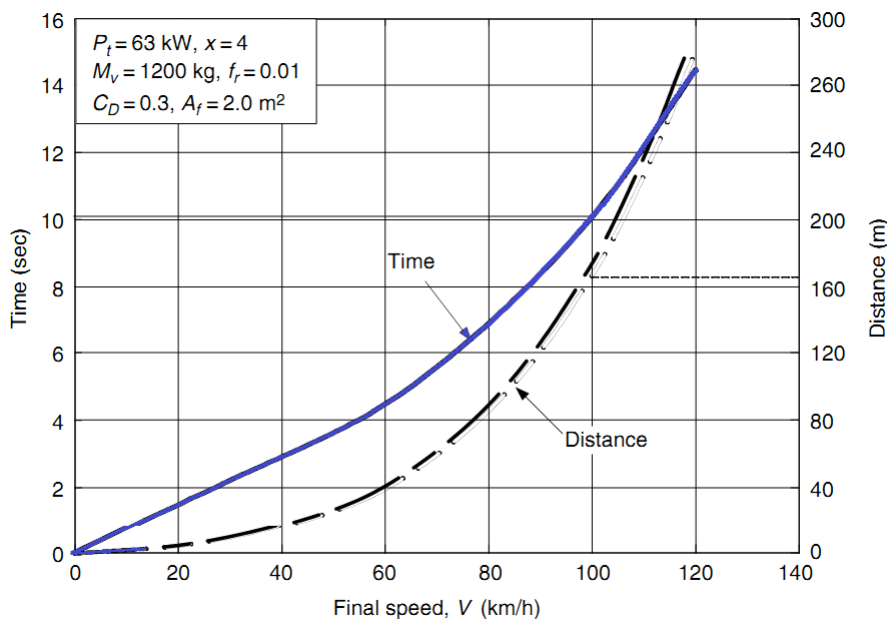


Figure 1.10: Acceleration time and distance vs. final speed

1.4.5 The tractive power

The tractive power, P_t , can then be expressed as

$$P_t = \frac{\delta M_v}{2t_a} (V_2^2 + V_1^2) \quad (1.17)$$

To determine the tractive power rating accurately, the power consumed in overcoming the rolling resistance and dynamic drag should be considered. The average drag power during acceleration can be expressed as [Hus11], [EGE09]

$$\bar{P}_{drag} = \frac{1}{t_a} \int_0^{t_a} (M_v g f_r V + \frac{1}{2} \rho c_d A_f V^2) dV \quad (1.18)$$

the vehicle speed V can be expressed using time t , as [EGE09]

$$V = V_2 \sqrt{\frac{t}{t_a}} \quad (1.19)$$

Substituting (1.19) in (1.18) and integrating, one obtains

$$\bar{P}_{drag} = \frac{2}{3}M_v g f_r V_2 + \frac{1}{5}\rho c_d A_f V_2^3 \quad (1.20)$$

Finally, the total tractive mechanical power for accelerating the vehicle from V_1 to speed V_2 in t seconds can be obtained as

$$P_t = \frac{\delta M_v}{2t_a}(V_2^2 + V_1^2) + \frac{2}{3}M_v g f_r V_2 + \frac{1}{5}\rho c_d A_f V_2^3 \quad (1.21)$$

1.4.6 Energy consumption

The energy unit used in transportation is usually kilowatt-hour (kWh). The energy consumption per unit distance in kWh/km is generally used to evaluate the vehicle energy consumption. However, for ICE vehicles the commonly used unit is a physical unit of fuel volume per unit distance, such as liters per 100 km (l/100 km)(miles per gallon (mpg)in USA). On the other hand, for battery-powered EVs, the original energy consumption unit in kWh, measured at the battery terminals, is more suitable. The battery energy capacity is usually measured in kWh and the driving range per battery charge can be easily calculated [EGE09].

Energy consumption is an integration of the power output at the battery terminals. For propelling, the battery power output is equal to resistance power and any power losses in the transmission and the motor drive, including power losses in electronics. The power losses in transmission and motor drive are represented by their efficiencies η_t and η_m , respectively. Thus, the battery power output can be expressed as [Hus11]

$$\bar{P}_{Bout} = \frac{V}{\eta_m \eta_n} \left[(M_v g f_r + i) + \frac{1}{2}\rho c_d A_f V^2 + M \delta \frac{dV}{dt} \right] \quad (1.22)$$

Here, the non-traction load (auxiliary load) is not included. In some cases, the auxiliary loads may be too significant to be ignored and should be added to the traction load. When regenerative braking is effective on an EV, a part of that braking energy (wasted in conventional vehicles) can be recovered by operating the motor drive as a generator and restoring it into the batteries. The regenerative braking power at the battery terminals can also be expressed as [RBE00]

$$P_{Bin} = \frac{\beta V}{\eta_m \eta_n} \left[(M_v g f_r + i) + \frac{1}{2}\rho c_d A_f V^2 + M \delta \frac{dV}{dt} \right] \quad (1.23)$$

Where road grade i or acceleration dV/dt or both of them are negative, and β ($0 < \beta < 1$) is the percentage of the total braking energy that can be applied by the electric motor, called the regenerative braking factor. The regenerative braking factor β is a function of the applied braking strength and the design of the power train [Ber05]. The net energy consumption from the batteries is

$$E_{out} = \int_{traction} P_{B_{out}} dt + \int_{braking} P_{B_{in}} dt \quad (1.24)$$

It should be noted that the braking power in (1.23) has a negative sign. When the net

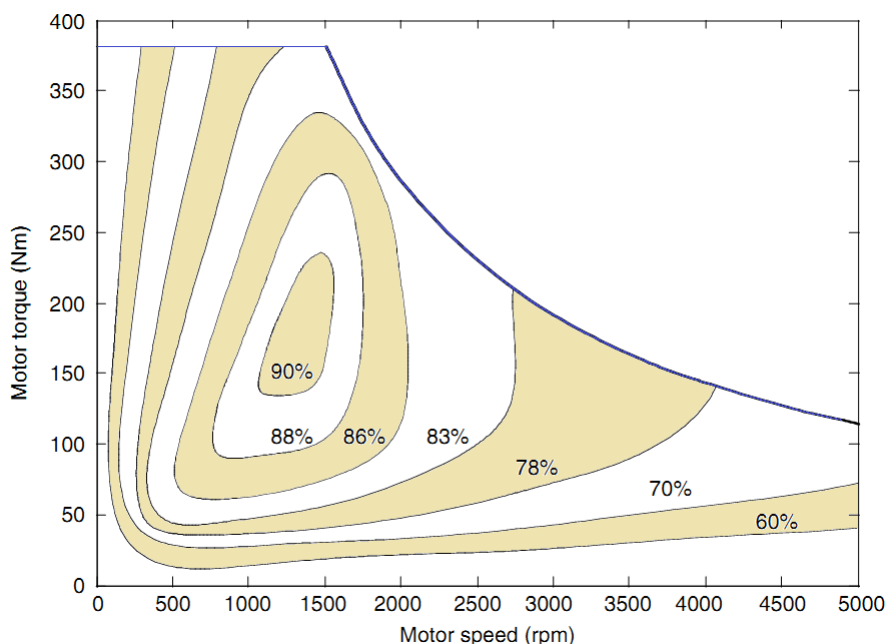


Figure 1.11: Typical electric motor efficiency characteristics [YWWS13]

battery energy consumption reaches the total energy in the batteries, measured at their terminal, the batteries are empty and need to be charged. The travelling distance between two charges (usually called effective travel range) is determined by the total energy carried by the batteries, the resistance power, and the effectiveness of the regenerative braking (β) [Ber05]. The efficiency of a traction motor varies with its operating points on the speed-torque (speed-power) plane as shown in Fig. 1.11 [EGE09], where the most efficient operating area exists.

1.5 Main configurations of EVs

There are various configurations of EVs and according to their energy sources, they are two global kinds: pure Electric vehicles and Hybrid vehicles.

1.5.1 Hybrid vehicle

A Hybrid Electric Vehicle (HEV) is a vehicle that uses two or more sources of power. The two sources are electricity from batteries and mechanical power from an internal combustion engine. This combination offers very low emissions of vehicles with the power and range of gasoline vehicles. They also offer up to 30 more miles per gallon perform as well or better than any comparable gasoline powered vehicle and never have to be plugged in for recharging [Ram03], [CBC10]. A hybrid road vehicle is one in which the propulsion energy during specified operational missions is available from two or more kinds or types of energy stores, sources, or converters, of which at least one store or converter must be on board. The second definition of hybrid road vehicle is proposed by Technical Committee 69 of Electric Road Vehicles of the International Electro-technical Commission. Many configurations are possible for HEVs as series and parallel HEVs.

1.5.1.1 Series HEV

A series hybrid is one in which only one energy converter can provide propulsion power. The heat engine or ICE acts as a prime mover in this configuration to drive an electric generator that delivers power to the battery or energy storage link and the propulsion motor [CBC10]. The component arrangement of a series HEV is shown in Fig. 1.5.1.1.

Advantages of series HEV [CBC10], [EGE09]:

- Flexibility of location of engine-generator set;
- Simplicity of drivetrain;
- Suitability for short trips.

Disadvantages of series HEV [EGE09]:

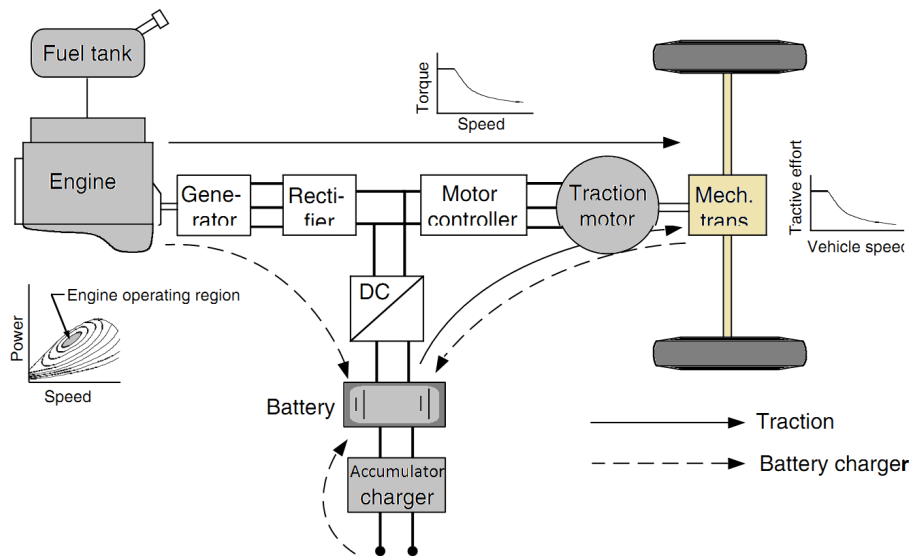


Figure 1.12: Series hybrid vehicle

- It needs three propulsion components: ICE, generator, and motor;
- The motor must be designed for the maximum sustained power that the vehicle may require, such as when climbing a high grade. However, the vehicle operates below the maximum power most of the time;
- All three drivetrain components need to be sized for maximum power for long-distance, sustained, high-speed driving. This is required, because the batteries will exhaust fairly quickly, leaving ICE to supply all the power through the generator.

1.5.1.2 Parallel HEV

A parallel hybrid is one in which more than one energy source can provide propulsion power. The heat engine and the electric motor are configured in parallel, with a mechanical coupling that blends the torque coming from the two sources. The component arrangements of a parallel hybrid are shown in Fig. 1.12 [CBC10].

Advantages of hybrid HEV [CBC10]:

- It needs only two propulsion components: ICE and motor/generator. In parallel HEV, the motor can be used as the generator and vice versa;
- A smaller engine and a smaller motor can be used to get the same performance,

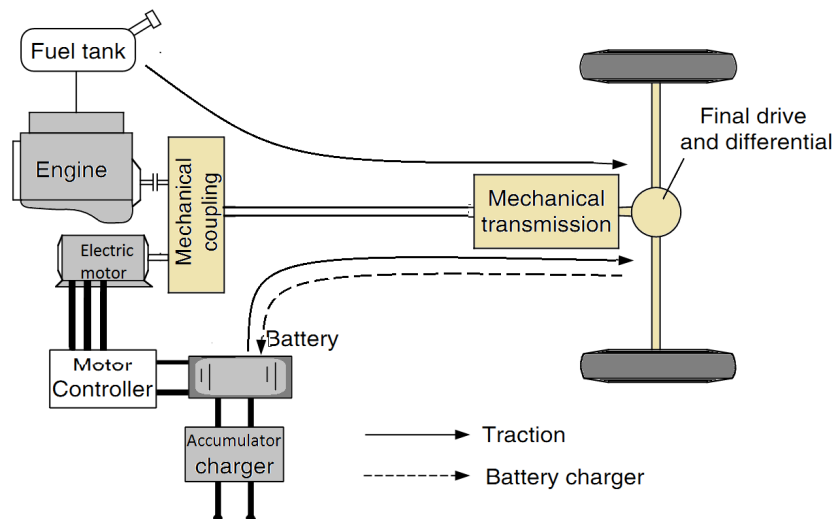


Figure 1.13: Parallel hybrid vehicle

until batteries are depleted. For short-trip missions, both can be rated at half the maximum power to provide the total power, assuming that the batteries are never depleted. For long-distance trips, the engine may be rated for the maximum power, while the motor-generator may still be rated to half the maximum power or even smaller.

Disadvantages of hybrid HEV:

- The control complexity increases significantly, because power flow has to be regulated and blended from two parallel sources;
- The power blending from the ICE and the motor necessitates a complex mechanical device.

1.5.1.3 Series-parallel combination

Although HEVs initially evolved as series or parallel, manufacturers later realized the advantages of a combination of the series and parallel configurations for practical road vehicles. In these combination hybrids, the heat engine can also be used to charge the battery. The recently available Toyota Prius is an example of such a hybrid, where a small series element is added to the primarily parallel HEV [Hus11]. The small series element (yellow element in Fig. 1.14) ensures that the battery remains charged in prolonged wait periods, such as at traffic lights or in a traffic jam. These hybrid combinations can be

categorically classified under parallel hybrids, because they retain the parallel structure of a component arrangement. It is important to stress the fact that the detailed configuration of an HEV depends on the application and the trade-off between cost and performance.

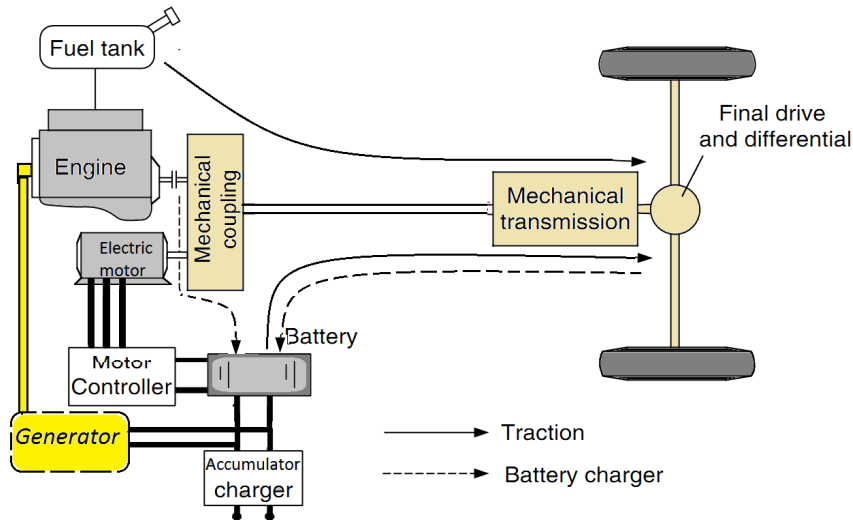


Figure 1.14: Serie-Parallel hybrid vehicle

Advantages of series-parallel hybrid HEV:

- high autonomy and travel range;
- The most sold;
- Rival to ICE vehicle;
- less polluting.

Disadvantages of hybrid HEV:

- High complexity of the drive train;
- High complexity of its management components;
- High cost and mass.

1.5.2 Pure Electric vehicle

Previously, the EV was mainly converted from the existing ICEV by replacing the internal combustion engine and fuel tank with an electric motor drive and battery pack

while retaining all the other components, as shown in Fig. 1.15 Drawbacks such as its heavy weight, lower flexibility, and performance degradation have caused the use of this type of EV to fade out. A modern electric drive train is conceptually illustrated in Fig.1.16, its drive train consists of three major subsystems: electric motor propulsion, energy source, and auxiliary. The electric propulsion subsystem is comprised of a vehicle controller, power electronic converter, electric motor, mechanical transmission, and driving wheels. The energy source subsystem involves the energy source, the energy management unit, and the energy refueling unit [CBC10]. The auxiliary subsystem consists of the power steering unit, the hotel climate control unit, and the auxiliary supply unit.

Advantages of pure EV:

- Zero mission;
- Silent;
- Easy use and driving.

Disadvantages of pure EV:

- Travel range obstacle;
- Oriented only for urban uses;
- High cost.

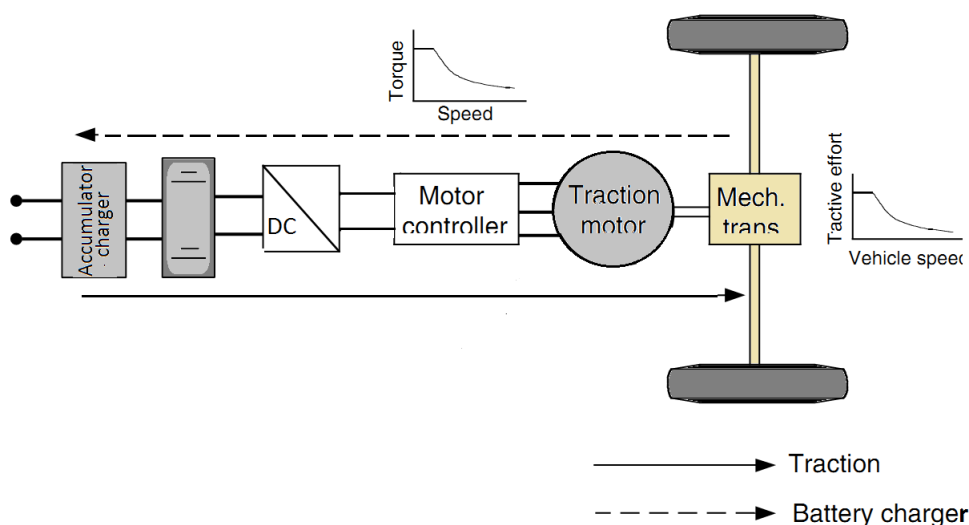


Figure 1.15: Pure electric vehicle

Based on the control inputs from the accelerator and brake pedals, the vehicle controller provides proper control signals to the electronic power converter, which functions to regulate the power flow between the electric motor and energy source. The backward power flow is due to the regenerative braking of the EV and this regenerated energy can be restored to the energy source, provided the energy source is receptive. Most EV batteries as well as ultracapacitors and flywheels readily possess the ability to accept regenerated energy. Currently, the proposed EVs are exclusively urban, their travel range is between 100 and 120 km with conventional technologies (lead-acid and cadmium-nickel) and 150 and 200 km with more advanced technologies (nikel metal hydride and lithium).

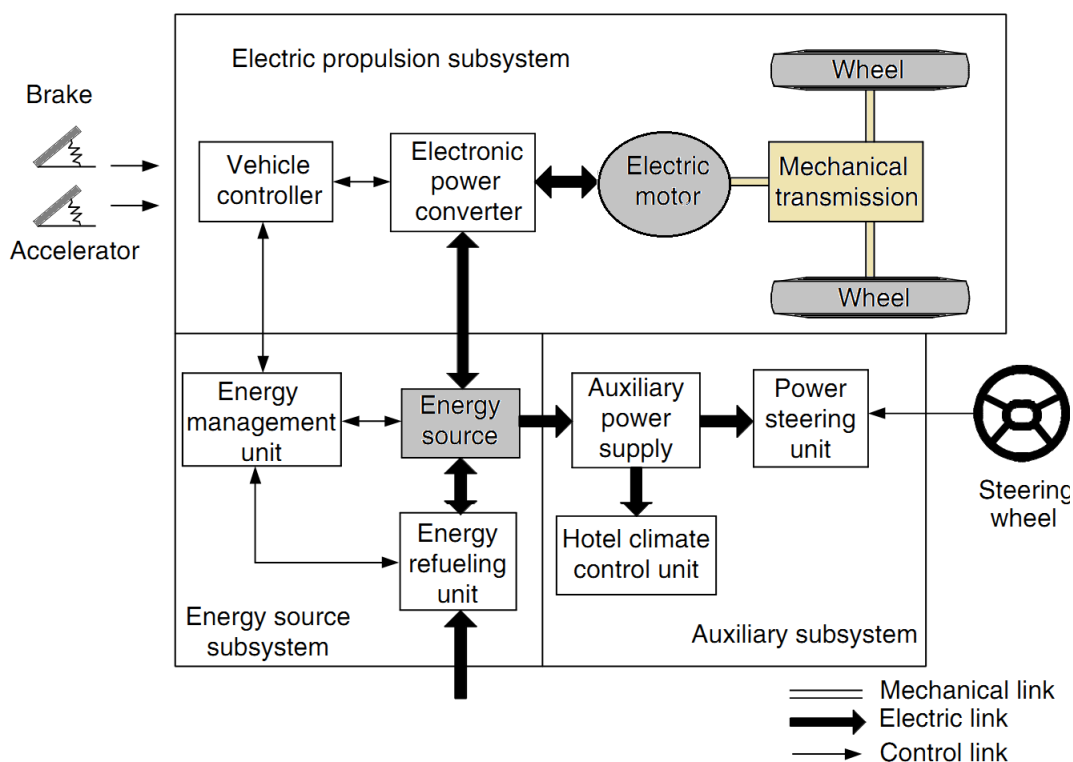


Figure 1.16: Modern electric vehicle

Regenerative braking allows to increase significantly the autonomy, especially in urban cycle (about 20%) [KT05]. It also allows to obtain an engine brake, for these reasons, it is necessary to have an energy management system. This last unit cooperates with the vehicle controller to control the regenerative braking and its energy recovery. It also works with the energy refueling unit to control the refueling unit, and to monitor the usability of the energy source. The auxiliary power supply provides the necessary power at different voltage levels for all the EV auxiliaries, especially the hotel climate control and power steering units.

1.6 Electric Vehicle Drive-train

1.6.1 Mechanical Transmission

The transmission requirements of a vehicle depend on the characteristics of the power plant and on the performance requirements of the vehicle. Basically, a well controlled electric machine such as the power plant of an electric vehicle will not need a multi-gears transmission. However, an internal combustion engine must have a multi-gears or continuously varying transmission to multiply its torque at low speed [MH94]. The term transmission here includes all those systems employed for transmitting engine power to the drive wheels. For automobile applications. There are a variety of possible EV configurations due to the variations in electric propulsion characteristics and energy sources, as shown in Fig. 1.17.

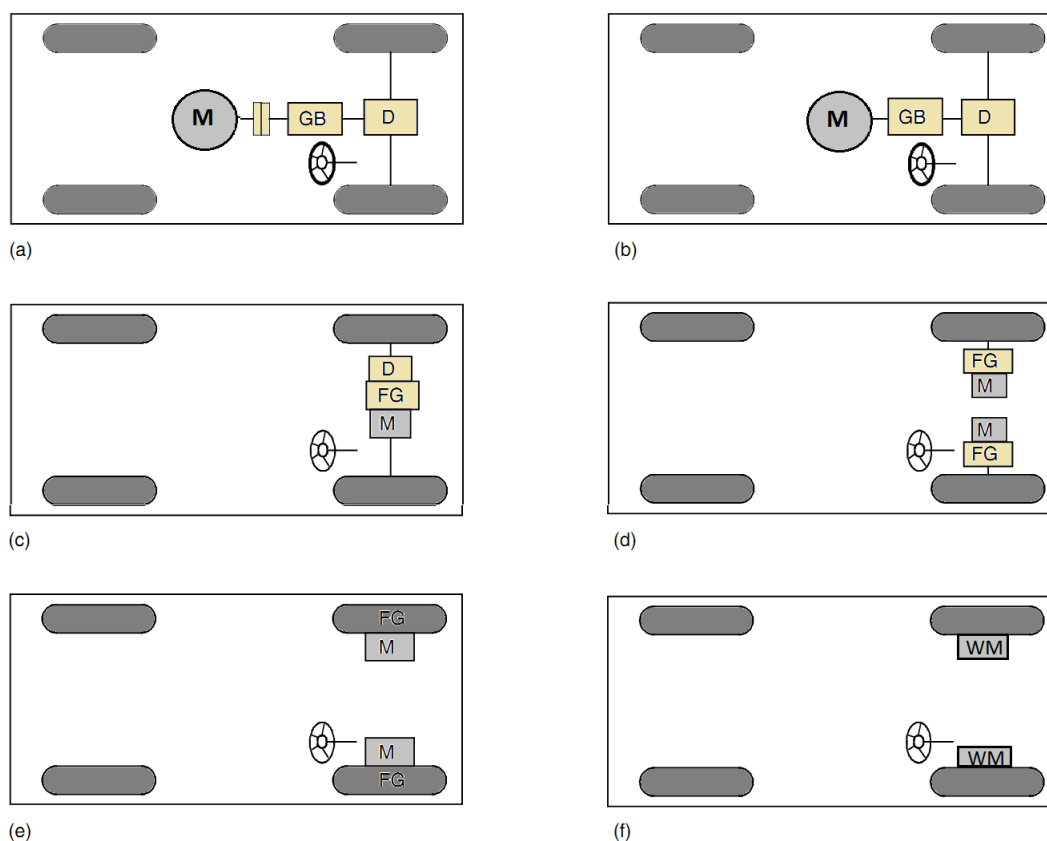


Figure 1.17: Possible EV configurations [Hus11], (C: Clutch, D: Differential, FG: Fixed gearing, GB: Gearbox, WM: Wheel Electric motor)

- (a) shows the configuration of the first alternative, in which electric propulsion replaces the IC engine of a conventional vehicle drive train. It consists of an electric

motor, a clutch, a gearbox, and a differential. The clutch and gearbox may be replaced by automatic transmission. The clutch is used to connect or disconnect the power of the electric motor from the driven wheels. The gearbox provides a set of gear ratios to modify the speed-power (torque) profile to match the load requirement. The differential is a mechanical device (usually a set of planetary gears), which enables the wheels of both sides to be driven at different speeds when the vehicle runs along a curved path.

- (b) With an electric motor that has constant power in a long speed range, a fixed gearing can replace the multi-speed gearbox and reduce the need for a clutch. This configuration not only reduces the size and weight of the mechanical transmission, but also simplifies the drive train control because gear shifting is not needed.
- (c) Similar to the drive train in (b), the electric motor, the fixed gearing and the differential can be further integrated into a single assembly while both axles point at both driving wheels. The whole drive train is further simplified and compacted.
- (d) the mechanical differential is replaced by using two traction motors. Each of them drives one side wheel and operates at a different speed when the vehicle is running along a curved path.
- (e) In order to further simplify the drive train, the traction motor can be placed inside a wheel. This arrangement is the so called in wheel drive. A thin planetary gear set may be used to reduce the motor speed and enhance the motor torque. The thin planetary gear set offers the advantage of a high-speed reduction ratio as well as an in line arrangement of the input and output shaft.
- (f) By fully abandoning any mechanical gearing between the electric motor and the driving wheel, the out-rotor of a low-speed electric motor in the in wheel drive can be directly connected to the driving wheel. The speed control of the electric motor is equivalent to the control of the wheel speed and hence the vehicle speed.

1.6.2 EV motor drives evaluation

In EVs, the electric motor is the propulsion unit, while in hybrid electric vehicles (HEVs), the electric motor and the ICE together in a series or parallel combinations

provide the propulsion power. In an EV or an HEV, the electric traction motor converts electrical energy from the energy storage unit to mechanical energy that drives the wheels of the vehicle. The major advantages of an electric motor over an IC engine are that the motor provides full torque at low speeds and the instantaneous power rating can be two or three times the rated power of the motor [Ber05]. These characteristics give the vehicle excellent acceleration with a nominally rated motor. As so far, four types of motor drives have been applied to EVs. They are Direct Current Motor (DCM) drives, Induction Motor (IM) drives, Permanent Magnet Synchronous Motor (PMSM) drives, and Switched Reluctance Motor (SRM) drives.

1.6.2.1 Direct current motor

Among the classic motors used in EV, the DCM with independent excitation, is the most economical solution through its armature chopper-type converter with two switches (the inductor is also powered by a small power chopper). This is the technology used by many automakers to commercialize EVs first generation. But the DCM has a number of well known drawbacks.

Positive attributes of DC machines are as follows:

- Ease of control due to linearity;
- Capability for independent torque and flux control;
- Established manufacturing technology.

Disadvantages of DC machines include the following:

- Brush wear that leads to high maintenance;
- Low maximum speed;
- Low power-to-weight ratio.

The separately excited DCM used in an EV or HEV has two separate DC/DC converters supplying the armature and field windings from the same energy source, The DC/DC converters process the fixed supply voltage of the energy source to deliver a variable DC to the armature and field circuits. The power rating of the converter supplying the armature windings is much larger than that of the converter supplying the field winding

[Hus11]. Control inputs to the converter circuits are the desired torque and speed of the motor. Control outputs of the converters are the voltages applied to the armature and field circuits of the DC motor. The performance analysis and modelling of used DCM in the studied EV will be shown in the next chapter.

1.6.2.2 Induction motor drives

Induction motors are of simple construction, reliability, ruggedness, low maintenance, low cost, and ability to operate in hostile environments. The absence of brush friction permits the motors to raise the limit for maximum speed, and the higher rating of speed enable these motors to develop high output. Speed variations of induction motors are achieved by changing the frequency of voltage. Field orientation control (FOC) of an IM can decouple its torque control from field control. This allows the motor to behave in the same manner as a separately excited DCM. This motor, however, does not suffer from the same speed limitations as in the DCM. Extended speed range operation beyond base speed is accomplished by flux weakening, once the motor has reached its rated power capability. A properly designed IM, e.g., spindle motor, with field oriented control can achieve field weakened range of 3-5 times the base speed [XCC08]. However, the controllers of IMs are at higher cost than the ones of DCM. Furthermore, the presence of a breakdown torque limits its extended constant-power operation. At the critical speed, the breakdown torque is reached. Generally, for a conventional IM, the critical speed is around two times the synchronous one. Any attempt to operate the motor at the maximum current beyond this speed will stall the motor. Although FOC may extend constant power operation, it results in an increased breakdown torque thereby resulting in an over-sizing of the motor. In addition, efficiency at a high speed range may suffer in addition to the fact that IMs efficiency is inherently lower than that of a Permanent Magnet Synchronous Motors (PMSM) and Switched Reluctance Motors (SRMs) due to the absence of rotor winding and rotor copper losses [Hus11].

1.6.2.3 Switched Reluctance Motor Drives

SRM drives are gaining much interest and are recognized to have a potential for EV applications. These motor drives have definite advantages such as simple and rugged construction, fault-tolerant operation, simple control, and outstanding torque-speed char-

acteristics. SRM drives can inherently operate with an extremely long constant-power range. The torque-speed characteristics of SRM drives match very well with the EV load characteristics. The SRM drive has high speed operation capability with a wide constant power region. The motor has high starting torque and high torque-inertia ratio.

The rotor structure is extremely simple without any windings, magnets, commutators or brushes. The fault-tolerance of the motor is also extremely good. Because of its simple construction and low rotor inertia, SRM has very rapid acceleration and extremely high speed operation. Because of its wide speed range operation, SRM is particularly suitable for gearless operation in EV propulsion [XCC08]. In addition, the absence of magnetic sources (i.e., windings or permanent magnets) on the rotor makes SRM relatively easy to cool and insensitive to high temperatures. The latter is of prime interest in automotive applications, which demand operation under harsh ambient conditions. An extended range of 2-3 times the base speed is usually possible using an appropriate control [XCC08]. The disadvantages of SRM drives are that they have to suffer from torque ripple and acoustic noise. However, these are not potential problems that prohibit its use for EVs application.

1.6.2.4 Permanent Magnet Synchronous Motors

The PMSM can be thought of as a cross between an AC IM and a brushless DCM . They have rotor structures similar to DCM motors which contain permanent magnets. Advantages of PMSM are well known. The greatest advantage is low volume of the PMSMs in contrast with other types of motors, it makes them suitable for wheel motor applications. On the other hand, the traction drive with PMSM has to meet special requirements typical for overhead line fed vehicles. The drives and specially their control should be robust to wide overhead line voltage tolerance (typically from -30 % to +20 %), voltage surges and input filter oscillations [XCC08]. These aspects may cause problems during flux weakening operation.

PMSM motor drives have the drawbacks in that the magnet is expensive and that the mechanical strength of the magnet makes it difficult to build a large torque into the motor. PM BLDC motors have no brush to limit speed, but questions persist over the fixing intensity of the magnet because it restricts the maximum speed if the motors are of an inner-rotor type. Furthermore, this motor suffers from a rather limited field weakening capability. This is due to the presence of the PM field which can only be weakened through

production of a stator field component which opposes the rotor magnetic field [XCC08]. Nevertheless, extended constant power operation is possible through the advancing of the commutation angle.

1.6.2.5 Comparison between four types of EV motor drives

The most appropriate choice for EVs among four types of motor drives is determined according to the following factors: weight factors in efficiency, weight, and cost. From the above summarized features of four types of motor drives for EVs, Table. 1.2 lists weight factors in efficiency, weight, and cost of four types of motor drives..

Table 1.2: Comparisons of four motors [XCC08]

Indes	DCM	IM	PMSM	SRM
efficiency	medium	high	high	high
Weigh	medium	medium	high	low
Cost	low	medium	high	high

The above table indicates that DCM drives will continue to be used in EVs because DC motor drives are available at the lowest cost. From the point of view of efficiency, PMSM motor drives are the best choice. SRM drives have the lowest weight among four types of motor drives for EVs. If the choice of motor drives for EVs is determined by three factors that are weight, efficiency and cost, it is clear that SRM drives are the best choice for EVs. Except for the efficiency, weight and cost, SRM drives also have the ascendancy in the aspects of cooling, maximum speed, fault tolerance, and reliability.

1.7 Conclusion

The main aim of this chapter was the analysis of the dynamic EV behavior based on the forces acting on a vehicle moving up a grade. The vehicle design depends on the speed-power (torque) characteristics of the traction motor which are determined by the tractive forces, the vehicle acceleration and the EV energy consumption.

Six types of the EV transmission systems of EV's drive-train had been discussed. The

drive-train scheme with the differential and single-level reduction gear is well suitable for electric motor drives with wide speed range and highly maximum speed in EVs. Furthermore, the main requests of EVs on electric motor drives and expected output characteristics of electric motor drives are presented. The comparative investigation in the weight factors in efficiency, weight, cost, cooling, maximum speed, and fault-tolerance, safety, and reliability has been accomplished for SRM, IM, PMSM, and DCM drives. To be specific, a) In the aspect of efficiency, PMSM drives are better than SRM drives, IM drives and DCM drives; b) The weight of SRM drives is lower than PMSM, IM, and DCM drives; c) Taking into account the aforementioned three criteria, SRM drives are superior to other three types of motor drives. d) DCM drives have the lowest cost for these four types of motor drives, Furthermore, DCM drives also according to the aspects of maximum speed, control simplicity and its cost, which make DCM drives are suitable for EV applications. In the main context of the EV development, it is the used supply sources and its less driving range, which is blocking the way of electric vehicles to the market. Therefore, a basic study of the different used sources and their principle were presented in the second chapter.

Electric Vehicle Supply Sources

2.1 Introduction

In the near future, EVs including HEVs, and pure battery EVs will dominate the clean vehicle market. By 2020, it is expected that more than half of new vehicle sales will likely be EV [YWWS13], [VMML06]. The key and the enabling technology to this revolutionary change is the energy storage. The energy storage is considered as the heart of an EV, and there are a number of energy storage requirements applied in an automotive application, such as specific energy, specific power, efficiency, maintenance requirement, management, cost, environmental adaptation and friendliness, and safety. For allocation on an EV, the specific energy is the first consideration since it limits the vehicle range.

In this chapter, the fundamentals and comparisons of EV battery, SCs and FC technologies, will be suggested and explained in order to find an answer to the following question "**Which best energy source for road transport in the future?**". There are several types of energy storages that have been proposed and used for EVs and HEV applications. These energy storages, so far, mainly include chemical batteries and supercapacitors. It is particularly important for power engineers to understand the basic principle of the different sources, and specific requirements of the EV supply source.

2.2 Electrochemical battery

Electrochemical batteries, more commonly referred to as batteries, are electrochemical devices that convert electrical energy into potential chemical energy during charging, and convert chemical energy into electric energy during discharging [KCC⁺12]. Many different battery types exist, e.g., lead-acid, nickel-metal hydride, lithium ion, etc. However, today the lithium ion is the preferred choice for the EV applications due to its relatively high specific energy and power [Ram03].

While the term "battery" is often used, the basic electrochemical unit being referred to is the "Battery cell". A battery consists of one or more of these cells, connected in series or parallel, or both, depending on the desired output voltage and capacity. The battery cell consists of three major components as shown in Fig. 2.1 [Red11]:

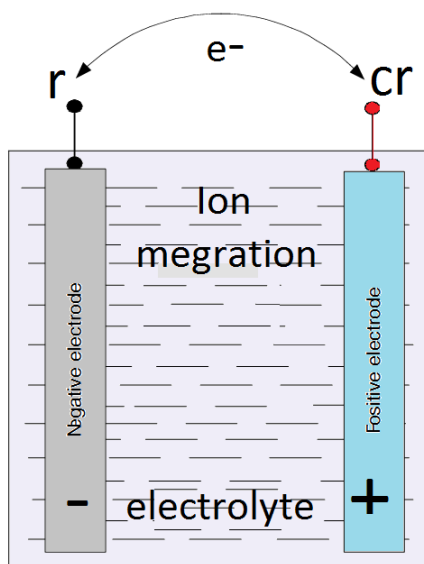


Figure 2.1: An electrochemical battery cell

1. The anode or negative electrode, the reducing or fuel electrode, which gives up electrons to the external circuit and is oxidized during the electrochemical reaction;
2. The cathode or positive electrode, the oxidizing electrode, which accepts electrons from the external circuit and it is reduced during the electrochemical reaction.
3. The electrolyte, the ionic conductor, which provides the medium for transfer of charge, as ions, inside the cell between the anode and cathode. The electrolyte is typically a liquid, such as water or other solvents, with dissolved salts, acids, or

alkalis to impart ionic conductivity. Some batteries use solid electrolytes, which are ionic conductors at the operating temperature of the cell [Red11].

There are many different battery types, the most popular types will be discussed in the following parts.

2.2.1 The Lead Acid battery

The lead-acid battery has been a successful commercial product for over a century and is still widely used as electrical energy storage in the automotive field and other applications. The main advantages and disadvantages of Lead-acid battery are given in Table. 2.1.

Table 2.1: Advantages and disadvantages of Lead Acid battery

Advantages	Disadvantages
<ul style="list-style-type: none">• Inexpensive and simple to manufacture• Mature, reliable and well-understood technology ;• Low self-discharge;• Low maintenance requirements ;	<ul style="list-style-type: none">• Low energy density;• Allows only a limited number of full discharge cycles;• Environmentally unfriendly ;• Thermal runaway can occur with improper charging.

Different lead-acid batteries with improved performance are being developed for EVs and HEVs. Improvements of the sealed lead-acid batteries in specific energy over 40 Wh/kg, with the possibility of rapid charge, have been attained. One of these advanced sealed lead-acid batteries is Electro-source's Horizon battery. It adopts the lead wire woven horizontal plate and hence offers the competitive advantages of high specific energy (43 Wh/kg), high specific power (285 W/kg), long cycle life (over 600 cycles for on-road EV application), rapid recharge capability (50% capacity in 8 min and 100% in less than 30 min), low cost (US\$2000-3000 an EV), mechanical ruggedness (robust structure of horizontal plate), maintenance-free conditions (sealed battery technology), and environmental friendliness [YWWS13].

2.2.2 The Nickel based battery

Nickel is a lighter metal than lead and has very good electrochemical properties desirable for battery applications. There are four different nickel-based battery technologies: nickel-iron, nickel-zinc, nickel-cadmium, and nickel-metal hydride. Two of them will be discussed.

2.2.2.1 The Nickel Cadmium (NiCd) battery

Nickel/cadmium technology has seen enormous technical improvement because of the advantages of high specific power (over 220 W/kg), long cycle life (up to 2000 cycles), a high tolerance of electric and mechanical abuse, a small voltage drop over a wide range of discharge currents, rapid charge capability (about 40 to 80% in 18 min), wide operating temperature (-40 to 85°C), low self-discharge rate ($< 0.5\%$ per day), excellent long-term storage due to negligible corrosion, and availability in a variety of size designs [YWWS13]. However, the nickel/cadmium battery has some disadvantages, given in Table. 2.2.

Table 2.2: Advantages and disadvantages of NiCd

Advantages	Disadvantages
<ul style="list-style-type: none">• High number of charge/discharge cycles;• Good load performance, the NiCd allows recharging at low temperatures;• The lowest cost battery in terms of cost per cycle;• Good low temperature performance.	<ul style="list-style-type: none">• Relatively low energy density compared with newer systems;• Its charge is complex because of the memory effect, the NiCd must periodically be exercised to prevent memory;• Environmentally unfriendly, the NiCd contains toxic metals;• Has relatively high self-discharge that needs recharging after storage.

2.2.3 The Nickel-Metal Hydride (NiMH) battery

The Ni-MH battery has been considered as an important near-term choice for EV and HEV applications. A number of battery manufacturers, such as GM Ovonic, GP, GS,

Panasonic, SAFT, *VARTA*¹, and *YUASA*², have actively engaged in the development of this battery technology, especially for powering EVs and HEVs. Since 1993, Ovonic battery has installed its Ni-MH battery in the Solectric GT Force EV for testing and demonstration. A 19-k/Wh battery has delivered over 65 Wh/kg, 134 km/h, acceleration from zero to 80 km/h in 14 sec, and a city driving range of 206 km [YWWS13]. Toyota and Honda have also used the Ni-MH battery in their new HEVs "Prius and Insight", respectively.

Table 2.3: Advantages and disadvantages of NiMH

Advantages	Disadvantages
<ul style="list-style-type: none"> • 30 to 40% higher capacity over a standard NiCd; • Less prone to memory than the NiCd, Periodic exercise cycles are required less often; • Simple storage and transportation, transportation conditions are not subject to regulatory control; • Environmentally friendly, contains only mild toxins; profitable for recycling. 	<ul style="list-style-type: none"> • Limited service life the performance starts to deteriorate after 200 to 300 cycles; • Limited discharge current; • More complex charge algorithm needed; • Performance degrades if stored at elevated temperatures; • 20% more expensive than NiCd;

2.2.4 The Lithium based battery

Lithium is the lightest of all metals and presents very interesting characteristics from an electrochemical point of view. Indeed, it allows a very high thermodynamic voltage, which results in a very high specific energy and specific power. There are two major technologies of lithium-based batteries [Red11]: lithium-polymer and lithium-ion.

¹VARTA is a company based in Germany manufacturing batteries for global automotive, industrial and consumer markets

²American manufacturer and distributor of replacement batteries for motorcycle

2.2.4.1 The Lithium Polymer battery

These batteries are considered solid state batteries, because their electrolytes are solids. The most common polymer electrolyte is polyethylene oxide compounded with an appropriate electrolyte salt. Li-poly batteries have the potential for the highest specific energy and power [YWWS13]. The solid polymers, replacing the more flammable liquid electrolytes in other type of batteries, can conduct ions at temperatures above 60°C. The use of solid polymers also has a great safety advantage in case of EV and HEV accidents [Hus11]. Because the lithium is intercalated into carbon electrodes, the lithium is in ionic form and is less reactive than pure lithium metal. The thin Li-poly cell gives the added advantage of forming a battery of any size or shape to suit the available space within the EV or HEV chassis.

Table 2.4: Advantages and disadvantages of Lithium Polymer battery

Advantages	Disadvantages
<ul style="list-style-type: none"> • Very low profile; • Flexible form factor, with high volume, any reasonable size can be produced economically; • Light weight; • Improved safety, more resistant to over-charge; less chance for electrolyte leakage. 	<ul style="list-style-type: none"> • Lower energy density and decreased cycle count compared to Li-ion; • Expensive to manufacture , once mass-produced; • Reduced control circuit offsets higher manufacturing costs.

2.2.4.2 Lithium-Ion (Li-Ion) Battery

Since the first announcement of the Li-ion battery in 1991 [Red11], Li-ion battery technology has seen an unprecedented rise to what is now considered to be the most promising rechargeable battery of the future thanks to its advantages as is indicated in Table. 2.5. Although still at the development stage, the Li-ion battery has already gained acceptance for EV and HEV applications.

Many battery manufacturers, such as SAFT, GS Hitachi, Panasonic, SONY, and VARTA, are actively engaged in the development of the Li-ion battery. Starting in 1993,

Table 2.5: Advantages and disadvantages of Lithium-Ion battery

Advantages	Disadvantages
<ul style="list-style-type: none"> • High energy density, potential for yet higher capacities.; • Flexible form factor, with high volume, any reasonable size can be produced economically; • Relatively low self-discharge, self-discharge is less than half that of NiCd and NiMH.; • Low maintenance and improved safety; 	<ul style="list-style-type: none"> • Requires protection circuit • Expensive to manufacture , once mass-produced;

SAFT focused on the nickel-based Li-ion battery. Recently, SAFT reported the development of Li-ion high-power batteries for HEV applications with a specific energy of 85 Wh/kg and a specific power of 1350 W/kg. They also announced high-energy batteries for EV applications with about 150 Wh/kg and 420 W/kg (at 80% SOC, 150 A current, and 30 sec) [Ber05], respectively.

Table. 2.6 shows the status of battery systems potentially available for EV. It can be seen that although specific energies are high in advanced batteries, the specific powers have to be improved. About 300 W/kg might be the optimistic estimation. However, SAFT³ has reported their Li-ion high-power for HEV application with a specific energy of 85Wh/kg, and a specific power of 1350 W/kg and their high-energy batteries for EV application with about 150 Wh/kg and 420 W/kg (at 80% SOC, 150 A current and 30 sec) [EGE09], respectively.

As shown in Table. 2.7, the current two major battery technologies used in EVs are nickel metal hydride (NiMH) and lithium ion (Li-ion). Nearly all HEVs available in the market today use NiMH batteries because of its mature technology. Due to the potential of obtaining higher specific energy and energy density, the adoption of Li-ion batteries is expected to grow fast in EVs, particularly in pure EVs and parallel HEVs [VMML06].

³Saft is a French company specializing in the design and manufacture of accumulators

Table 2.6: Different chemical battery technologies[Red11] (E_s : specific energy wh/kg)

Cell Reaction			
Battery	charge(\Leftarrow)	discharge(\Rightarrow)	E_s
Acidic aqueous solution			
PbO_2 Pb	$PbO_2 + 2H_2SO_4 + Pb$	$\Leftrightarrow 2PbSO_4 + 2H_2$	170
Alkaline aqueous solution			
$NiOOH$ Cd	$2NiOOH + 2H_2O + Cd$	$\Leftrightarrow 2Ni(OH)_2 + Cd(OH)_2$	217
$NiOOH$ Fe	$2NiOOH + 2H_2O + fe$	$\Leftrightarrow 2Ni(OH)_2 + Fe(OH)_2$	287
$NiOOH$ Zn	$2NiOOH + 2H_2O + Zn$	$\Leftrightarrow 2Ni(OH)_2 + Zn(OH)_2$	341
$NiOOH$ H_2	$2NiOOH + H_2$	$\Leftrightarrow 2Ni(OH)_2$	387
MnO_2 Zn	$2MnO_2 + 2H_2O + Zn$	$\Leftrightarrow 2MnOOH + ZnO$	317
O_2 Al	$4Al + 6H_2O + 3O_2$	$\Leftrightarrow 2Al(OH_2)_3$	2815
O_2 Fe	$2Fe + 2H_2O + O_2$	$\Leftrightarrow 2Fe(OH)_2$	764
O_2 Zn	$3Zn + 2H_2O + O_2$	$\Leftrightarrow 2PbSO_4 + 2H_2$	288
Flow			
Br_2 Zn	$Zn + Cl_2$	$\Leftrightarrow ZnBr_2$	436
Cl_2 Zn	$Zn + Br_2$	$\Leftrightarrow ZnCl_2$	833
$(VO_2)_2SO_4$ VSO_4	$(VO_2)_2 + SO_2 + 2HVSO_2 + 2H_2SO_4$	$\Leftrightarrow 2VoSO_4 + V_2(SO_4)_3 + H_2O$	114
Melten salt			
S Na	$2Na + 3S$	$\Leftrightarrow 2NaS_3$	760
$Nicl_2$ Na	$2NA + NcCl_2$	$\Leftrightarrow 2NaCl$	790
F_2S_2 $LiAl$	$4LiAl + F_2S_2$	$\Leftrightarrow 2Li_2S + 4Al + F_2$	650
Organic lithium			
$LiCoO_2$ LiC	$Li_{(y+x)}C_6 + Li_{(1-(y-x))}CoO_2$	$\Leftrightarrow LI_y + Li_{1-y}CoO_2$	320

Table 2.7: Used batteries technologies in EV's manufacturers [YWWS13]

Company	Country	Vehicle model	Battery technology
GM	USA	Chevy-Volt	Li-ion
GM	USA	Saturn Vue Hybrid	NiMH
Ford	USA	Escape, Fusion, MKZ HEV	NiMH
Ford	USA	Escape PHEV	Li-ion
Toyota	Japan	Prius, Lexus	NiMH
Honda	Japan	Civic, Insight	NiMH
Hyundai	South Korea	Sonata	Lithium polymer
Chrysler	USA	Chrysler 200C EV	Li-ion
BMW	Germany	X6	NiMH
BMW	Germany	Mini E (2012)	Li-ion
BYD	China	E6	Li-ion
Daimler Benz	Germany	ML450, S400	NiMH
Daimler Benz	Germany	Smart EV (2010)	Li-ion
Mitsubishi	Japan	iMiEV (2010)	Li-ion
Nissan	Japan	Altima	NiMH
Nissan	Japan	Leaf EV (2010)	Li-ion
Tesla	USA	Roadster (2009)	Li-ion
Think	Norway	Think EV	Li-ion

2.2.5 Electric model of battery

The battery can be modelled in steady-state, i.e., the dynamic behavior is not considered [EGE09]. The electric equivalent circuit diagram can be seen in Fig. 2.2 [Cha00]. The battery model consists of an internal voltage source (V_{int}) and an inner resistances (R_{int}), caused by chemical reaction. This latter represents the voltage drop, ΔV , which is associated with the battery current (for more details see [Red11]). Battery currents (i) are treated as positive currents, i.e., charging currents are then negative.

$$V_{bat} = V_{bat_{int}} - R_{int}i \quad (2.1)$$

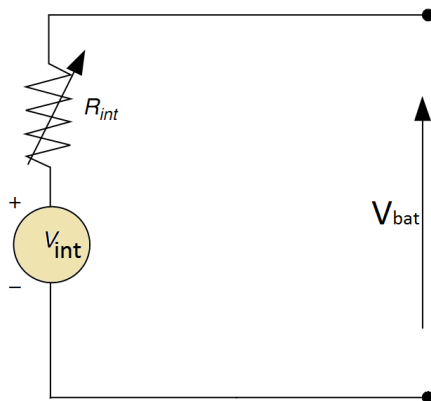


Figure 2.2: The battery's equivalent circuit .

2.2.5.1 Specific power

Specific power is important in the reduction of a battery weight, especially in high power demand applications, such as EV and HEV applications. The specific power of a chemical battery depends mostly on the battery's internal resistance [EGE09]. With the battery model as shown in Fig. 2.2, the maximum power that the battery can supply to the load is

$$P_s = \frac{V_{int}^2}{4(R_c + R_{int})} \quad (Wh/kg) \quad (2.2)$$

2.2.5.2 Energy efficiency

The energy or power losses during a battery discharging and charging appear in the form of voltage losses. Thus, the efficiency of the battery during discharging and charging can be defined at any operating point as the ratio of the cell operating voltage to the thermodynamic voltage, that is [Red11]:

$$\begin{cases} \eta_d = \frac{v}{v_{int}} \\ \eta_c = \frac{v_{int}}{v} \end{cases} \quad (2.3)$$

where η_d , and η_c are the energy efficiency during discharging and charging, respectively. The terminal voltage, as a function of battery current and energy stored in it or battery State Of Charge (SOS), is lower in discharging and higher in charging than the electrical potential produced by a chemical reaction. Fig. 2.3 shows the efficiency of the lead-acid battery during discharging and charging. The battery has a high discharging efficiency

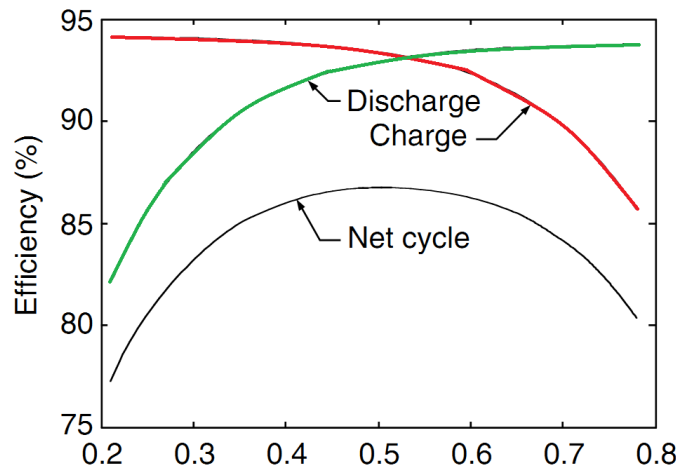


Figure 2.3: Typical battery charge and discharge efficiency [EGE09].

with high SOC and a high charging efficiency with low SOC. The net cycle efficiency has a maximum in the middle range of the SOC.

2.2.5.3 Battery state of charge

The SOC is the equivalent of a fuel gauge for the battery pack in an EV. There is not an units for SOC and it is expressed in percentage points (0% = empty; 100% = full), In many literatures [YWWS13], [KBA+13], [TCDH09], the change of SOC in a time interval dt , with discharging or charging current i_{bat} may be expressed as:

$$\begin{cases} \Delta SOC = \frac{idt}{Q} \\ SOC(t) = SOC(0) - \int \frac{i_{bat}(t)}{Q} dt \end{cases} \quad (2.4)$$

where Q is amp-hour capacity of the battery at current rate i_{bat} . For discharging, the battery's current (i_{bat}) is positive and for charging it is negative.

2.3 Supercapacitors

For the EV applications, the energy source, mainly batteries and fuel cells, have a high specific energy whereas the power source has a high specific power. The power sources can be recharged from the energy source during less demanding driving or regenerative braking. The power source that has received wide attention is the Supercapacitors (SCs). The electric double-layer capacitor effect was first noticed in 1957 by General Electric

engineers experimenting with devices using porous carbon electrode [SB10]. It was believed that the energy was stored in the carbon pores and it exhibited "exceptionally high capacitance", although the mechanism was unknown at that time. SCs are electrochemical devices that have an unusually high energy density, but its main disadvantage is its lower specific energy compared to the chemical batteries, which limits the uses of SC in transient dynamic performance of the EV (accelerations and deceleration) [TCDH09].

2.3.1 Basic principles of supercapacitors

Electrochemical SC consists of two electrodes separated by an ion permeable membrane (separator), and an electrolyte connecting electrically the both electrodes. By applying a voltage to the capacitor an electric double layer at both electrodes is formed, which has a positive or negative layer of ions deposited in a mirror image on the opposite electrode [SB10]. The basic principle of a double-layer capacitor is illustrated in Fig. 2.4. When two carbon rods are immersed in a thin sulphuric acid solution, separated from each other and charged with voltage increasing from zero to 1.5 V, almost nothing happens up to 1 V; then at a little over 1.2 V, a small bubbles will appear on the surface of both the electrodes. Those bubbles at a voltage above 1 V indicate electrical decomposition of water. Below the decomposition voltage, while the current does not flow, an "electric double layer" then occurs at the boundary of electrode and electrolyte, then electrons are charged across the double layer [Bar11].

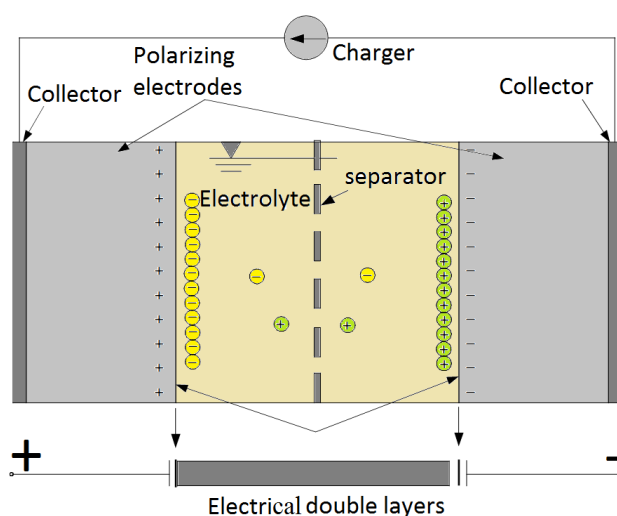


Figure 2.4: Principle construction of a supercapacitor

2.3.2 Electric model of supercapacitor

There are different electric equivalent circuits of SC in literature. The frequent electrical model given by (2.5) is deduced from the SC equivalent circuit shown in Fig. 2.5 [ABH11]. In this model, the differential capacitance is represented by two capacitors: a constant capacitor C_0 and a linear voltage dependent capacitor kV_0 , where k is a constant corresponding to the slope voltage [ABH11].

$$\begin{cases} \frac{dV_0}{dt} = \frac{1}{C_0 + kV_0} I_{SC} \\ V_{SC} = R_{SC} I_{SC} + V_0 \end{cases} \quad (2.5)$$

where $C_0 + kV_0 > 0$

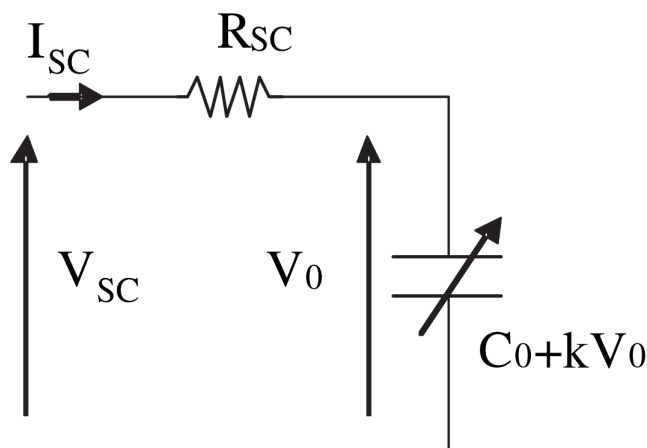


Figure 2.5: Supercapacitor equivalent circuit [ABH11]

The SC's stored energy, E_{SC} , is expressed as [YWWS13]

$$E_{SC} = \frac{1}{2} C V_{SC}^2 \quad (2.6)$$

where C is the capacitance in Faraday.

2.3.2.1 Supercapacitor's state of charge

Many searching works such as in [CY13], [IT11] and [SJS⁺10] gave approximate functions to determine the SC's SOC. An SC is usually given a bottom voltage (V_{SC_b}), below which the SC will stop delivering energy. Consequently, the available or useful energy for use is less than its fully charged energy, which can be expressed as [Hus11]

$$E_{SC_u} = \frac{1}{2} C (V_{SC_b}^2 - V_{SC_r}^2) \quad (2.7)$$

where V_{SC_r} is the rated voltage of the SC. At its bottom voltage, the SOC can be written as [Hus11]

$$SOC = \frac{E_{SC_u}}{E_{SC_c}} = \left(\frac{V_{SC_b}}{V_{SC_r}} \right)^2 \quad (2.8)$$

For example, when the cell voltage drops from rated voltage to 60% of the rated voltage, 64% of the total energy is available for use, as it is shown in Fig. 2.6.

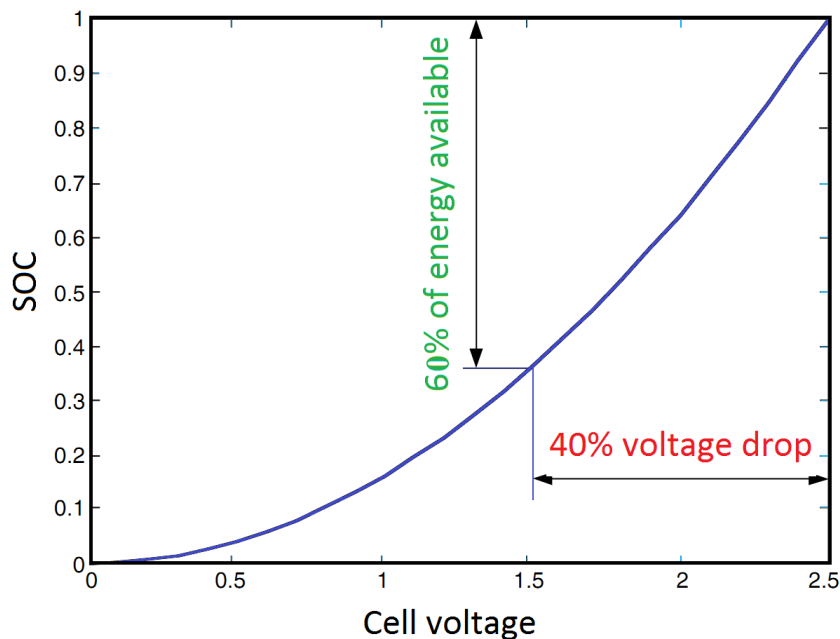


Figure 2.6: Typical supercapacitor's SOC [EGE09]

2.4 Fuel cell vehicle

In recent decades, a new kind of an EV prototype has appeared thanks to the application of fuel cells in vehicles, which have been the focus of increased attention. The Fuel Cell is considered only as a generator of electrical energy rather than energy storage device unlike the batteries or SCs.

2.4.1 Fuel cell history

The FC technology was actually invented in the 19th century in 1839 by Sir William Grove, a Welsh judge and scientist. Since then, FCs have been primarily used in research settings. The National Aeronautics and Space Administration selected PEMFCs for the space program in the 1960s, rejecting both nuclear power, which had a higher safety risk,

and solar power, which had a higher cost [PSP04], [Puk03]. FCs provided power for the Gemini and Apollo missions and, at present, provide water and electricity to the space shuttle. Despite their high-profile use in the space program, the commercialization of a FC technology was not explored until the early 1980s [Puk03]. The first applications in "vehicles" were by implantation demonstrators in the late 1950s, to the result of the work of FT Bacon at the University of Cambridge on an alkaline FC operating above 200° C. In August 1959, a system of an alkaline FC hydrogen/oxygen with 6 kw was developed and tested on machine tools and a forklift. In recent decades, the appearance prototype replacing part of the battery by a fuel cell generator pack, made the advanced vehicle technology research turned to the **FC vehicles**⁴ [Ber05].

2.4.2 Basic principle of the fuel cell

A FC consists of an electrolyte sandwiched between two electrodes. The electrolyte has a special property that allows positive ions (protons) to pass through while blocking electrons. Hydrogen gas passes over one electrode, called an anode, and with the help of a catalyst, separates into electrons and hydrogen protons as shown in Fig. 2.5 [Bar13]. The chemical reaction in a fuel cell is similar to that in a chemical battery and it is expressed as



The protons flow to the other electrode, called a cathode, through the electrolyte while the electrons flow through an external circuit, thus creating electricity. The hydrogen protons and electrons combine with oxygen flow through the cathode, and produce water [PSP04], [Bar13].



The overall FC reaction is therefore



The voltage produced from one FC is 0 to 1(V) depending on FC operating conditions and the size of load connected to it [Puk03]. The typically value of FC voltage is about 0.7(V) [PSP04], [Puk03]. To get higher voltage, multiple cells are stacked in series, the

⁴is an EV kind which is supplied by a FC.

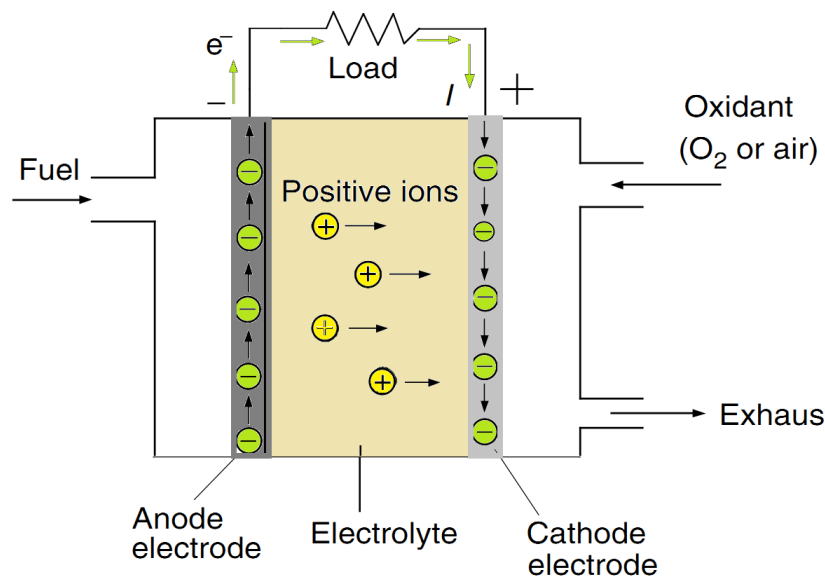


Figure 2.7: Basic operation of a fuel cell

total stack voltage is the number of cells \times the average cell voltage. Like other electric devices, there are electrical resistances in the FC, the loss associated with the resistance is dissipated in the form of heat, In other word, heat is released from the FC chemical reactions [Puk03].

Depending on the type of FC electrolyte, six major types of fuel cells can be distinguished [Hus11] as shown in Table. 2.8.

2.4.3 Fuel cell advantages and disadvantages

In contrast to a chemical battery, compared with the battery-powered electric vehicles (EVs), the FCs are suitable for the EV applications specially PEMFC, thanks to their high power density, a solid electrolyte, long life, as well as low corrosion, and they operate in the temperature range of $50 - 100^\circ\text{C}$ [VMML06], [PSP04], which allows safer operating and eliminating the need of thermal insulation. the FC generates electrical energy and continues to do so as long as a fuel supply is maintained that make the FC-powered vehicle has the advantages of a longer driving range. Compared with the internal combustion engine (ICE) vehicles, the FC has the advantages of high energy efficiency and zero emissions due to the direct conversion of free energy in the fuel into electric energy, without undergoing combustion.

However, their uses in the EV field remains at the prototype stage because there are

Table 2.8: Fuel cell types characteristics [Hus11]

Fuel Cell Variety	Fuel	Electrolyte	$T_{operating}$
Phosphoric acid	H_2 , reformat(LNG, methanol)	Phosphoric acid	200° C
Alkaline	H_2	Potassium hydroxide solution	80° C
Proton exchange membrane	H_2 , reformat (LNG, methanol)	Polymer ion exchange	80° C
Direct methanol	Methanol ethanol	Solid polymer	90 – 100° C
Molten carbonate	H_2 CO (coal gas, LNG, methanol)	Carbonate	600 – 700° C
Solid oxide	H_2 , CO (coal gas, LNG, methanol)	Yttria-stabilized zirconia	1000° C
Fuel Cell Variety	Efficiency	Applications	
Phosphoric acid	40-50%	Stationary (>250 kW)	
Alkaline	-50%	Mobile	
Proton exchange membrane	40-50%	EV and HEV, industrial up to 80 kW	
Direct methanol	30%	EV and HEVs, small portable devices	
Molten carbonate	50-60%	Stationary (>250 kW)	
Solid oxide	50-65%	Stationary	

many obstacles such as hydrogen storage, and complexity of their annexes component e.g. pressure regulation, compression, radiator, air and heat management system as shown in Fig. 2.8 . On the other hand, the large scale hydrogen distribution would require a complete update of the distribution system current fuel that makes the FC technology so expensive [VMML06] and the main FC vehicle disadvantage is its slowest transient dynamic performance.

In the following sections, only PEMFC type will be studied and simulated as a discussed example.

2.4.4 Fuel cell modelling

In the literature, different models of PEMFC are reported and can be divided into two types: steady-state (static) and dynamic models, depending on the main FC feature the model is focused on. Steady-state models reproduce the curve emphasizing the operating temperature and pressure effects [BCLM08], [RX01]. These models correctly match the fuel cell behaviour only for slow transients, neglecting short time intervals. Yet, in power supply system design, the source transient response must be accurately characterized, due to the load burst power consumption profile in terms of current value and slew-rate.

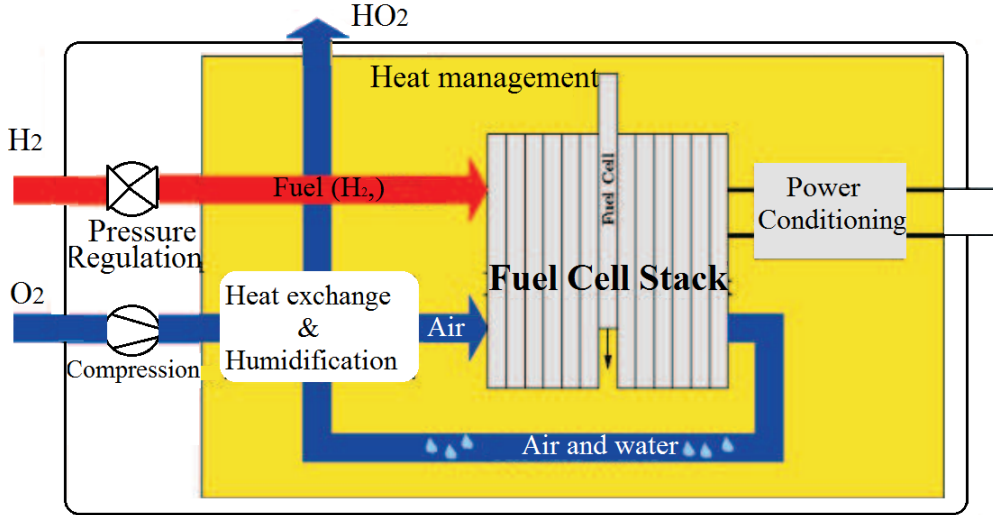


Figure 2.8: Fuel cell system.

Dynamic models, on the other hand, focus on the fuel cell transient performances, by just considering the operating parameters effects of major interest or completely neglecting steady-state effects [BCLM08].

2.4.5 Fuel cell static model

The variation of the individual cell voltage is found from the maximum cell voltage and the various voltage drops (losses). The FC output voltage V_{FC} can be defined by a nonlinear Larminie and Dicks static model as given in [ABH11]:

$$V_{FC} = E_0 - A \log \left(\frac{i_{FC} - i_n}{i_0} \right) - \left[R_m (i_{FC} - i_n) + B \log \left(1 - \frac{i_{FC} - i_n}{i_{Lim}} \right) \right] \quad (2.12)$$

Hence $V_{FC} = f(i_{FC})$, E_0 is the reversible no loss voltage of the FC, i_{FC} is the delivered current, i_0 is the exchange current, A is the slope of the Tafel line, i_{Lim} is the limiting current, B is the constant in the mass transfer, i_n is the internal current and R_m is the membrane and contact resistances. Theoretically, A and B are given by [SBAA13]:

$$A = \frac{R_1 T_{FC}}{2\alpha F} \quad (2.13)$$

$$B = \frac{R_1 T_{FC}}{2F}$$

Where, R_1 , T_{FC} and F are the universal gas constant, the temperature (K) and a Faraday number respectively. α is called the charge transfer coefficient, its value depends

on the reaction involved and the electrode material, but it must be in the range from 0 to 1 [SBAA13].

A simplified model has been developed by [MTD12] (Fig. 2.9), it represents a particular fuel cell stack operating at nominal conditions of temperature and pressure. The parameters of the equivalent circuit can be modified based on the polarization curve obtained from the manufacturer datasheet. It just has to input in the value of the voltage at 0 and 1 A, the nominal and the maximum operating points, for the parameters to be calculated. A diode is used to prevent the flow of negative current into the stack [MTD12]

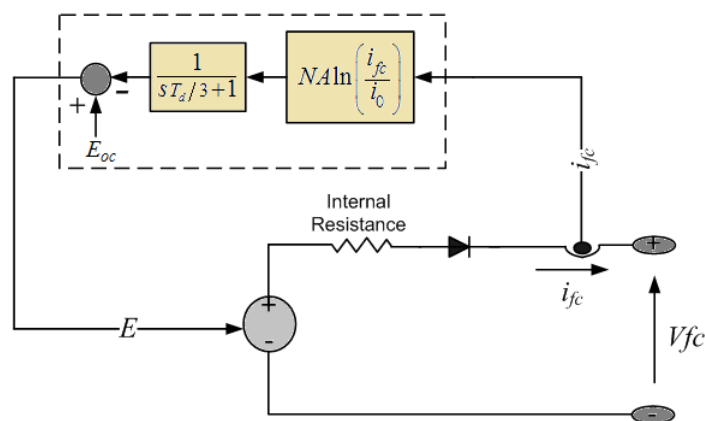


Figure 2.9: A fuel cell equivalent electric circuit [Mat]

The ideal typical polarization curve for a single FC has three major regions, as it is shown in Fig. 2.10 (Matlab simulation of the model given in (2.12)). The first region represents **the activation polarization** at low current densities, the cell potential drops exponentially due to the slowness of the chemical reactions taking place at electrode surfaces. Depending on the temperature and operating pressure, type of electrode, and catalyst used, this region is more or less wide. The second region represents **the ohmic polarization** at intermediate current densities. The voltage loss caused by ohmic resistance becomes significant and results mainly from resistance to flow of ions in the electrolyte and resistance to the flow of electrons through the electrode [Bar13], as it is shown in Fig. 2.10. At high current densities, the mass effects dominate due to the transport limit of reactant gas through the pore structure of the gas diffusion layers and electro-catalyst, and cell performance drops drastically [Bar13].

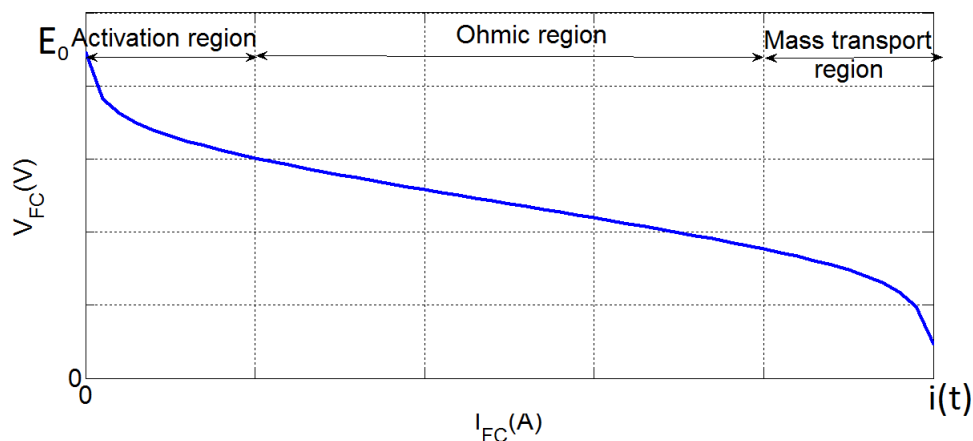


Figure 2.10: A PEMFC typical polarization curve

2.5 Different hybrid sources of an electrical vehicle

Currently, the battery is still the most extensive energy storage device for providing and delivering electricity in the EV [KBA+13]. But it is expected that the fuel cell vehicles will be the main source for the future vehicle, especially after improving the FC power operations by using an auxiliary energy storage device to manage the load power peaks during acceleration and braking. The hybrid source combines the advantages of the used technologies (e.g. specific energy and power, energy recovery thought regenerative breaking, etc). In this section, a comparative study of FC vehicles hybridization with battery or SCs storage device will be presented, it is addressed to find a satisfied answer of the following question "Which hybrid energy source for road transport in the future?".

2.5.1 FC-battery vs FC-subercapacitors

The main important point in hybrid systems presented in literatures is to balance the energy between the FC main source, the auxiliary source, and the load [MTD12]. The role of the FC and the batteries is to supply mean power to the load, whereas the storage device (SCs) can be used as a power source: it manages load power peaks during acceleration and braking. The FC power (or current) dynamics have been intentionally reduced, the auxiliary source supplies all load variations. The advantages of a FC hybrid source could include improved vehicle performance, fuel economy and lower stem (minimise the FC or the battery sizing). The degree of hybridization benefits from [PPMTD11]:

- FC efficiency characteristics;

- FC downsizing;
- Energy recovery through regenerative braking.

The comparison between the FC-battery and the FC-SCs hybrid sources depends completely on the comparison between SCs and battery characteristics.

2.5.2 Battery vs Supercapacitor

To compare the power characteristics of SCs and batteries, and to know which one can be better auxiliary source to FC, the comparison should be made for the same charge/discharge efficiency. Both types of devices (battery and SCs) are capable of high-power pulses, although batteries are not intended to be charged/discharged for long periods at these high power levels, which allow assessing directly the relative performance of SCs and power batteries from the pulse power tests. The battery pulse testing is usually done at a specified partial SOC, as only a small fraction of the energy stored in the battery is used in the cycle tests. Of particular interest in the pulse tests is the round-trip efficiency of the devices [MT10], [Hus11]. This is determined from the ratio of the energy out of the devices to the energy into the devices during the test cycle. For SCs, their charge/discharge efficiency is high, and the energy lost to heat during each a cycle is relatively small and readily removed. The energy lost to heat in batteries is a much larger amount, making heat removal more crucial and its extraction costs much more. This is to say that the cycle efficiency of batteries is around 80%, and the cycle efficiency of SCs is around 95% [EGE09]. For a corresponding high-efficiency discharge, batteries would have a much lower power capability.

The main advantage of SC is its short charging time, depending on a high charging current (power) that is available from the main source, depending on a high charging current (power) that is available from the main source. Whereas the batteries is a slow charging time, due to it is limited charging current [MT10]. According to specific power and energy, the battery has the largest energy density as shown in Fig. 2.11, (i.e., more energy is stored per weight than other technologies), it is important to consider the availability of such that energy. e.g. with a time constant of less than 0.1 s, energy can be taken from a capacitor at a very high rate [Bar11]. On the contrary, a battery of the same size will not be able to supply the necessary energy in the same time period. Also,

the SC can withstand a very large number of charge/discharge cycles without degradation unlike the battery, it means that the supercapacitors cycle life is much higher than that

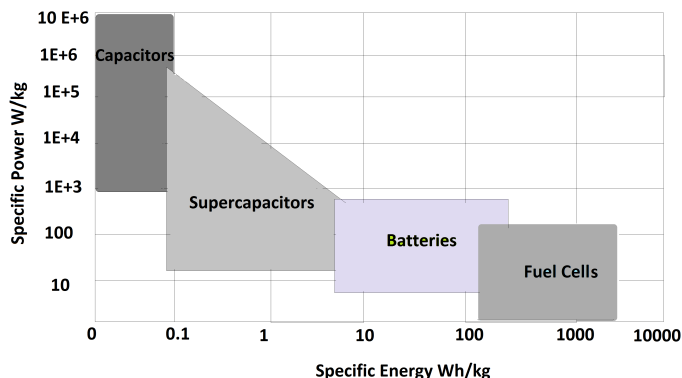


Figure 2.11: Energetic comparison between capacitors, SCs, batteries and FCs.

of batteries [CBLM09].

The tests of SC and Li-battery presented in [MT10], proved when both devices are compared with similar cell mass, the SCs efficiency is greater than high power lithium batteries in all operative conditions. Furthermore, the SC efficiency is very high in symmetrical cycles characterized by high power density both in charging and discharging operations as shown in Table. 2.9. As a consequence, the SCs have better performances

Table 2.9: Measured Li-battery and simulated SC (650 F) efficiencies [MT10]

Power in discharge (W/kg)	Power in charge (W/kg)	Measured Li-battery efficiency (%)	Simulated SC efficiency%
2100	330	87.6	90.3
2070	330	84.8	90.8
2030	330	83.7	90.8
1980	330	83	91
1910	330	82.5	91.2
1450	330	87	93.1

than the battery, to be an auxiliary source with a FC in EVs application. The hybrid FC-SC source has advantages of FC plus the SCs advantages that eliminate the drawbacks

of the FC transient dynamic performance and recovery the energy through regenerative braking, because the SCs can more effectively assist the FC to meet the transient power demand. Nonetheless, an FC hybrid vehicle with SCs will be deficient during the vehicle start-up because of the start-up time of a PEMFC of around 5-10 min, in which the battery has higher specific energy than the SC. Consequently, a more practical solution is proposed using a FC, battery and SCs hybrid power source to increase the battery lifetime due to the reduction of high-current charges and discharges. The SCs is added to supply or to absorb the load transient power and not the battery. Nonetheless, due to its high volume, weight and cost this system is still under study.

2.6 Conclusion

A fundamental study of different nowadays and future EVs supply sources, had been presented in this chapter. Nearly, all EVs available in the market today use the chemical batteries, the current two major battery technologies used in EV are nickel metal hydride (NiMH) and lithium ion (Li-ion), due to their potential of obtaining of higher specific energy and energy density. However, the driving range of the battery is still considered as the main obstacle and challenge of the EV battery development. The fuel cells have potentially higher energy density than batteries, the FCs and specially PEMFC are suitable for EV applications. But, due to its system complexity specially their weakness transient power, and high cost and weight, the FC technology is so expensive and that limits the FC vehicle marketable. Accordingly, the battery and FC may be used as main sources in VE, thanks to their higher specific energy and energy density but the low driving range of the battery and the weakest transient performance of FC are still considered as obstacles and challenge. The SC has an unusually high energy density, but its main disadvantage is its lower specific energy, which limits the uses of SC only in transient dynamic performance, so they can be used only as auxiliary sources. In hybrid source, the SCs have better performances than the battery, where the hybrid FC-SC source has advantages of FC plus the SCs advantages that eliminate the drawbacks of the FC transient dynamic performance and recovery quickly the regenerative braking energy.

Energy management of hybrid sources

3.1 Introduction

The academic and industrial researches are widely addressed on the control problem (DC link stabilization), due it is important in many power electronic applications, such as control methods for AC and DC machines applications [Mul13], control of renewable energy systems such as solar and wind energy systems [SFS⁺13]. Nowadays, it is considered as one of the most important research subject of the electric and hybrid vehicles in the industrial researches [TT13]. Currently, the classical regulators are used to solve this problem. They are based on a linearized model of the power converter and proportional-integral (PI) or proportional-integral-derivative (PID) feedback controllers.

In this chapter, we presented control strategy of a fuel cell stack using a non-isolated DC/DC converter. This control is ensured by hybrid dual loop control, which includes a voltage loops with a linear PI controllers and a fast current loops with a non-linear sliding controllers. This FC's control system has been validated on an experimental test bench at reduced power (120 W) at ESM laboratory. Also, a flatness-sliding mode controller has been developped for the energy management of an EV power-train. It includes a FC to supply the mean power to the load (primary source) and charge SC storage device (auxiliary power source). The auxiliary source role is to manage the load power peaks during the dynamic transient variations and to recover the energy through regenerative braking. Our contribution is based on a new combination of the sliding and flatness controllers to manage a hybrid FC/SCs DC link voltage of an EV or HEV applications. Basically,

its principle lies in the control of the FC and energies to their reference trajectories by using a flatness control. The sliding mode controller is used to ensure instantaneously the power sharing between the DC-bus inverters, it ensures that the the SC and FC currents track well their references, which are calculated from the SC and FC powers.

3.2 Fuel cell control

This section includes the control of a fuel cell stack using a non-isolated DC/DC converter. This last has been proposed and designed by R. SAADI [SBA⁺14]. It consists of two cascade stages. The first stage is an interleaved boost converter and the second is a floating-interleaved boost. The choice of each converter is based on the efficiency of the converter with high voltage ratio and small input current undulations (more details are given in [SBA⁺14]).

3.2.1 Modelling of the studied system

The studied converter structure is constituted by two cascaded converters in order to ensure a high voltage ratio and a small power source current undulation. This DC-DC converter structure is obtained by cascading Interleaved Boost and an Interleaved Double Dual Boost Converters (IBC and IDDBC) as it is shown in Fig. 3.1.

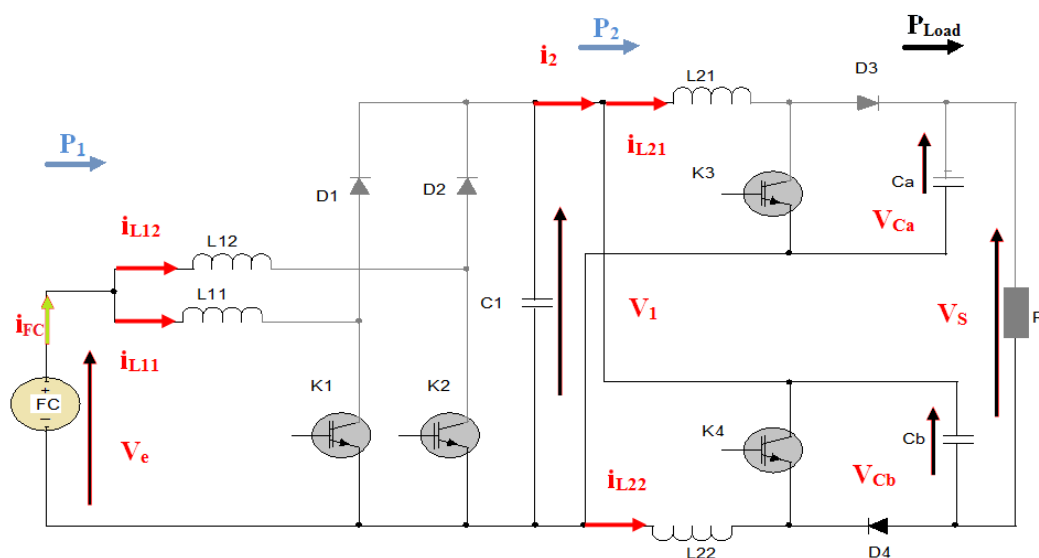


Figure 3.1: Circuit of the studied FC converter [SBA⁺14]

The following expressions that are presented in 3.1 and 3.7, define respectively the small-signal models of the IBC and IDDBC [SBA⁺14]:

$$\left\{ \begin{array}{l} \frac{d\tilde{i}_{L11}}{dt} = \frac{1}{L_{11}}[\tilde{V}_e - (1 - U_1)\tilde{V}_1 - v_1.\tilde{u}_1 - R_{L11}\tilde{i}_{L11}] \\ \frac{d\tilde{i}_{L21}}{dt} = \frac{1}{L_{12}}[\tilde{V}_e - (1 - U_2)\tilde{V}_1 - v_1.\tilde{u}_2 - R_{L12}\tilde{i}_{L12}] \\ \frac{d\tilde{V}_1}{dt} = \frac{1}{C_1}[(1 - U_1)\tilde{i}_{L11} + (1 - U_2)\tilde{i}_{L12} - \tilde{i}_2 + i_{L11}\tilde{u}_1 + i_{L12}\tilde{u}_2] \end{array} \right. \quad (3.1)$$

$$\left\{ \begin{array}{l} \frac{d\tilde{i}_{L21}}{dt} = \frac{1}{L_{21}}[\tilde{V}_1 - U_3\tilde{V}_{C_a} + v_{C_b}\tilde{u}_3 - R_{L21}\tilde{i}_{L21} - U_3R_{C_a}C_a\frac{d\tilde{V}_{C_a}}{dt}] \\ \frac{d\tilde{i}_{L22}}{dt} = \frac{1}{L_{21}}[\tilde{V}_1 - U_4\tilde{V}_{C_b} + v_{C_b}\tilde{u}_4 - R_{L21}\tilde{i}_{L21} - U_4R_{C_b}C_b\frac{d\tilde{V}_{C_b}}{dt}] \\ \frac{d\tilde{V}_{C_a}}{dt} = \frac{1}{C_a}[U_3\tilde{i}_{L21} + i_{L21}\tilde{u}_3 - i_{Load}] \\ \frac{d\tilde{V}_{C_b}}{dt} = \frac{1}{C_b}[U_4\tilde{i}_{L22} + i_{L22}\tilde{u}_4 - i_{Load}] \end{array} \right. \quad (3.2)$$

where $\tilde{V}_e, \tilde{V}_1, \tilde{V}_{C_a}, \tilde{V}_{C_b}$ and \tilde{u}_i are small perturbations around operating points of the FC, IBC and IDDBC respectively. The nominal operating point of the first stage sizing for: $i_{L_{1i}} = 33.33A$ and $V_1 = 150V$ is obtained for a voltage undulation of 1% and 5% of an input current undulation. The sizing values of the system parameters are give in Table 3.7 [SBA⁺14]:

The transfer functions in the open-loop after Laplace transformation of IBC converter were obtained from the average small-signal model:

$$H_{i_x} = \frac{\tilde{i}_{L_x}}{\tilde{u}} = \frac{2v_1}{R(1 - U_1)^2} \frac{1 + \frac{RC}{2}s}{1 + \frac{L_x}{R(1 - U_1)}s + \frac{L_x C}{(1 - U_1)^2}s^2} \quad (3.3)$$

$$G_{V_1} = \frac{\tilde{V}_1}{\tilde{i}_{L_x}} = \frac{R(1 - U_1)}{2} \frac{1 - \frac{L_x}{R(1 - U_1)^2}s}{1 + \frac{RC}{2}s} \quad (3.4)$$

Similarly, the transfer functions of IDDBC current and voltage are expressed in 3.5 and 3.6, respectively.

$$H_{i_{x2}} = \frac{\tilde{i}_{L_{3,4}}}{\tilde{u}} = \frac{(U_2 + 3)}{(1 - U_2)} \frac{(1 + \frac{RC}{U_2 + 3})s}{R(1 - U_2)^2 + L_x s + RL_x C s^2} \quad (3.5)$$

$$G_{V_s} = \frac{\tilde{V}_s}{\tilde{i}_{L_{3,4}}} = \frac{R(1 - U_2)V_s - \frac{(2rL_x)}{(1 + U_2)}s}{r(1 - U_2)^2 + L_x s + RL_x C s^2} \quad (3.6)$$

Then, the Open loop of the each phase of the IB and IDDB converters is presented in the following figure.

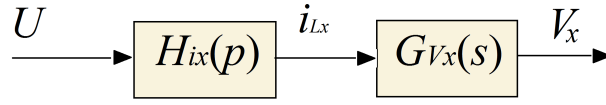


Figure 3.2: Open-loop of each converter stage.

3.2.2 Sliding mode based closed-loop control of the studied converter

Both stages of the proposed converter are controlled by dual closed-loop control that contains a linear PI regulator. Hence, the total reference currents (i_{xT}) is obtained using PI controller and then is shared out between to phases of the converter stage. For IBC , the total current is divided by 2 (number of phases of each stage) as it is shown in Fig. 3.3. Then, the sliding mode controllers are used to ensure that IBC and IDDB current track well their references. The block diagram of the closed-loop control of each IBC phase is shown in Fig. 3.3.

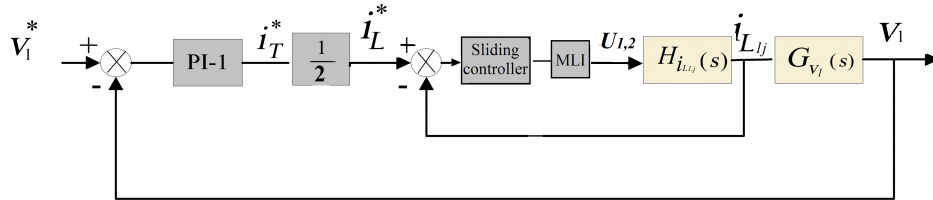


Figure 3.3: The closed-loop structure of the IBC phases.

The block diagram of the closed-loop control of each IDDBC phase is shown in Fig. 3.4.

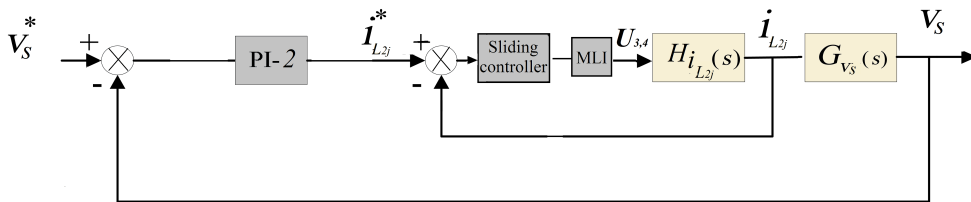


Figure 3.4: The closed-loop structure of the IDDBC phases.

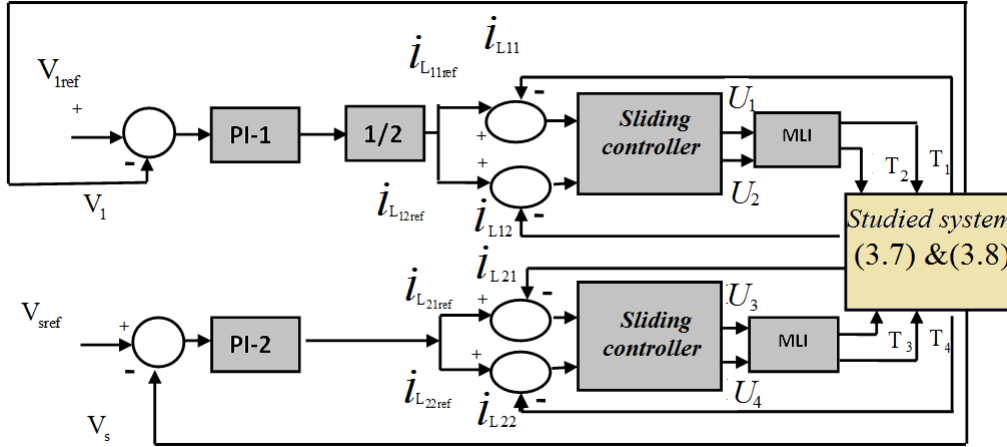


Figure 3.5: Control of system

The parameters of the regulators PI-1 and PI-2 (shown in Table. 3.7) are calculated using the graphical poles-placement of the transfer functions $G_{V_1}(s)$ and $G_{V_s}(s)$ under Matlab's SISO-Tool as it is shown in Fig 3.6.

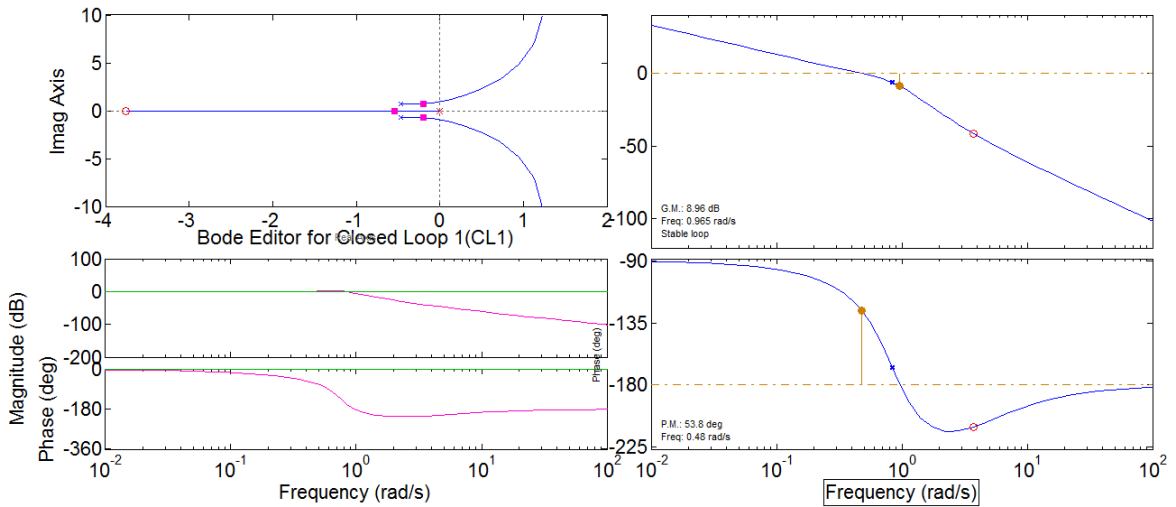


Figure 3.6: SISO design task

The following expressions present the average models of the IBC and IDDB, respectively [SBA⁺14]:

$$\left\{ \begin{array}{l} \frac{di_{L11}}{dt} = \frac{1}{L_{11}} [V_e - (1 - U_1) \cdot V_1 - R_{L11} i_{L11}] \\ \frac{di_{L12}}{dt} = \frac{1}{L_{12}} [V_e - (1 - U_2) \cdot V_1 - R_{L12} i_{L12}] \\ \frac{dV_1}{dt} = \frac{1}{C_1} [(1 - U_1) i_{L11} + (1 - U_2) i_{L12} - i_2] \end{array} \right. \quad (3.7)$$

$$\left\{ \begin{array}{l} \frac{di_{L21}}{dt} = \frac{1}{2L_{21}} [(U_3 + 1)V_e + (U_3 - 1)V_s - 2R_{L21} i_{L21}] \\ \frac{di_{L22}}{dt} = \frac{1}{2L_{22}} [(U_4 - 1)V_e + (U_4 - 1)V_s - 2R_{L22} i_{L22}] \\ \frac{dV_{C_a}}{dt} = \frac{1}{C_a} [(1 - U_3) i_{L21} - i_{Load}] \\ \frac{dV_{C_b}}{dt} = \frac{1}{C_b} [(1 - U_4) i_{L22} - i_{Load}] \end{array} \right. \quad (3.8)$$

The sliding surfaces of the IBC and the IDDB currents are defined by the following expressions:

$$\left\{ \begin{array}{l} S_{i_{L1i}} = (i_{L1i}^* - i_{L1i}) + K_{i_{L1i}} \int (i_{L1i}^* - i_{L1i}) dt \\ S_{i_{L2i}} = (i_{L2i}^* - i_{L2i}) + K_{i_{L2i}} \int (i_{L2i}^* - i_{L2i}) dt \end{array} \right. \quad (3.9)$$

In order to set the system dynamic, the reaching law has been defined as

$$\left\{ \dot{S} = -\lambda S \right. \quad (3.10)$$

We use the expression of $\frac{di_{L1j}}{dt}$ and $\frac{di_{L2j}}{dt}$ that are presented in 3.7 and 3.8, we find:

$$\left\{ \begin{array}{l} U_{1,2} = 1 - \frac{V_e - r_{1i} i_{L1i} + L_{1i} [\dot{i}_{L1i}^* - \lambda_1 S_{i_{L1i}} + K_{i_{L1i}} (i_{L1i}^* - i_{L1i})]}{V_1} \\ U_{3,4} = 1 - \frac{2(V_1 + r_{2i} i_{L2i} + L_{2i} [\dot{i}_{L2i}^* - \lambda_2 S_{i_{L2i}} + K_{i_{L2i}} (i_{L2i}^* - i_{L2i})])}{V_1 + V_s} \end{array} \right. \quad (3.11)$$

By deriving 3.9 then substituting \dot{S} by λS the expressions of the controlled currents become:

$$\left\{ \begin{array}{l} (\dot{i}_{L1i}^* - \dot{i}_{L1i}) + (\lambda_1 + K_{i_{L1i}})(i_{L1i}^* - i_{L1i}) + \lambda_1 K_{i_{L1i}} \int (i_{L1i}^* - i_{L1i}) dt = 0 \\ (\dot{i}_{L2i}^* - \dot{i}_{L2i}) + (\lambda_2 + K_{i_{L2i}})(i_{L2i}^* - i_{L2i}) + \lambda_2 K_{i_{L2i}} \int (i_{L2i}^* - i_{L2i}) dt = 0 \end{array} \right. \quad (3.12)$$

The parameters $K_{i_{L1i}}$, $K_{i_{L2i}}$, λ_1 and λ_2 are then determined by solving the following equations using the graphical poles-placement under Matlab's SISO-Tool.

$$\left\{ \begin{array}{l} \ddot{Z}_1 + (\lambda_1 + K_{i_{L1i}})\dot{Z}_1 + \lambda_1 K_{i_{L1i}} Z_1 = 0 \\ \ddot{Z}_2 + (\lambda_2 + K_{i_{L2i}})\dot{Z}_2 + \lambda_2 K_{i_{L2i}} Z_2 = 0 \end{array} \right. \quad (3.13)$$

where $Z_1 = i_{L1i}^* - i_{L1i}$, and $Z_2 = i_{L2i}^* - i_{L2i}$.

3.2.3 Stability

Consider the following Lyapunov function:

$$V = \frac{1}{2}(S_{i_{L_{1i}}} + S_{i_{L_{2i}}}) \quad (3.14)$$

where $S_{i_{L_{1i}}}$ and $S_{i_{L_{2i}}}$ are the sliding surface of currents $i_{L_{1i}}$ and $i_{L_{2i}}$, respectively.

Then the derivatives of the functions V along the trajectory is:

$$\dot{V} = -(\lambda_1 S_{i_{L_{1i}}} \dot{S}_{i_{L_{1i}}} + \lambda_2 S_{i_{L_{2i}}} \dot{S}_{i_{L_{2i}}}) = -(\lambda_1 S_{i_{L_{1i}}}^2 + \lambda_2 S_{i_{L_{2i}}}^2) < 0 \quad (3.15)$$

with $\lambda_2 > 0$ and $\lambda_1 > 0$.

Hence, the origin with the sliding surfaces given in (??), the system is stable since the Lyapunov function (3.14) is radially unbounded and its derivative is strictly negative when $S \neq 0$ and $V = 0 \iff S = 0$ [LSL61].

3.2.4 Simulation results

The whole FC pack and the used converter had been simulated under the Matlab-Simulink Software, Table. 3.7 shows the parameters associated to the system.

The Fig. 3.8 and 3.9 show the behaviour of the output voltages during a positive step load change. It changes from 57 ohm to 67 ohm as it is shown in Fig. 3.7. It is clear that the IBC voltage tracks well its reference and it proves that the sliding mode controller of the both converter stages show an excellent dynamic performance during the load cycle with acceptable overshoots because of the load's changes.

The following results shown in Fig. 3.10 and 3.11 show the behaviour of the IBC and IDBBC's currents (second order dynamics with $D\% < 10\%$). They arrived quickly at their references, which are given by PI regulators. Consequently, the sliding mode control gives an excellent tracking and short response time with a low overshoot.

Table 3.1: Parameters of the FC-converter system.

Parameter	Value
FC rated power, P_{Fc}	5[Kw]
FC rated voltage, V_{FC}	42[V]
FC rated current, I_{FC}	120[A]
Output voltage V_1	150[V]
Output voltage V_s	540[V]
Switching frequency F_s	10[kHz]
Output currents of stage 1 and 2	33.33 and 9.25[A]
Cyclical ratio of stage 1 and 2(U_1 and U_2)	0,72 and 0.56
Effective currents of (K_1, K_2) and (K_3, K_4)	50.93 and 15.99[A]
Effective currents (D_1, D_2) and (D_3, D_4)	31.76 and 14.17[A]
Effective currents of C_1 and (C_a, C_b)	27.78 and 19.0[A]
Capacitance values C_1 and C_a ($C_a = C_b$)	488 and 189.83[uF]
Maximum current of ($L_{11} = L_{12}$) and ($L_{21} = L_{22}$)	65 and 35 [A]
Inductance values ($L_{11} = L_{12}$) and ($L_{21} = L_{22}$)	308 and 1.62 [mH]
Internal resistances ($R_{L11} = R_{L12}$) and ($R_{L21} = R_{L22}$)	0.071and0.18[Ω]
PI-1's parameters	$K_{p1} = 60$ and $K_{i1} = 0.5$
PI-2's parameters	$K_{p2} = 200$ and $K_{i2} = 0.7$

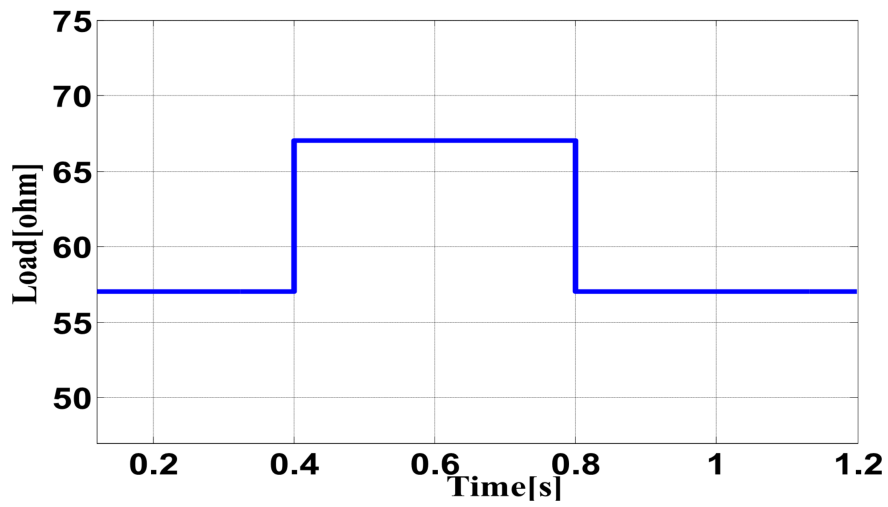


Figure 3.7: Load cycle.

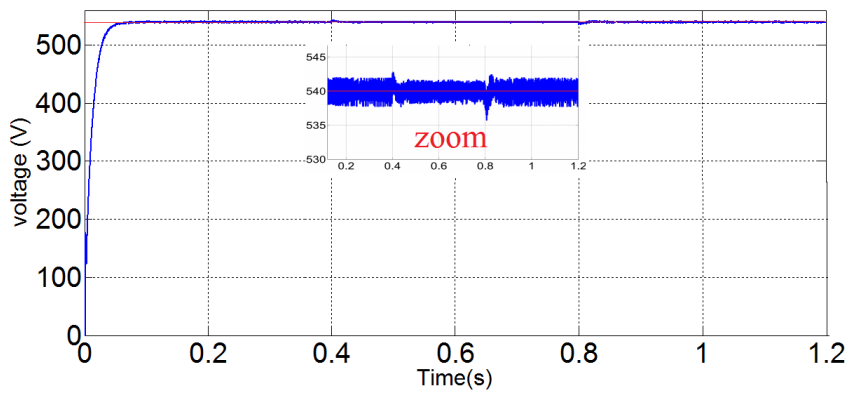


Figure 3.8: IDDBC Output voltage V_s .

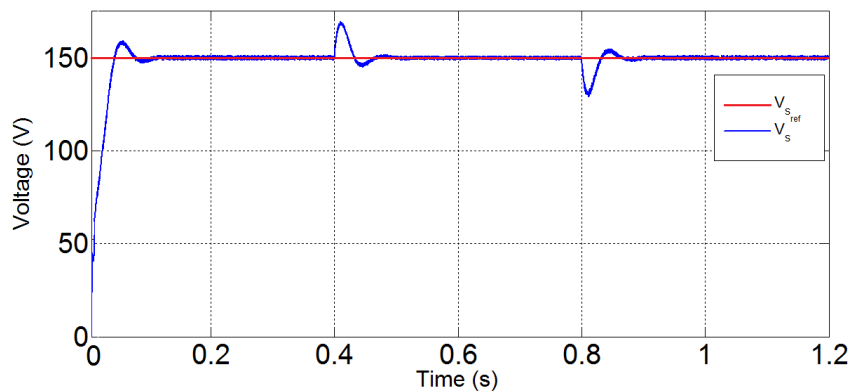


Figure 3.9: IBC output voltage V_1 .

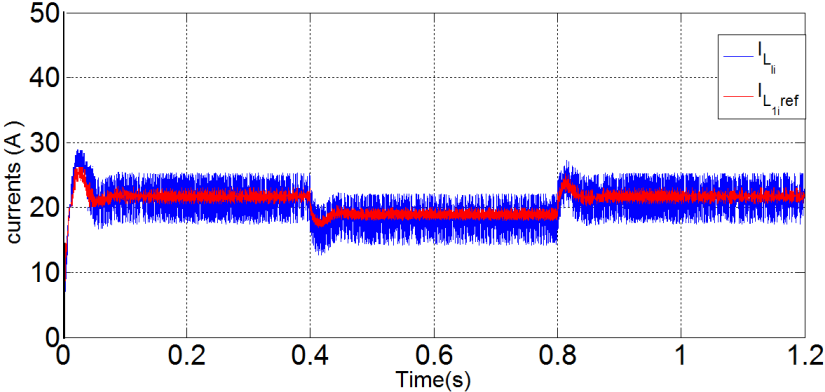


Figure 3.10: Inductors current of IDDBC stage and its reference.

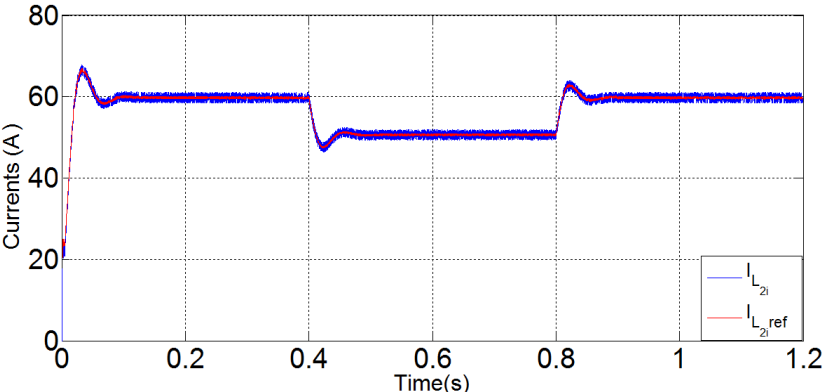


Figure 3.11: Inductors current of IBC stage and its reference.

3.2.5 Experimental results

In order to validate the proposed command combination of PI closed-loop and the sliding mode control. A prototype experimental test bench of the studied converter has been released by S. Ramzi at MSE laboratory and. This test bench shown in 3.12 was carried out on an experimental bench at reduced power (120 watts) of equipment available at our Laboratory of Energy System Modelling (LESM). The maximum output voltage of the programmable source is adjusted to 50 V, which corresponds to 60 A current. The IBC reference voltage (V_1) equals 45V and the output voltage V_s equals 150V. The load is a variable resistive (it changes from 150 Ω to 450 Ω). The FC's cascade boost is controlled by means of a real time card dSpace DS1104. Measurements are performed by means of current and voltage sensors associated with a carte driver SKHI 22. To investigate the

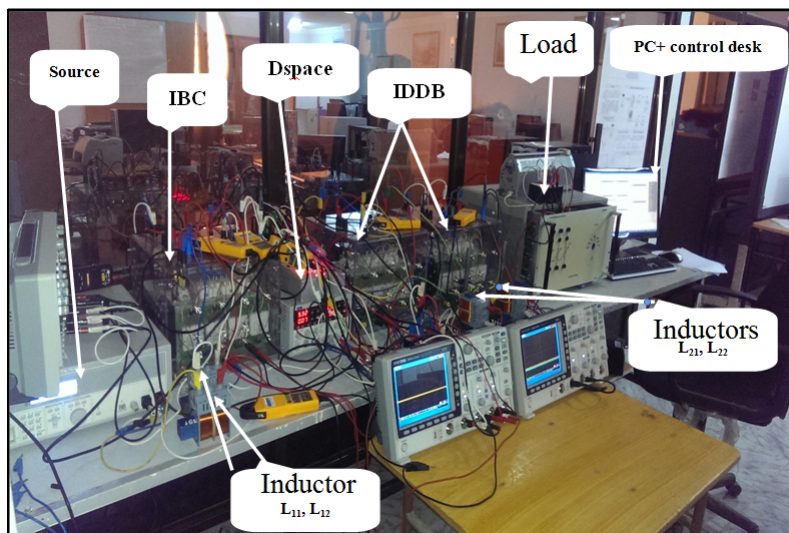


Figure 3.12: Experimental setup of the studied converter.

studied system behaviour in different operating modes, a variable pulse current load is imposed on the system with the current profile shown in Fig. 3.13 (a). As the converter connected to the load is controlled such that the system output voltages are 150 V for IDDBC and 45 V for IBC. The experimental results shown in Fig. 3.13 (b) show the controlled voltages V_s and V_1 track well their references under a very small steady state error (less than 5%).

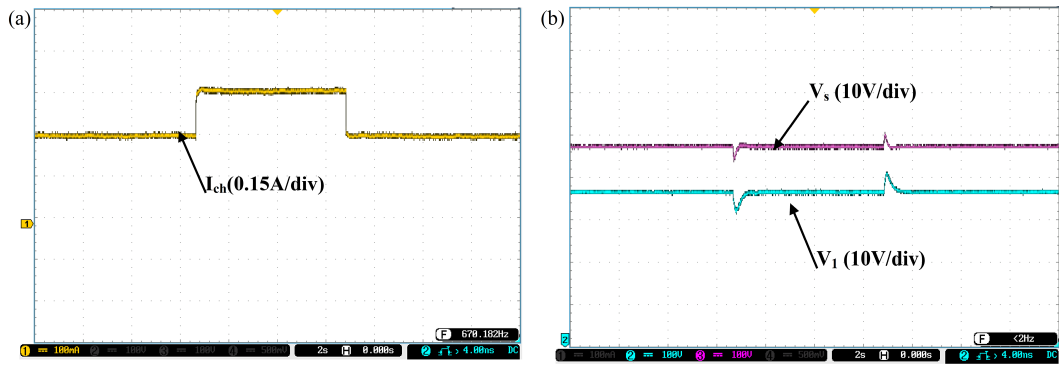


Figure 3.13: Experimental results of the closed-loop control law: (a) load current cycle; (b) IBC and IDDBC voltages.

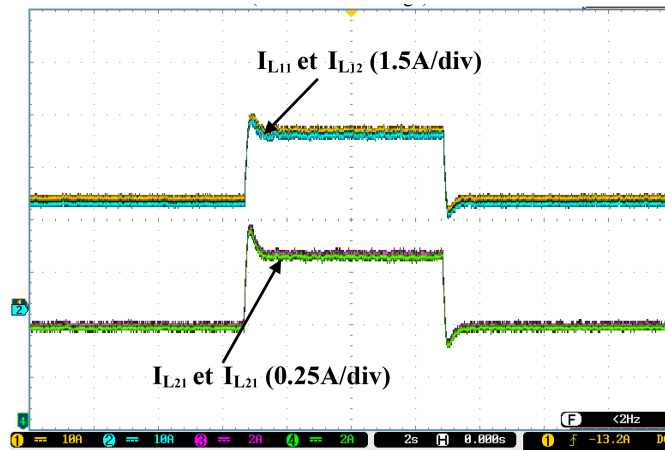


Figure 3.14: Experimental results: IBC and IDDBC currents.

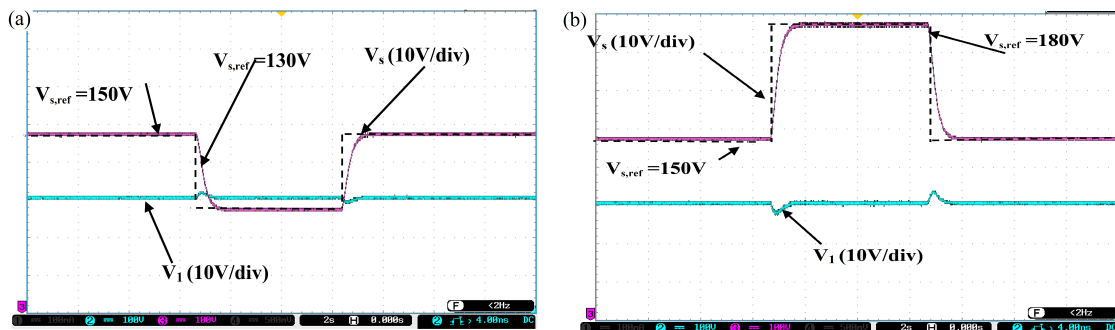


Figure 3.15: The IBC and IDDBC's voltages while the V_s 's (a) increasing and (b) decreasing.

The Fig. 3.14 presents the behaviour of currents $I_{L_{1i}}$ and $I_{L_{2i}}$, and for transient responses obtained while the load current changing. The test is performed by sharply changing the load current I_L . The IBC and IDBBC's currents have a second order dynamics behaviour with acceptable overshoot. Furthermore, the good tracking of the IBC and IDBBC's currents to their references shows that the used sliding mode regulators work favourably

The figures 3.15 present the experimental results of the voltages V_1 and V_s that are obtained during the a positive and negative variations of the output voltage V_s . The control system works very well and the voltage of each converter stage tracks its reference with the desired behaviour in spite of the voltage V_s changes.

3.3 Hybridization of energy storages

The hybridization of sources is to combine two or more energy sources devices together so that the advantages of each one can be brought out and the disadvantages can be compensated by others. For instance, the hybridization of a chemical FC or battery with an SCs can overcome such problems as low specific power of electrochemical batteries (or FC) and low specific energy of SCs, therefore achieving high specific energy and high specific power.

Basically in literatures, the hybridized energy sources consists of two basic energy sources: one with high specific energy (FC or battery) and the other with high specific power (SCs). The basic operation modes of this system are shown in Fig 3.16 [EGE09]:

- In Fig. 3.16(a): in high power demand operations, such as acceleration and hill climbing of the EV, where the steady-state load power is greater than the main source's limited maximum power, in this mode the both basic energy storages deliver their powers to the load.
- In Fig.3.16(b): in low power demand operation, such as constant speed cruising operations, the high specific energy storage will deliver its power to the load and charge the high specific power storage to recover its charge lost during high power demand operation.
- In Fig. 3.16(c): in regenerative braking operations, the peak power will be absorbed by the high specific power storage (case of battery as a primary source), and only a limited part is absorbed by the high specific energy storage.

By this way, the whole system would be much smaller in weight and size than if any one of them alone [EGE09].

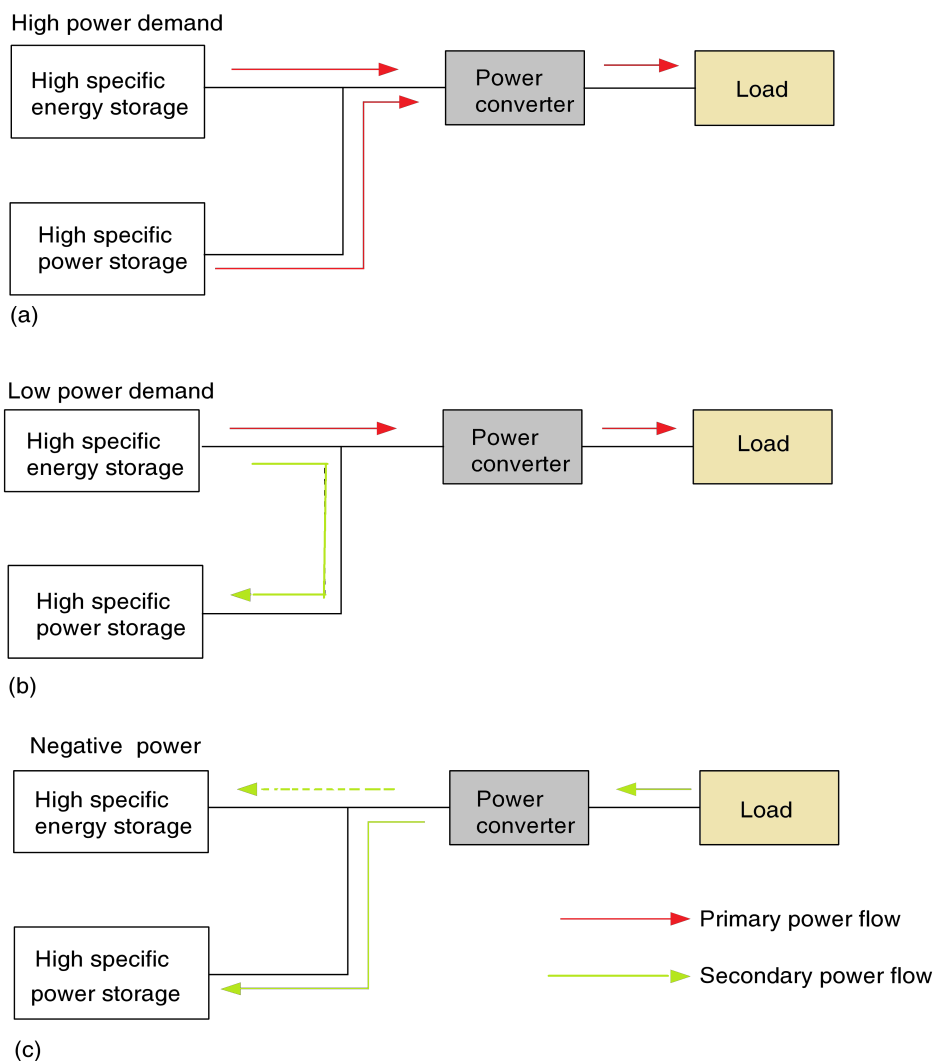


Figure 3.16: Concept of hybrid energy storage operation modes.

3.4 Modelling of studied FC-SC hybrid source

As recommended in literature [ZWZ12], [TS07], one must operate an FC with slow dynamics in order to prevent the fuel starvation phenomenon and thus improve its stack lifetime. The slow dynamics of an FC can be compensated by faster dynamics from storage devices. In contrast to batteries, SCs have lower energy density but higher power density and provide very fast current charge/discharge cycles because of their low equivalent series resistance. SC can provide more cycles than batteries and are well suited to very high

dynamic cycles.

The Fig. 3.17 shows the studied architecture of a FC-SC hybrid source in an EV power train system. It is a hybrid system composed of a FC and SCs as the main and auxiliary sources, respectively. We used the nonlinear Larminie and Dicks static model that was presented in second chapter in (2.12) and the studied SC model expressed in (2.5).

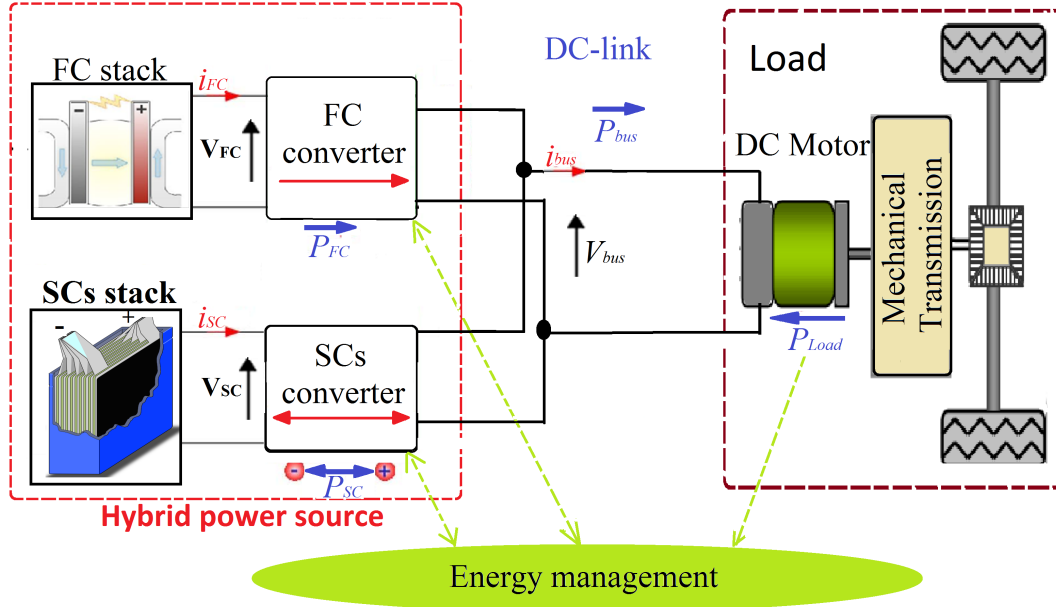


Figure 3.17: Studied structure of the FC-SCs hybrid power source of an EV,

3.4.1 Modelling of the FC-SCs DC bus voltage

Fuel cell operates by giving direct current at a low voltage; thereby, the two-phase IBC converter, presented in Fig. 3.18, is selected to adapt the low voltage delivered by the FC. The IBC is employed to reduce the input current undulation. Interleaving adds additional benefits such as reduced undulation current in both input and output circuits [SBK⁺13], [MKB⁺14]. Here, the FC's voltage (V_{FC}) is given by a nonlinear Larminie and Dicks static model as shown in 3.16.

$$V_{FC} = E_0 - A \log \left(\frac{i_{FC} - i_n}{i_0} \right) - \left[R_m (i_{FC} - i_n) + B \log \left(1 - \frac{i_{FC} - i_n}{i_{lim}} \right) \right] \quad (3.16)$$

The following state space model of studied hybrid source is an overall dynamical model

based on differential equations. It is used to describe the studied hybrid DC link.

$$\left\{ \begin{array}{l} \frac{di_{FC}}{dt} = \frac{1}{L_{FC}}[(1 - U_{FC})V_{bus} + V_{FC}] \\ \frac{dV_{bus}}{dt} = \frac{1}{C_{bus}}[(1 - U_{FC})V_{FC} + (1 - U_{SC})i_{SC} + i_{bus}] \\ \frac{dV_{SC}}{dt} = \frac{1}{C_{SC}}i_{SC} \\ \frac{di_{SC}}{dt} = \frac{1}{L_{SC}}[-(1 - U_{SC})V_{bus} + V_{SC}] \\ \frac{di_{bus}}{dt} = \frac{1}{L_L}[V_{bus} - R_L i_{bus} - E_L] \end{array} \right. \quad (3.17)$$

with

- U_{FC} and U_{SC} : are the control signals of the FC and SC converters, respectively;
- V_{FC} and i_{FC} : are the voltage and current of the FC, respectively;
- V_{SC} and i_{SC} : are the voltage and current of the SC, respectively;
- V_{bus} and i_{bus} : are the voltage and current of the DC bus, respectively.

The Table. 3.2 shows the parameters of studied hybrid source.

3.5 Flatness-sliding mode control of the DC-bus energies

The energy management of hybrid power sources using a flatness or a sliding mode controls has been already studied recently, for example, Phatiphat [TTD14], Sikkabu [SFP+13], who worked on an unregulated voltage FC-battery and SC hybrid sources by developing a flatness based energy management controller, by Ayad et al. [ABH11], who studied the control of an DC link voltage battery/SC hybrid sources based sliding mode strategy.

In this thesis, a new combination of the sliding and flatness controllers is proposed, the flatness strategy is used to determine the desired reference of the FC and SC powers (P_{FC} and P_{SC}) by applying the law given in (3.34), it is possible to determine the desired reference values of FC and SC currents using (3.41). Then, sliding mode controllers are used to ensure instantaneous share of power between the inverters, and a good energy management of the power delivered in the hybrid FC/SCs DC link.

3.5.1 Differential flatness principle

The concept of flatness was first defined by Fliess et al. [Jar12] using the formalism of differential algebra, where a system is viewed as a differential field generated by a set of variables (states and inputs). Consider the system:

$$\begin{cases} \dot{x} = f(x, u) \\ x = [x_1, x_2, \dots, x_n]^T; \quad x \in \mathbb{R}^n \\ u = [u_1, u_2, \dots, u_m]^T; \quad u \in \mathbb{R}^m \\ y = [y_1, y_2, \dots, y_m]^T; \quad y \in \mathbb{R}^m \end{cases} \quad (3.18)$$

Where x is the state variables, u is the vector of input (control) variables, and $(n, m) \in \mathbb{N}^2$. We say the system given in 3.18 is flat if we can find a set of outputs such that all states and inputs can be determined from these outputs without integration. More precisely, if the system is flat if we can find outputs y of the form [SBK+13], [PPMTD11]:

$$y = \phi(x, u, \dot{u}, \dots, u^\alpha) \quad (3.19)$$

Such that

$$\begin{cases} x = \varphi(y, \dot{y}, \dots, y^{(\kappa)}) \\ u = \nabla(y, \dot{y}, \dots, y^{(\kappa+1)}) \end{cases} \quad (3.20)$$

where α and κ are finite numbers of derivatives.

If the output variables of interest (y) can be proven to be flat outputs, reference control design y_{ref} becomes straightforward. The dynamics of the resulting linear error dynamics can be specified (control law) [SBK+13], [TTD14], must be regulated.

$$(y^{(\kappa+1)} - y_{ref}^{(\kappa+1)}) + \beta_\kappa(y^{(\kappa)} - y_{ref}^{(\kappa)}) + \dots + \beta_0(y - y_{ref}) = 0 \quad (3.21)$$

where $\beta_\kappa, \dots, \beta_0$ are the set of controller parameters. Then, there is no differential equation of the form:

$$\zeta(y, \dot{y}, \dots, y^{(\kappa+1)}) = 0 \quad (3.22)$$

The flat outputs y and their derivatives provide an alternate representation of the system dynamics such that if the flat output profiles are known as a function of time, then one can obtain the profiles of all the system states and the corresponding the state and inputs (control) variables (u and x). Clearly, an advantage of the differential flatness approach is that the trajectories of the system, i.e. (x, u) , are calculated in a straightforward

manner by the trajectories of y and their derivatives without integrating any differential equations [TTD14].

3.5.2 Flatness control of FC-SC hybrid source

Regarding the values of the inductances and capacitors and the corresponding currents and voltages, the energies stored in the inductors are very much less than that in the capacitors. Therefore, only the electrostatic energies given by (3.23) are stored in C_{SC} and C_{bus} , they are represented by y_T and y_{bus} , respectively.

$$\begin{cases} y_T = \frac{1}{2}C_{SC}V_{SC}^2 + \frac{1}{2}C_{bus}V_{bus}^2 \\ y_{bus} = \frac{1}{2}C_{bus}V_{bus}^2 \end{cases} \quad (3.23)$$

The equation (3.24) presents the DC-bus capacitive energy variation \dot{y}_{bus} in terms of P_{FC_0} , P_{SC_0} and P_{Load} (load's power) [SBK+13].

$$\dot{y}_{bus} = P_{FC_0} + P_{SC_0} - P_{Load} \quad (3.24)$$

where P_{FC_0} and P_{SC_0} are the output powers of FC and SC converters, respectively. The FC and SC powers are given by the following expressions:

$$\begin{cases} P_{FC} = P_{FC_0} + r_{FC} \left(\frac{P_{FC}}{V_{FC}} \right)^2 \\ P_{SC} = P_{SC_0} + r_{SC} \left(\frac{P_{SC}}{V_{SC}} \right)^2 \\ P_{Load} = V_{bus} \cdot i_{Load} \end{cases} \quad (3.25)$$

In the system (3.41), the electrostatic energy y_{bus} and y_T stored in DC-link are assumed to be the flat output components. We consider the system:

$$\begin{cases} y = [y_{Bus}, y_T]^T \\ u = [P_{FC}, P_{SC}]^T \\ x = [V_{Bus}, V_{SC}]^T \end{cases} \quad (3.26)$$

From (3.23), the V_{bus} can be written as:

$$V_{bus} = \sqrt{\frac{2y_{bus}}{C_{bus}}} V_{SC} = \sqrt{\frac{2(y_T - y_{bus})}{C_{SC}}} \quad (3.27)$$

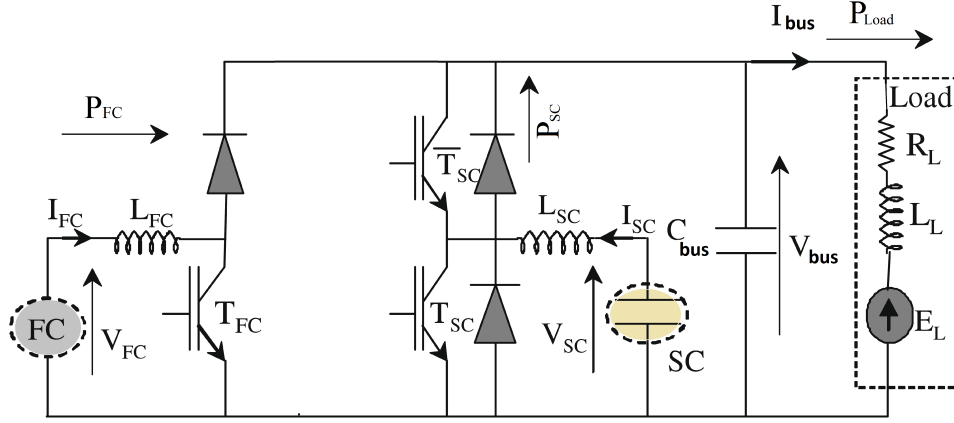


Figure 3.18: The studied hybrid power source

Substituting the voltages V_{bus} by its expression given in (3.27), the load powers is written as:

$$\left\{ \begin{array}{l} P_{Load} = V_{bus} \cdot i_{Load} = \sqrt{\frac{2y_{bus}}{C_{bus}}} i_{bus} \end{array} \right. \quad (3.28)$$

From (3.27), the state variables x_1 and x_2 can be written as:

$$\left\{ \begin{array}{l} x_1 = \sqrt{\frac{2y_{Bus}}{C_{bus}}} = \varphi_1(y_{bus}) \\ x_2 = \sqrt{\frac{2(y_T - y_{bus})}{C_{SC}}} = \varphi_2(y_T, y_{bus}) \end{array} \right. \quad (3.29)$$

The study given in [?] proved that the powers P_{FC} and P_{SC} of the boost and buck boost converters can be written by (2.C) by using (3.24) and 3.28).

$$\left\{ \begin{array}{l} P_{FC} = 2P_{FC_{max}} \left(1 - \sqrt{1 - \frac{\dot{y}_T + P_{Load}}{P_{FC_{max}}}} \right) \\ P_{SC} = 2P_{SC_{max}} \left(1 - \sqrt{1 - \frac{\dot{y}_{bus} + P_{load} - P_{FC_0}}{P_{SC_{max}}}} \right) \end{array} \right. \quad (3.30)$$

Then, after substituting the load's power P_{Load} by its expression given in (3.28), the control variables u_1 and u_2 can be expressed in terms of the flat outputs y_{bus} and y_T and their time derivatives as:

$$\left\{ \begin{array}{l} u_1 = P_{FC} = 2P_{FC_{max}} \left(1 - \sqrt{1 - \frac{\dot{y}_T + \sqrt{\frac{2y_{bus}}{C_{bus}}} i_{bus}}{P_{FC_{max}}}} \right) = \nabla_1(y_{bus}, \dot{y}_T) \\ u_2 = P_{SC} = 2P_{SC_{max}} \left(1 - \sqrt{1 - \frac{\dot{y}_{bus} + \sqrt{\frac{2y_{bus}}{C_{bus}}} i_{bus} - P_{FC_0}}{P_{SC_{max}}}} \right) = \nabla_2(y_{bus}, \dot{y}_{bus},) \end{array} \right. \quad (3.31)$$

where $P_{FC_{max}}$ and $P_{SC_{max}}$ are the limited maximum powers from the FC and SC. They are given by:

$$\begin{cases} P_{FC_{max}} = \frac{V_{FC}^2}{4r_1} \\ P_{SC_{max}} = \frac{V_{SC}^2}{4r_2} \end{cases} \quad (3.32)$$

Finally, it is apparent that $x_1 = \varphi_1(y_{bus})$, $x_2 = \varphi_2(y_T, y_{bus})$, $u_1 = \nabla_1(y_{bus}, \dot{y}_T)$ and $u_2 = \nabla_2(y_{bus}, \dot{y}_{bus})$ correspond to (3.20). Consequently, the proposed mathematical model for the FC-SCs hybrid source is a flat system.

3.5.3 Trajectory planning

one of the major advantage of the flat system is the possibility of planning the flat output trajectories, which allows determining the trajectories of the other components. Clearly, this advantage of the differential flatness approach is that the trajectories of the system $(x;u)$, are calculated in a straightforward manner by the trajectories of y given by (3.33) and their derivatives without integrating any differential equations.

$$\begin{cases} y_{bus_{ref}} = \frac{1}{2}C_{bus}V_{bus_{ref}}^2 \\ y_{T_{ref}} = \frac{1}{2}C_{SC}V_{SC_{ref}}^2 + y_{bus_{ref}} \end{cases} \quad (3.33)$$

A linearizing feedback control law achieving an exponential asymptotic tracking of the desired references of the DC-bus energies is given by the following expression:

$$\begin{cases} (\dot{y}_{bus} - \dot{y}_{bus_{ref}}) + K_{11}(y_{bus} - y_{bus_{ref}}) + K_{12} \int_0^t (y_{bus} - y_{bus_{ref}})dt = 0 \\ (\dot{y}_T - \dot{y}_{T_{ref}}) + K_{21}(y_T - y_{T_{ref}}) + K_{22} \int_0^t (y_T - y_{T_{ref}})dt = 0 \end{cases} \quad (3.34)$$

where the set of controller parameters K_{i1} and K_{i2} ($i = 1, 2$) are chosen such that the poles of the closed loop characteristic polynomial, in the complex variables are the roots of the following equation [SBK⁺13]:

$$P(s) = s^2 + K_{i1}s + K_{i2} \quad (3.35)$$

where $P(s)$ is a Hurwitz polynomial. Obviously, the tracking error e_1 between a y_{bus} and $y_{bus_{ref}}$ (or e_2 between a y_{SC} and $y_{SC_{ref}}$), satisfies

$$\begin{cases} \ddot{e}_1 + K_{11}\dot{e}_1 + K_{12}e_1 = 0 \\ \ddot{e}_2 + K_{21}\dot{e}_2 + K_{22}e_2 = 0 \end{cases} \quad (3.36)$$

The choice of the designed controller parameters is done by matching the polynomial $P(s)$, to a desired characteristic polynomial, with pre-specified root locations. It may be set as a desired characteristic polynomial:

$$\begin{cases} P(s) = s^2 + 2\xi_i\omega_{in}s + \omega_{in}^2 & i = 1, 2 \\ K_{i1} = 2\xi_i\omega_{in} \\ K_{i2} = \omega_{in}^2 \end{cases} \quad (3.37)$$

where ξ and ω_n are the desired dominant damping ratio and natural frequency.

Finally, by virtue of the system being flat, we can write the trajectories of u satisfying the differential equation in terms of the flat output and its derivatives:

$$\begin{cases} P_{FCref} = 2P_{FCmax} \left(1 - \sqrt{1 - \frac{\dot{y}_{Tref} - K_{21}e_2 - K_{22} \int_0^t e_2 dt + P_{Load}}{P_{FCmax}}} \right) \\ P_{SCref} = 2P_{SCmax} \left(1 - \sqrt{1 - \frac{\dot{y}_{busref} - K_{11}e_1 - K_{12} \int_0^t e_1 dt + P_{load} - P_{FC0}}{P_{SCmax}}} \right) \end{cases} \quad (3.38)$$

The output signals of flatness controllers will be the input targets of the sliding mode controllers in the next control step as it is shown in Fig. 3.19.

3.6 Sliding Mode controller

The sliding mode controller is used to ensure, instantaneously, the power sharing between the DC-link inverters, they ensure that the sliding surface equals zero by tracking the SC and FC currents to their references calculated from the estimated energies. However, because of the fast response requested in the transient power and the possibility of working with a constant or variable frequency, a sliding mode control has been chosen for the DC-DC SC and FC converters. The bidirectional property of the SC converter allows the management of charge-discharge cycles of the SC tank [ABH11].

The FC and SC current references (i_{FCref}, i_{SCref}) are calculated by means of a flatness loop control.

$$\begin{cases} i_{FCref} = \frac{P_{FCref}}{V_{FC}} \\ i_{SCref} = \frac{P_{SCref}}{V_{SC}} \end{cases} \quad (3.39)$$

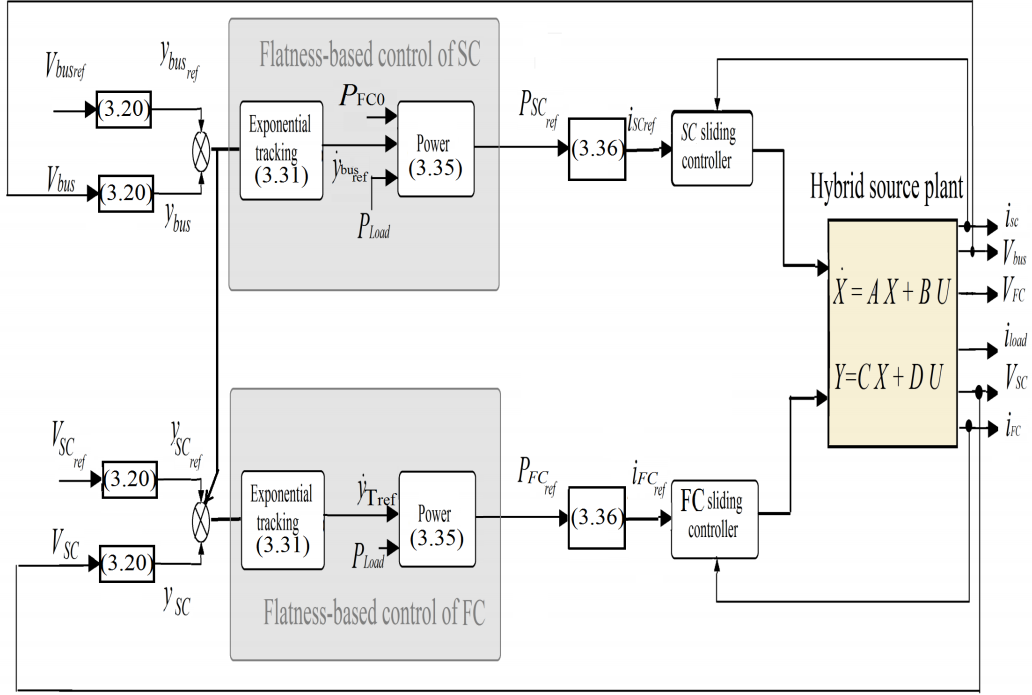


Figure 3.19: Structure of flatness and sliding mode based control of a FC-SCs DC bus.

where $P_{FC_{ref}}$ and $P_{SC_{ref}}$ are generated from the regulated flat outputs y_{bus} and y_{SC} as shown in (3.31). The proposed sliding surface is defined as:

$$\begin{cases} S_{FC} = (i_{FC_{ref}} - i_{FC}) + K_{FC} \int i_{FC_{ref}} - i_{FC} dt \\ S_{SC} = (i_{SC_{ref}} - i_{SC}) + K_{SC} \int i_{SC_{ref}} - i_{SC} dt \end{cases} \quad (3.40)$$

In order to set the system dynamic, the reaching law has been defined as

$$\begin{cases} \dot{S} = -\lambda S \end{cases} \quad (3.41)$$

It is possible to determine the continuous equivalent control, which allows to maintain the state trajectories of FC and SC currents on the sliding surface. From (3.17), we find:

$$\begin{cases} U_{FC} = 1 + \frac{V_{FC} - L_{FC}[\dot{i}_{FC_{ref}} - \lambda_1 S_{FC} + K_{FC}(i_{FC_{ref}} - i_{FC})]}{V_{bus}} \\ U_{SC} = 1 - \frac{V_{SC} - L_{SC}[\dot{i}_{SC_{ref}} - \lambda_2 S_{SC} + K_{SC}(i_{SC_{ref}} - i_{SC})]}{V_{bus}} \end{cases} \quad (3.42)$$

The parameters K_{FC} , K_{SC} , λ_1 and λ_2 are then determined by solving the following equations:

$$\begin{cases} \ddot{Z}_1 + (\lambda_1 + K_{FC})\dot{Z}_1 + \lambda_1 K_{FC} Z_1 = 0 \\ \ddot{Z}_2 + (\lambda_2 + K_{SC})\dot{Z}_2 + \lambda_2 K_{SC} Z_2 = 0 \end{cases} \quad (3.43)$$

where $Z_1 = (i_{FC_{ref}} - i_{FC})$, and $Z_2 = (i_{SC_{ref}} - i_{SC})$.

3.6.1 Stability of the flatness control system

The control system stability depends on the roots values of the characteristic polynomial. According to Routh-Hurwitz criterion law for second order polynomial, "all the roots are in the left half plane and the system with characteristic equation $P(s)$ is stable, if all the coefficients satisfy [Gop08] K_{i1} and $K_{i2} > 0$, (ξ_i and $\omega_{in} > 0$). Once the flat outputs are stabilized, the whole system is stable because all the variables of the system are expressed in terms of the flat outputs y_{bus} and y_{SC} [TTD14].

3.7 Simulation results

In order to validate the proposed control strategy of the hybrid source, The maximum output power main source is adjusted to 300 W. The following simulation study demonstrates the power enhancement capability of a controlled hybrid system using the proposed controller. The SC initial voltage is set to 15 V and its maximum power is limited to [-800 800] W. To investigate the system behaviour in different operating modes, a variable pulse load power is imposed on the system with the load power cycle shown in Fig. 3.22. As the DC-DC converter connected to the load is controlled such that the system output voltage V_{bus} is 42 V. The parameters of the system are given in Table I.

- Control the voltage V_{bus} to its reference (42[V]);
Manage the distribution of energy between the FC and SC;
- Set the SC's charging mode as a propriety of the FC;

As Fig. 3.20 and 3.21 show, the proposed control strategy guaranties the output voltage (V_{bus}) and DC-bus energy (y_{bus}) in their constant desired values in the different operating modes even at the moment of the load variation. During periods of high power demand (discharge mode), the fuel cell is controlled to generate its rated power and the SC is discharged to satisfy the extra power requirements that exceed the fuel cell capability. Moreover, the dynamics of $y_{bus_{ref}}$ is controlled according to the fuel cell characteristic as it is presented in fig 3.34.

Table 3.2: Parameters of the FC-SC hybrid source.

Parameter	Value
$V_{bus_{ref}}$	42 [V]
E the reversible no loss voltage of the fuel cell	27.1[V] at $T = 55^{\circ}C$, 23 cells
i_o the exchange current	6.54e-3[A]
Rm the membrane and contact resistances	0.08[Ω]
A the slope of the Tafel line	1.35[V]
B the constant in the mass transfer	1.19[V]
i_{Lim} the limiting current	100[A]
i_n the internal current	0.23[A]
L_{FC} boost's inductance	3000e-6[H]
L_{bus}	10e - 6H
C_{bus} the total capacitance at DC bus	32e - 6[F]
C_{SC} the total capacitance of supercapacitor module	175 [F]
L_{SC} buck-boost's inductance	100e-6 [H]
r_{FC} the internal resistance of the inductance L_{FC}	0.1[Ω]
r_{SC} the internal resistance of the inductance L_{FC}	0.05[Ω]

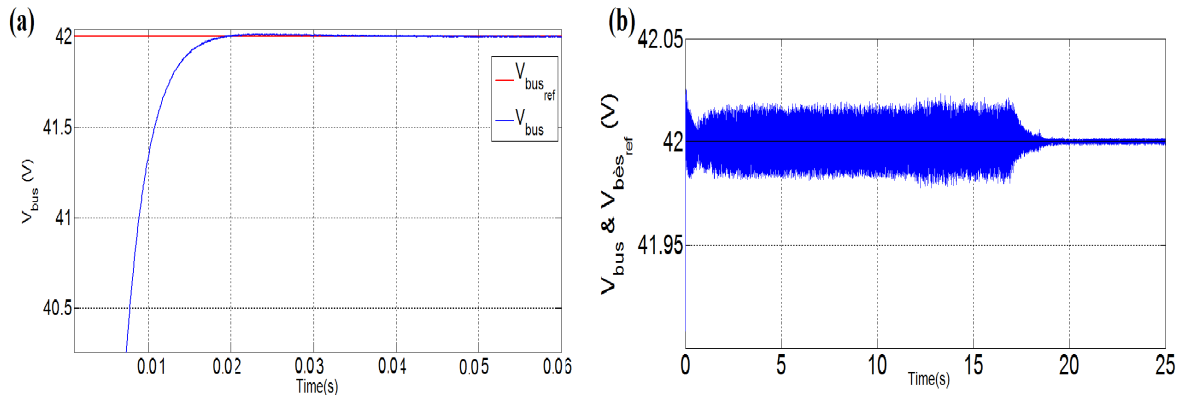


Figure 3.20: The DC link voltage (a) transient behaviour;(b) steady behaviour.

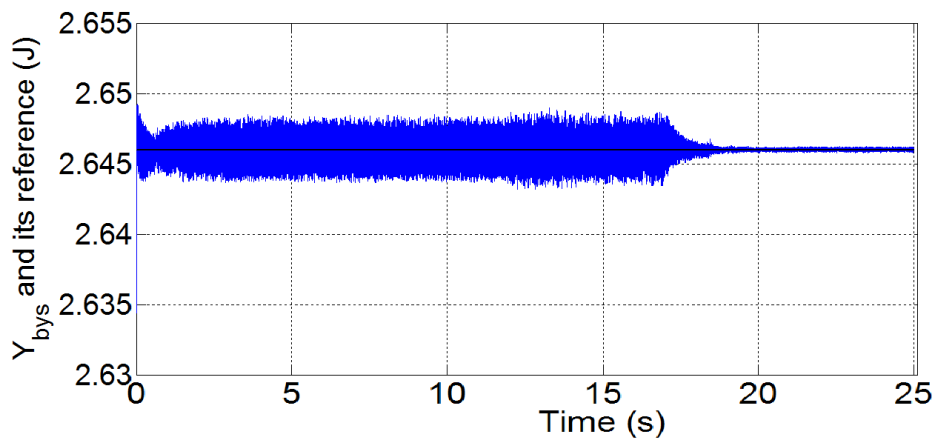


Figure 3.21: Energy of DC link voltage and its reference

Therefore, the SC supplies load at the moment of the load transient variation because of its fast dynamic. Furthermore, the Fig. 3.24 and 3.26 show the good tracking of the FC and SC currents to their references, it demonstrates that the used sliding regulators work favourably.

The Fig. 3.29 and 3.30 show the voltage and current of the auxiliary storage source (SC) during the discharging and charging mode , respectively.

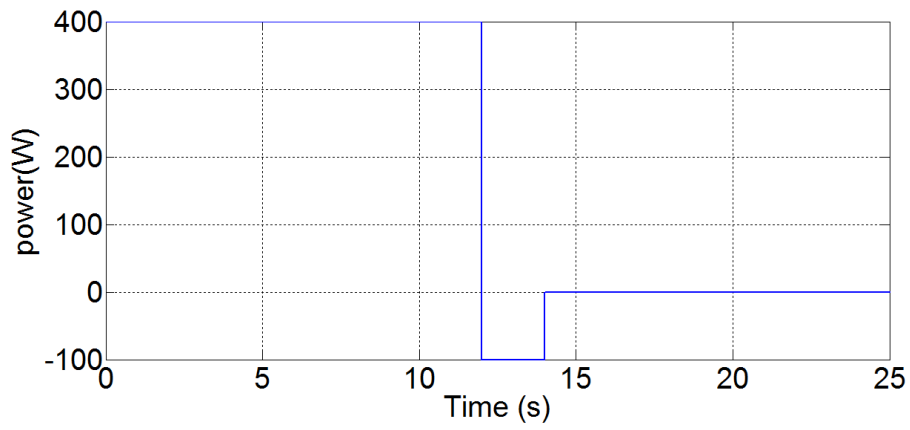


Figure 3.22: The power reference of load

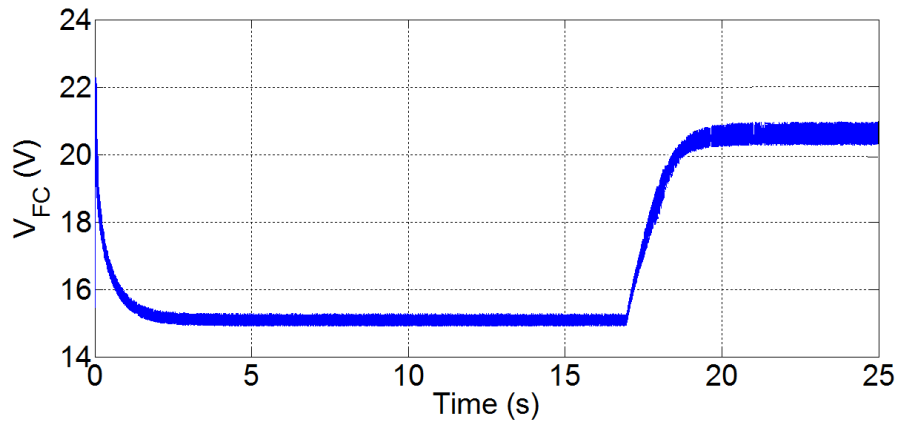


Figure 3.23: The FC's voltage

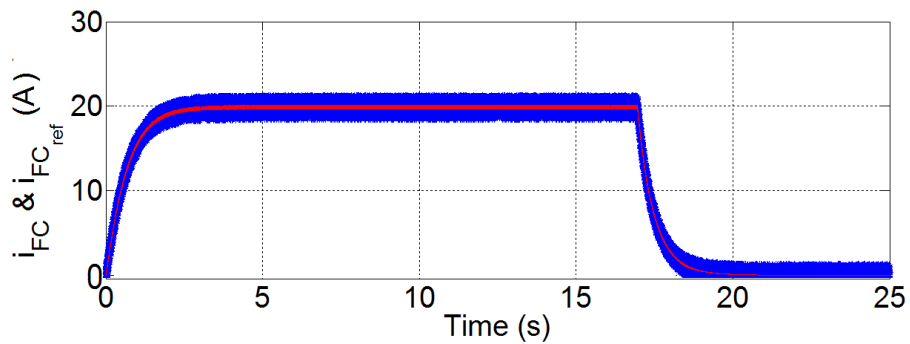


Figure 3.24: The FC's current and its reference

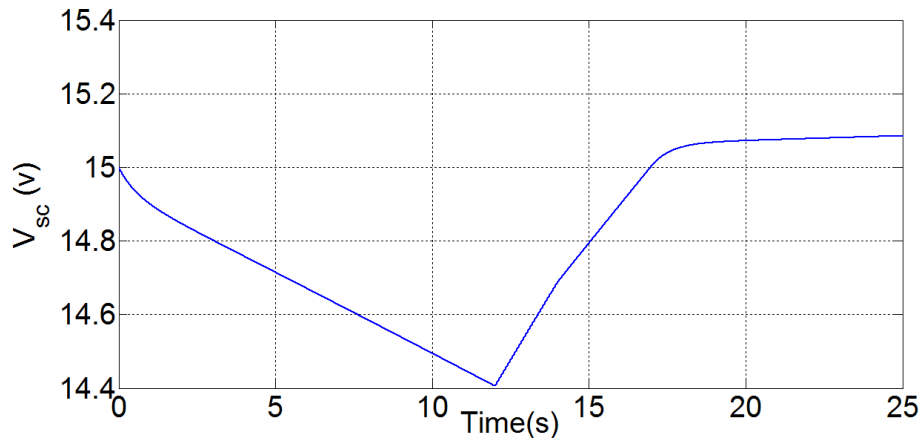


Figure 3.25: The SC's voltage

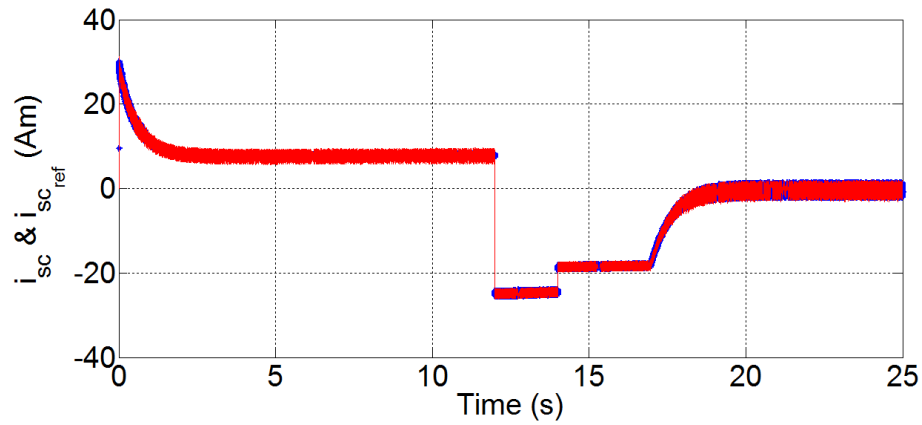


Figure 3.26: The SC's current and its reference

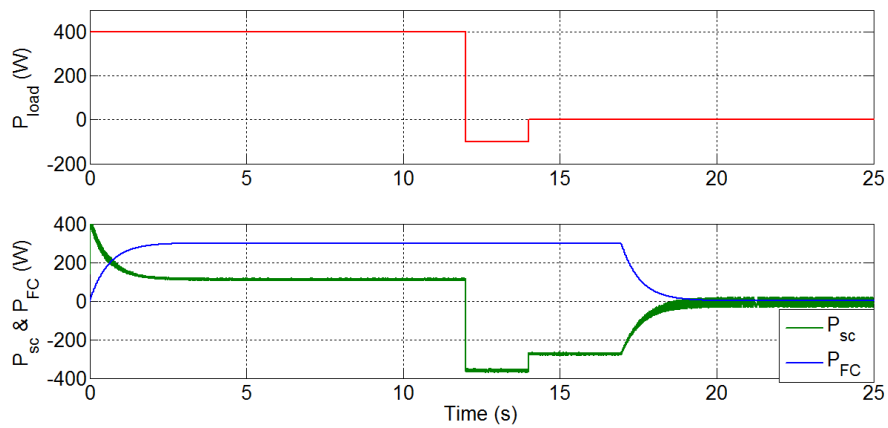


Figure 3.27: Load, FC and SC power responses

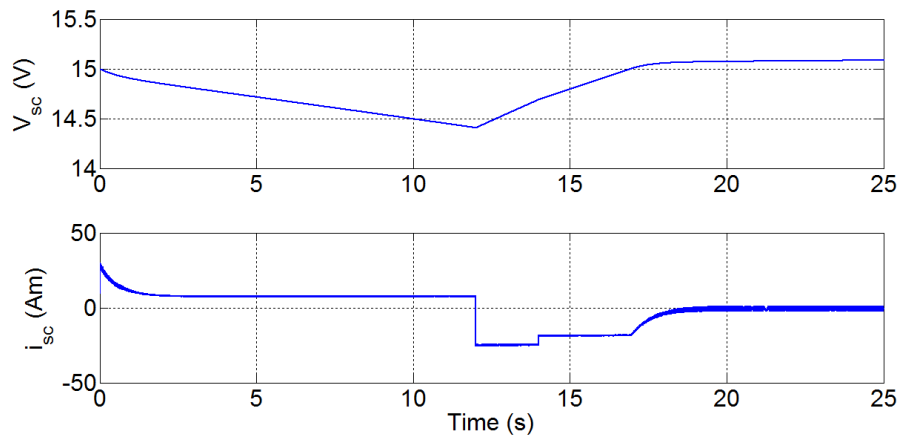


Figure 3.28: SC's voltage and current

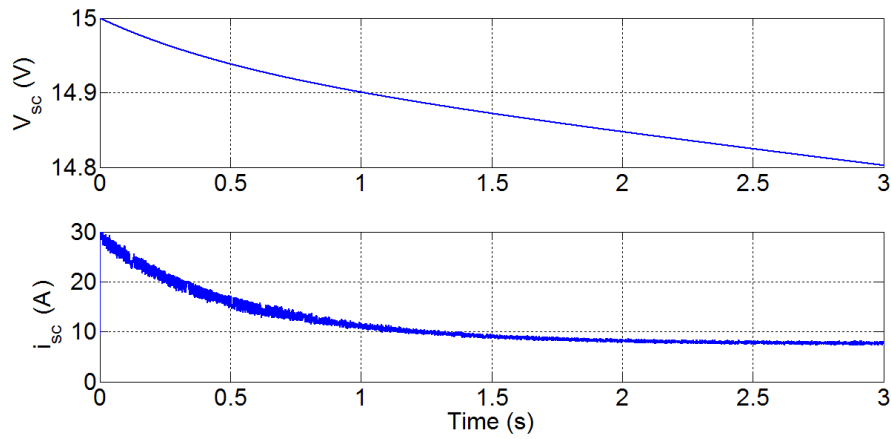


Figure 3.29: SC's voltage and current in discharging mode

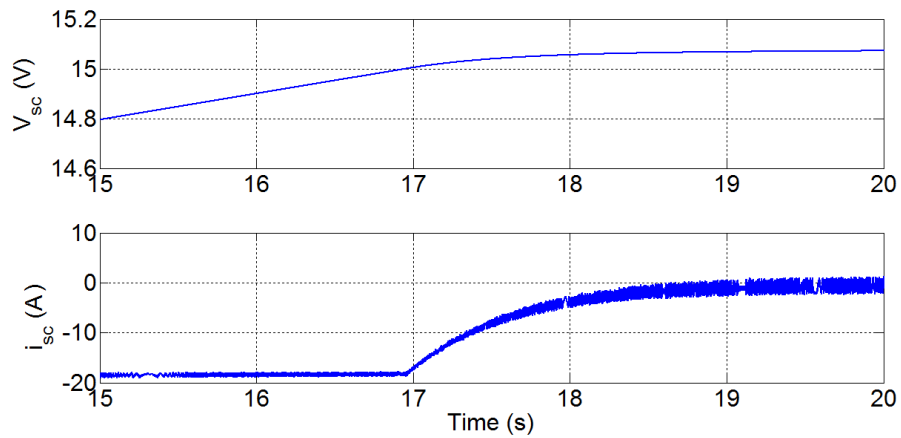


Figure 3.30: SC's voltage and current in charging mode

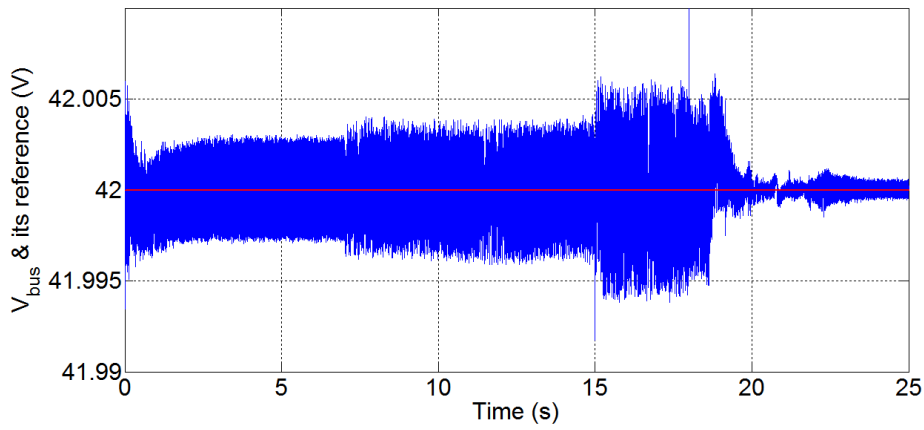


Figure 3.31: DC-bus's voltage and its reference

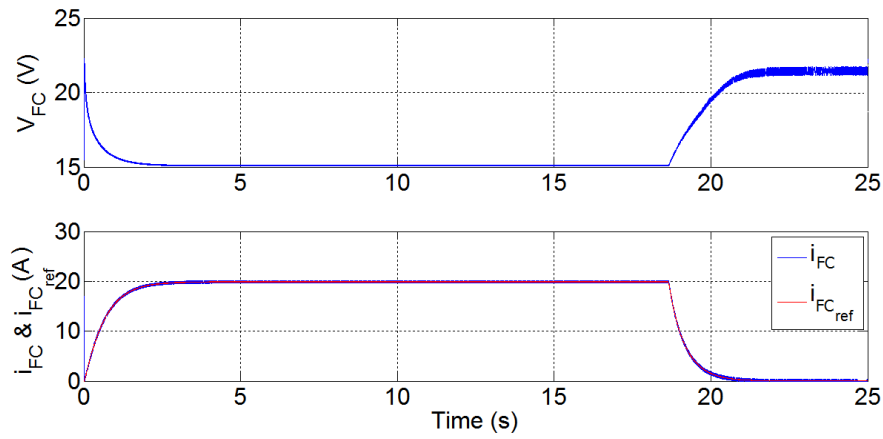


Figure 3.32: FC's voltage and current with its reference

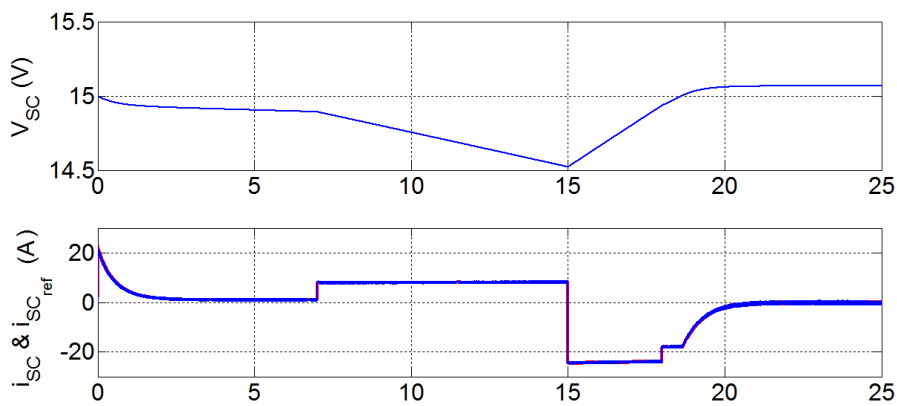


Figure 3.33: SC's voltage and current with its reference

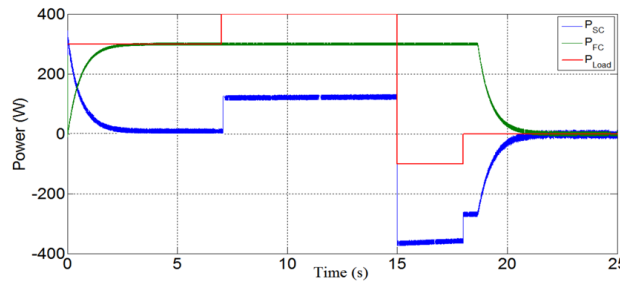


Figure 3.34: Response of system powers

The Fig. 3.34 shows the basic operation modes of the studied FC-SC hybrid source. The initial state has a load power = $300W$, and the SC storage device is full of charge, i.e., $V_{SC} = 15,1V$; as a result, the SC power is zero, and the FC power equals to $300W$ for the load power demanded. At $t = 7s$, the load power steps to a constant value of $400W$, whereas the final FC power is in its limited maximum power of $300W$. Thus, the SC, which supplies most of the transient power that is required during stepped load, remains in a discharge state after the stepped load because the steady-state load power ($400W$) is greater than the FC limited maximum power ($300W$). Subsequently, at $t = 40s$, the load power steps from $400W$ to $-100W$. As a result, the SC changes its state from discharging to charging, demonstrating the three mode. First, the FC supplies its limited maximum power of $300W$ for charging the supercapacitor, which absorbs simultaneously the regenerative braking power from load. Second, at $t = 18s$ until $19s$ the load power is zero, then, only the FC charges the SC. Third, at $t=19s$, the SC is nearly fully charged at $15V$ as it is shown in Fig. 3.33, which then reduces the charging power. Finally, at $t = 20s$, the supercapacitor is fully charged, and the supercapacitor charging power is zero. One can observe that the DC-bus voltage waveform is stable during the constant load power, the large positive load step, and the negative load step, which is of major importance when employing SC to improve the dynamic performance of the whole system using the differential flatness-sliding based energy management law.

3.8 conclusion

In this chapter, a control strategy of a fuel cell stack using a non-isolated DC/DC converter had been presented and validated. This control is ensured by hybrid dual

loop control, which includes a voltage loops with a linear PI controllers and a fast current loops with a non-linear sliding controllers. the simulation and experimental results showed the good efficiency and functionality of the converter and control strategy. Also, a new energy management method has been presented, it is based on the flatness and the sliding mode control to control a hybrid system composed of a fuel cell and a supercapacitor as the main and auxiliary sources, respectively. The nonlinear flatness strategy is used to achieve a linearizing feedback control law that gives an exponential asymptotic reference trajectories of the FC and SCs powers. The proposed flatness control determines the desired FC and SCs powers that allow decoupling the hybrid system into two decoupled sources such that each subsystem has a separated control target expressed in terms of a sliding surface. The role of sliding mode controllers is instantaneously to ensure the power sharing between the DC-link converters. The simulation results show that the produced energy of the studies sources satisfies the load's demands in different examined conditions and the energy control using flatness and sliding mode is managed successfully in the hybrid system with stable and robust performance.

Control of an electric vehicle

4.1 Introduction

With the rapid development of the science and technology, the emergence of new complex systems has never ceased. In order to answer the new constraints of this challenge, an Energetic Macroscopic Representation (EMR) is proposed. It does not have the role to replace the traditional representations, but rather to supplement them by a more overall view. The use of EMR allows developing a MCS, which can be obtained from the inversion of the considered EMR modelling. In the MCS, the inversion of stander elements (conversion or coupling elements) is easier than the inversion of accumulation elements, which is based on the use of PI or PID regulators.

In this chapter, a specific Adaptive Fuzzy Logic system integrated into MCS has been designed to control EV speed. The speed control parameters and the EV operation mode are also on-line adapted according to the battery SOC and the distance between vehicle and the nearest charging station (this distance is provided by the algorithm of the charging station location), in order to reduce the energy used by EV and meet the requested autonomy. Also, a states space model is presented in this chapter for modelling the electromechanical behaviour of the EV. The states feedback control has been used to control an EV speed, by using two types of methods to determine the values of the controller parameters, the first one is pole placement and the second one is Linear Quadratic Regulator.

4.2 Energetic macroscopic representation

The EMR has been first developed in 2000 at Laboratory of Power electronics (Lille, France) and has been applied to the energetic and multi-physic systems by Femto-ST CNRS Lab (Belfort, France). EMR is a graphical modelling tool, which is based on the action-reaction principle to organize the interconnection of sub-systems according to the physical causality (i.e. integral causality) [Fra05]. This description highlights energetic properties of the system (energy accumulation, conversion and source).

4.2.1 Action reaction principle

The power is transmitted between connected elements by a combination of "action" and "reaction". For example, a current source (s_1) is connected to a capacitor (s_2), the action of s_1 is its current and the voltage is its reaction s_2 as it is shown in Fig. 4.1. The transmitted power is the product of the action and the reaction.

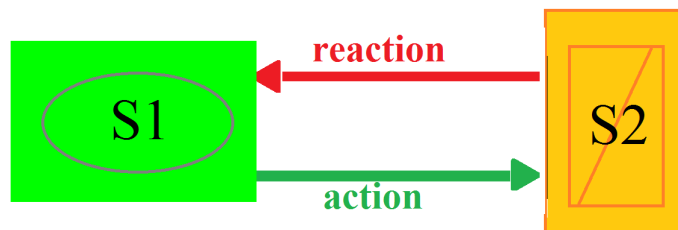


Figure 4.1: Causality principle

4.2.2 Integral causality

In real time systems, integration means the surface of the past, but derivation means the trend of the future, which can not be determined before. Thereby, the EMR considers integral causality as the only allowable physical causality. Integral causality indicates what are the inputs of system and what are the outputs. In other words, for a system modelled by an integral equation, integrand(cause) is the input of system and the integration(effect) is the output [Sye12]. For instance, as viewed from capacitor equation (4.1), the current is the cause (input) and the voltage is the effect (output), contrary to an inductor. Whereas, the conversion and coupling elements have no time-dependant behaviour i.g. in the resistor, the voltage or current can be considered as input or output,

that depends on the system connected with it.

$$V_{SC} = \frac{1}{C} \cdot \int I_{SC}(t)dt \quad (4.1)$$

4.2.3 EMR elements

EMR has four basic kinds of elements: source elements, conversion elements, accumulation elements and coupling elements. Source elements (ovals) are terminal elements, which deliver or receive energy (e.g. a battery). Conversion elements are considered as energy conversion without energy accumulation (integral or derivative causality). They are described by squares for electrical conversion, circles for electromechanical conversion and triangles for mechanical conversion. Accumulation elements (rectangles) store energy, which leads to state variables. Coupling elements (overlapped pictogram) are introduced energy (e.g series or parallel relationship of electrical circuits) [Fra05].

Table 4.1: Energetic macroscopic representation blocks

Energetic macroscopic elements blocks		Inversion based control blocks	
Source		Accumulation	
Electrical conversion		Multi-physical conversions	
Electrical coupling		Multi-physical coupling	
		Indirect inversion	
		Direct inversion	
		Coupling inversion	

4.2.4 Inversion based control of an EMR

The control structure of a system is considered as an inversion model of the system. Firstly, tuning chains are defined according to the objective and constraints of system. Then, control chains are deduced by inversions of the tuning chains. According to these control chains, EMR is inverted element by element. All control blocks are depicted by parallelograms as it is shown in Fig. 4.2. Conversion elements can be directly inverted, as

they have no time-dependence behaviour. Coupling elements may require supplementary inputs for inversion. Since accumulation elements cannot be inverted physically to avoid derivation, an indirect inversion is thus made using a closed loop controller. Since an accumulation represents a time-dependence relationship, a controller is required [LDBB05]. Small circle means sensor. Real arrow line with sensor means that this measurement is necessary. Dashed arrow line with sensor means the disturb compensation, which should be taken into account in the first step [Fra05]. By this way, MCS can be obtained under the assumption that all variable are measurable. From this MCS, some simplifications and estimations can be made and then a practical control structure can be obtained.

4.3 Modelling of the electric vehicle

4.3.1 Architecture of the studied EV

The general scheme of the studied EV is represented by Fig. 4.2, which couples the dynamics of the vehicle to the electrical motorization. The EV is driven by a DC machine with a differential mechanical device. It is supplied by a battery through a DC/DC converter.

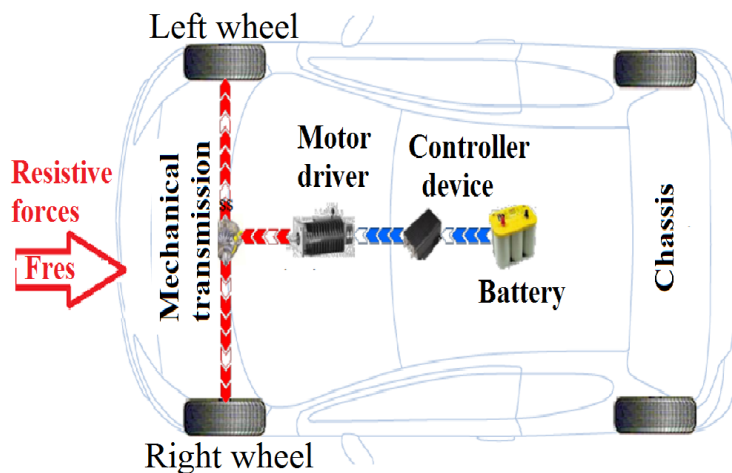


Figure 4.2: The studied electric vehicle structure

4.3.2 EMR of the electric vehicle

4.3.2.1 The EV supply source

In this chapter a simple battery has been used. The battery can be modelled as an equivalent circuit such as a voltage source in serial with an internal resistor. The following equation allows finding an acceptable approximation of the SOC as it is presented in (2.2.5.3).

$$SOC(t) = SOC(0) - \frac{100}{Q} \cdot \int I_{bat}(t) dt \quad (4.2)$$

4.3.2.2 Chopper

Chopper is an electric converter (without energy accumulation and supposed without losses). It is represented as a conversion element (square pictogram) and its expression is:

$$\begin{cases} U_{chop} = \alpha_{chop} V_{bat} \\ I_{chop} = \frac{1}{\alpha_{chop}} I_{bat} \end{cases} \quad (4.3)$$

Where α_{chop} is the chopper amplification gain where ($\alpha_{chop} = \frac{1}{1-\alpha}$) and α is the duty ratio. I_{chop} , U_{chop} are the chopper current and voltage, and V_{bat} is the battery voltage.

4.3.2.3 Motor drive

The used motorization consists of a Direct Current Motor supplied by a chopper. DCM is modelled with classical relationships. The armature current (I_{arm}) is the state variable of armature windings and is obtained from the supply voltage and the electromotive force e_{em} :

$$L_{arm} \frac{dI_{arm}}{dt} = U_{chop} - e_{em} - R_{arm} I_{arm} \quad (4.4)$$

Where R_{arm} and L_{arm} are the resistance and inductance of the armature windings. This device is thus an accumulation element due to the presence of the inductance. An electromechanical conversion link current to the produced motor torque (T_{mot}). As shown in (4.5), the e_{em} is also deduced from the nominal motor rotation W_{nom} [KBA+13]:

$$\begin{cases} T_{mot} = k\phi I_{arm} \\ e_{em} = k\phi W_{nom} \\ k\phi = \frac{U_{arm}^{nominal} - R_{arm} I_{arm}^{nominal}}{W_{nom}} \end{cases} \quad (4.5)$$

where k is the machine constant parameter related to the torque and to the e.m.f. ϕ is the magnetic flux.

The following equation allows finding the numerical value for the mechanical conversion (shaft + gearbox).

$$\begin{cases} T_{gear} = k_{gear} T_{mot} \\ W_{mot} = k_{gear} W_{gear} \end{cases} \quad (4.6)$$

where T_{gear} and W_{gear} are the torque and speed rotation after reduction, k_{gear} is the gearbox reduction coefficient and W_{mot} is the motor rotation speed.

4.3.3 Modelling of the mechanical coupling

4.3.3.1 Mechanical differential

The torque reduction is shared fairly on the left and the right wheels, as well the rotation speed as shown in (4.7)[KBA+13].

$$\begin{cases} T_{diff_{left}} = \frac{1}{2} T_{gear} \\ T_{diff_{right}} = \frac{1}{2} T_{gear} \\ W_{diff} = \frac{1}{2} (W_{left} + W_{right}) \end{cases} \quad (4.7)$$

Where W_{diff} , $T_{diff_{left}}$ and $T_{diff_{right}}$ are the differential speed rotation and torques of left and right wheels after differential, respectively.

4.3.3.2 Left and right wheels

The wheels have to produce a linear motion from a rotational motion. The traction forces can be calculated from the torque of the differential, and the wheel rotation from the vehicle velocity [NBDEB07].

$$\begin{cases} F_{left} = \frac{1}{R_{wheel}} T_{diff_{left}} \\ W_{left} = \frac{1}{R_{wheel}} V_{veh_{left}} \\ F_{right} = \frac{1}{R_{wheel}} T_{diff_{right}} \\ W_{right} = \frac{1}{R_{wheel}} V_{veh_{right}} \end{cases} \quad (4.8)$$

By differentiating linear velocities of both the left and right wheels, one can take into account the radius of curvature (R_{courb}) and the width of the vehicle (l_{veh}) (distance between the rear wheels).

$$\begin{cases} F_t = F_{left} + F_{right} \\ v_{veh_{left}} = \frac{R_{courb} + \frac{l_{veh}}{2}}{R_{courb}} v_{veh} \\ v_{veh_{right}} = \frac{R_{courb} - \frac{l_{veh}}{2}}{R_{courb}} v_{veh} \end{cases} \quad (4.9)$$

4.3.3.3 Chassis

We saw, in the first chapter, that the vehicle velocity V_{veh} is obtained with the Newton dynamics relationship from the the total tractive force of the vehicle F_t and the resistance force F_{tr} as it is shown in the following expression (more details are given in first chapter 1.3):

$$M \frac{dV_{veh}}{dt} = F_t - F_{tr} \quad (4.10)$$

where M is the vehicle mass. The chassis is an accumulation element, hence the velocity is chosen as a state variable.

4.3.3.4 Environment

The external environment of the vehicle is considered as a mechanical load and is modelled in EMR with a mechanical source element which is used for both source and load. It yields a resistive force F_{tr} to the motion from the vehicle velocity as it is explained in first chapter (1.3.1). The modelling of the traction system using EMR simulator allows the implementation of some controls such as the MCS and the speed control.

4.4 Inversion of EMR simulator

4.4.1 Inversion of standard elements

The electric or mechanical conversion elements are directly inverted to obtain the reference output. The inversion of the mechanical coupling allows the repartition of the estimated force on the two wheels, where the inversion of the wheels is directly obtained and leads to the reference torque of mechanical differential.

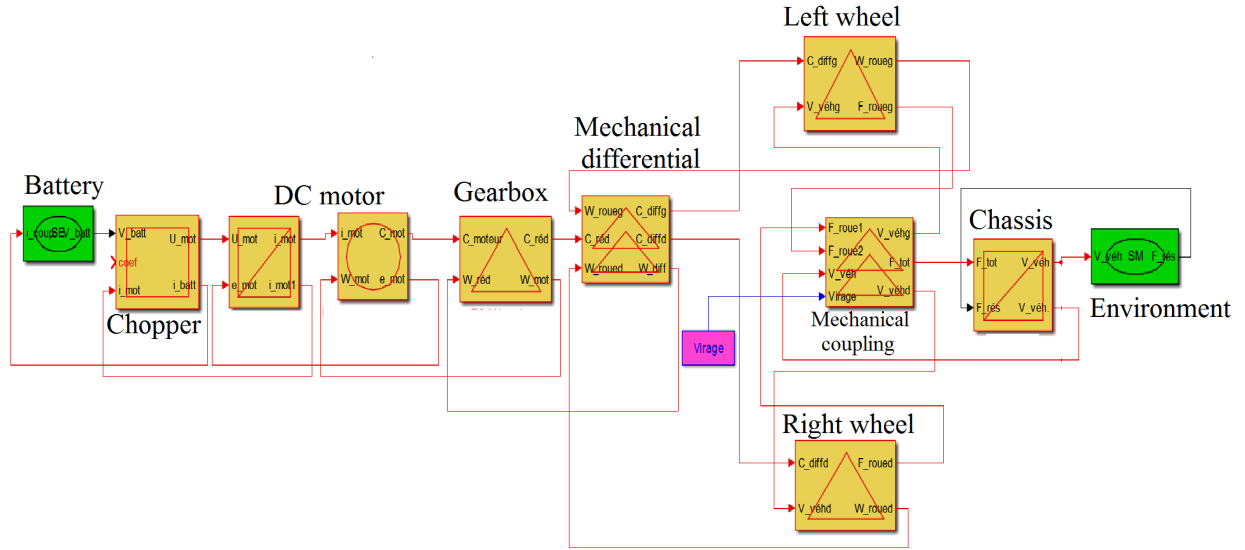


Figure 4.3: EMR simulator of the studied EV in Matlab/simulink .

4.4.2 Inversion of accumulation elements

The classical inversion of accumulation bloc using the PID or IP controller needs the calculation of the controller parameters (integral and proportional gains). This task is not obvious and parameters are constant whatever the batteries SOC. In order to overcome this problem, authors propose to use the FL technique instead of the PI or IP controller which provides an easy and parametric way to control the system and to adjust the vehicle mode.

4.4.2.1 Inversion of chassis

The inversion of the accumulation element associated with the chassis that is presented by (4.10) leads to a velocity controller:

$$F_{t-ref} = Con(V_{veh-ref} - V_{veh-mes}) \quad (4.11)$$

where $Con(x_{ref} - x_{mes})$ is the controller of the measured value (x_{mes}) of variable x toward its reference.

In this paper, a specific AFLC is proposed and developed by author to invert this accumulation element contrary to other works that used an IP (Integral + Proportional) [MHPA11], [NBDEB07].

4.4.3 Inversion of Armature

The inversion of the armature winding leads to the armature current controller IP and the e.m.f. e_{em} compensation.

$$U_{chop-ref} = Con(I_{arm-ref} - I_{arm-mes}) + e_{em} \quad (4.12)$$

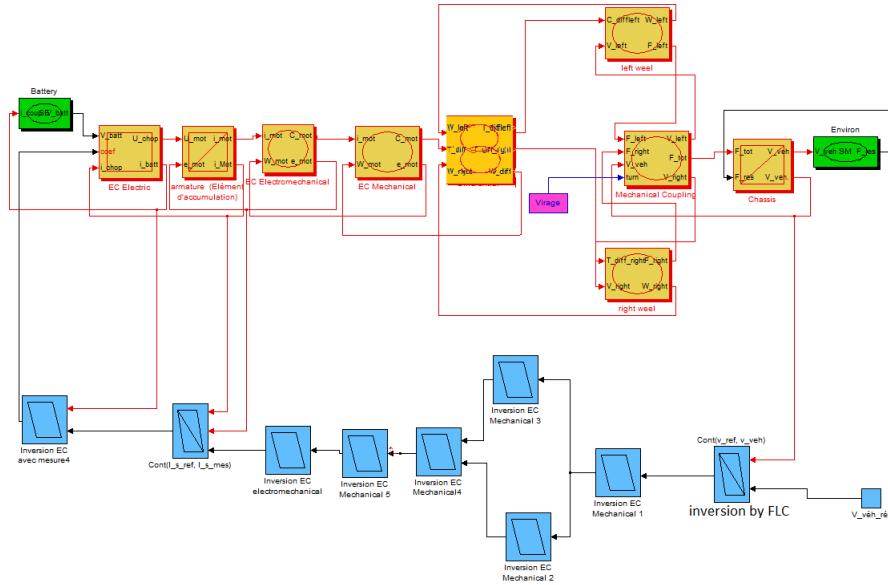


Figure 4.4: EMR and MCS simulator of the studied EV in Matlab/simulink .

4.5 Development of fuzzy logic-based control

The basic idea in this work is the use of an AFLC to invert the accumulation element in MCS and to adapt the performance of the EV. Then, the EV can work in an adaptive operation mode.

4.5.1 Adaptive fuzzy logic control design

The developed AFLC includes two fuzzy logic structure (FLS). The first one is FLC which was adopted to invert the accumulation element associated with the chassis, the second one is a simple FLS, which acts on the values of output MFs range (FLC-MFs) to vary them during the control of the system to obtain the desired Operation Mode as presented in Fig. 4.5. The FLS inputs are the battery SOC and the signal U which represents the information of the nearest charging station. For example location-based

services built into most EVs allows providing the locations of nearby charging stations. The FLS outputs are the range value of FLC output MFs. This FLC is nonlinear system [PH11], which allows determining the $F_{t_{ref}}$ corresponding to the torque reference and to apply it to the EV motor.

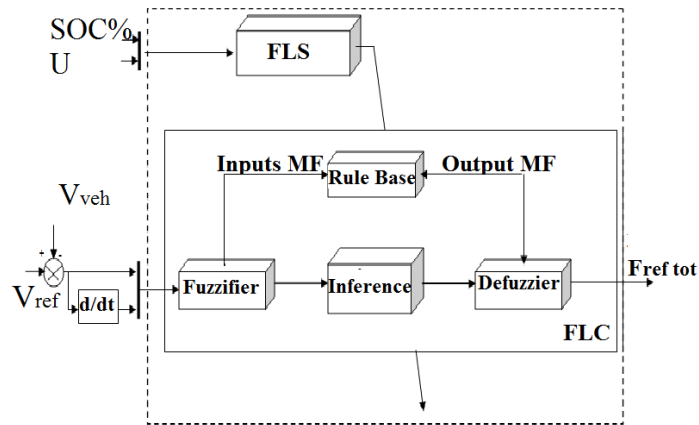


Figure 4.5: (a) A typical structure of the developed AFLC.

Table 4.2: The rule base system of FLC.

$\frac{d\xi}{dt}$	NB	NA	NS	ZE	PS	PA	PB
ξ							
NB	NB	NB	NB	NA	NS	P	PB
NA	NB	NB	NA	NS	NS	ZEN	PS
NS	NA	NA	NS	NS	ZEN	PS	PS
ZE	NS	ZEN	ZEN	ZE	ZE	ZEP	PS
PS	NS	NS	ZE	PS	PS	PA	PB
PA	NS	ZE	PS	PS	PA	PB	PB
PB	PB	PS	PS	PA	PB	PB	PB

4.5.2 Basic concepts of fuzzy logic

4.5.2.1 Fuzzification interface

It transforms the inputs SOC, the signal U , the error (ξ) and the change of error ($\frac{d\xi}{dt}$) between $v_{veh_{ref}}$ and $v_{veh_{mes}}$, of the AFLC from distinct quantities to fuzzy quantities [SA10]. The nine-term sets are negative big (NB), negative average (NA), negative

Table 4.3: The rule base of FLS.

SOC	low	avg	high
U			
SoFAR	E	E	D
FAR	E	ED	D
NEARBY	ED	D	D

small (NS), zero negative (ZEN), zero (ZE), zero positive (ZEP), positive small (PS), positive average (PA) and positive big (PB) are used to define FLC output and inputs linguistic variables. The seven-term sets: low, average (avg), high, Economic Choice (EC), SoFAR, FAR and NEARBY are applied to define input linguistic variable of FLS (SOC and U). For the FLS output, (E), (ED) and (D) terms are defined. Where E, ED and D are corresponding to predefined vector of FLC-MFs values that allow improving and the adjustment of the EV performance (fast, medium or slow EV response).

4.5.2.2 Rule base system

The fuzzy rule base is a set of linguistic rules defined with IF-THEN conditions. The rule base which has the M number of rules ($j = 1, 2, \dots, M$) is shown in (4.13).

$$\begin{aligned}
 R^j &: \text{IF } x_1 \text{ is } A_1^j \text{ and } x_2 \text{ is } A_2^j \text{ and } \dots \text{ and } x_n \text{ is } A_n^j \\
 &\text{THEN } z \text{ is } B^j
 \end{aligned} \tag{4.13}$$

$x_i (i = 1, 2, \dots, n)$ are the fuzzy system input parameters. The fuzzy output variables are denoted z . The Membership Functions (MF) $\mu_\xi(x_i)$ and $\mu_{\frac{d\xi}{dt}_i}(x_i)$ are represented as the input linguistic terms A_i^j . B^j is the linguistic terms for the fuzzy output [Ros13]. All rule base system of FLC and FLS and FLC memberships function are shown in Table. 4.2 and Fig. 4.7 respectively.

4.6 Simulation results

The EMR and MCS are directly converted into a Matlab/Simulink model as illustrated in Fig. 4.4. In the following simulations, battery, chopper and gears are considered ideal and without losses. The parameters of the DCM, main geometrical data and inertial

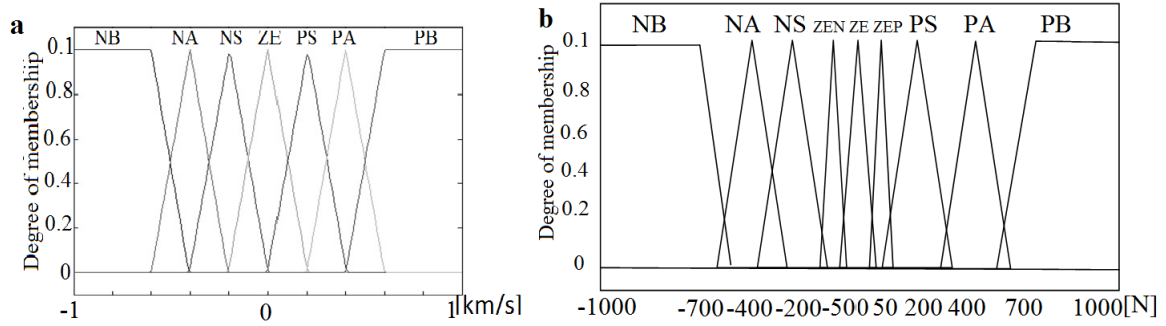


Figure 4.6: (a) FLC's MF for the input ξ ; (b) FLC's MF for the output $F_{t_{ref}}$.

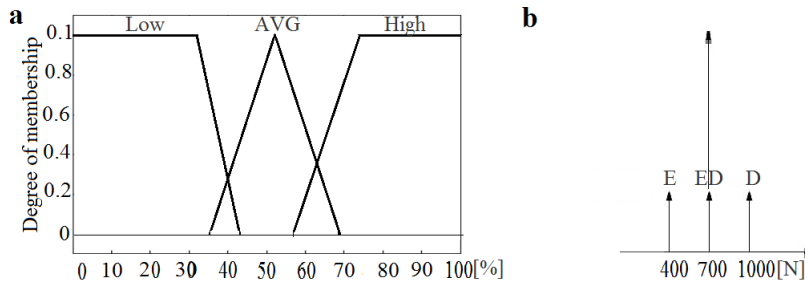


Figure 4.7: (a) FS's MF for the input; (b) FS's MF for the output $F_{t_{ref}}$'s range.

properties of the vehicle and wheels are shown in the Table. 4.6. Simulation was carried out with a part of the european driving cycles.

The Fig. 4.8 shows a comparison between the reference and the vehicle velocity controlled using AFLC based MCS. The EV works with two different operation modes. One corresponds to a dynamic vehicle fast dynamic vehicle) as shown in Fig. 4.8(a). The second is an EOM Fig. 4.8 (b), a slow dynamic is imposed in order to safe the energy consumption and to obtain an economic vehicle. It is clearly seen that the vehicle velocity follows its reference without steady error and overshoot. By using the EMR and AFLC-SMC of EV, the velocities of wheels are presented in Fig. 4.9 (b). At 65 s the vehicle makes a turn during 3.46 s which is considered as a disturbance for testing the control robustness.

Indeed, when the vehicle makes a turn, the wheels left and right are not running with the same speed. Where the left wheel slow down and the right wheel speed up. The results in Fig. 4.10 show the are obtained results for different values of SOC(0) where the EV is simulated with the AOM ($U = FAR$). It is clear that the AFLC works better and acts on the EV dynamic performance to adapt it during the control of system according to the SOC. Under the same driving cycles and simulation conditions, a comparison between

Table 4.4: Parameters of the EV system.

Parameters	Value
V_{batt}	300V
M_{veh} (vehicle mass)	1000kg
l_{veh} width of the vehicle	1.6m
R_{wheel} wheel radius	0.26m
J_{weel} inertia of wheel	4.3Kg.m ²
A_f frontal surface of vehicle	21.6m ²
ρ density of the air	1.2Kg/m ³
P_{nom} nominal power	32kW
L_{arm} armature's inductance	0,0065H
R_{arm} armature's resistance	0,35Ω
J_m Rotor's inertia	0,12kg.m ²

the EV autonomy of DOM (sport vehicle) and AOM is presented in Fig. 4.11. The AOM saves 10% of SOC %, whereas with the classical DOM, SOC% is null when using the same driving cycle.

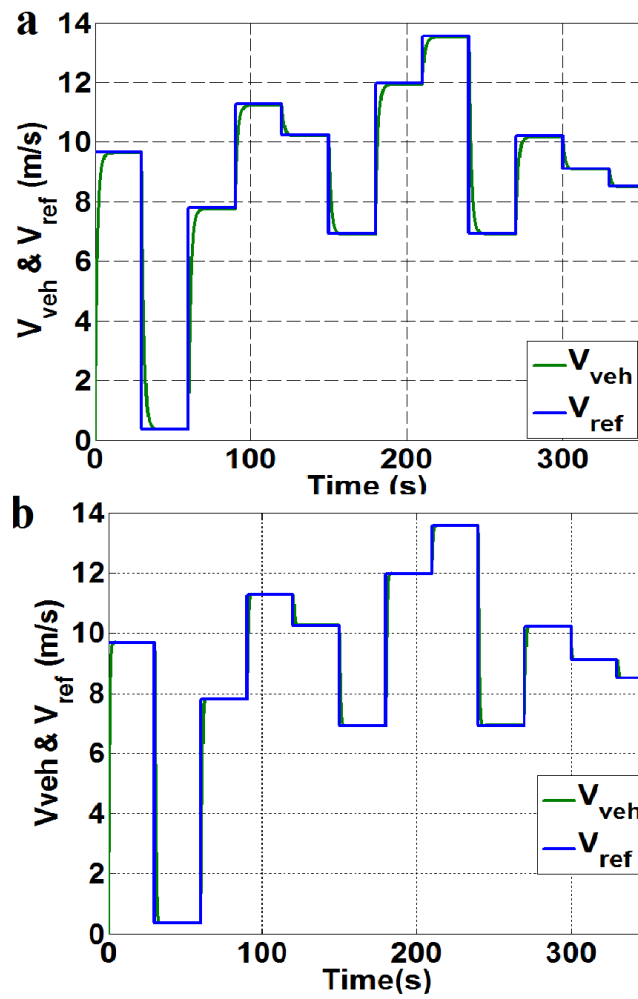


Figure 4.8: Reference and vehicle velocities with (a) EOM (b) DOM.

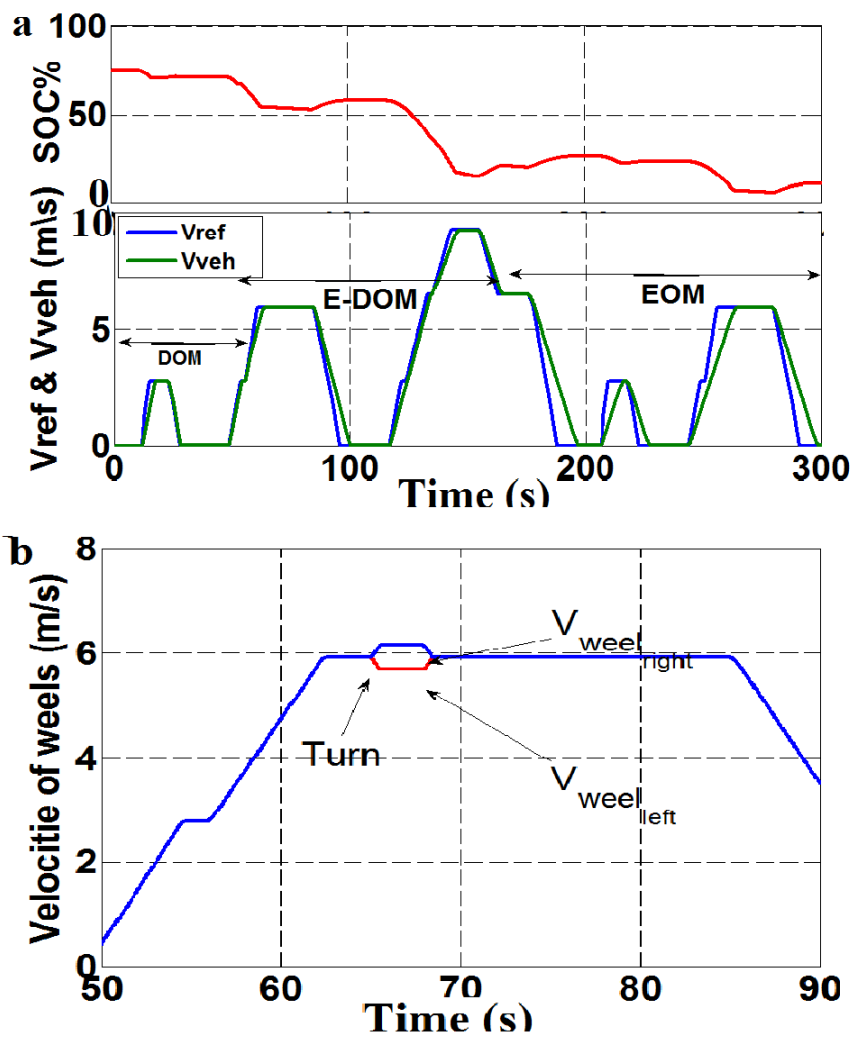


Figure 4.9: (a)Reference and measured EV speeds with the AOM SOC%=78%;(b)Left and right vehicle velocities.

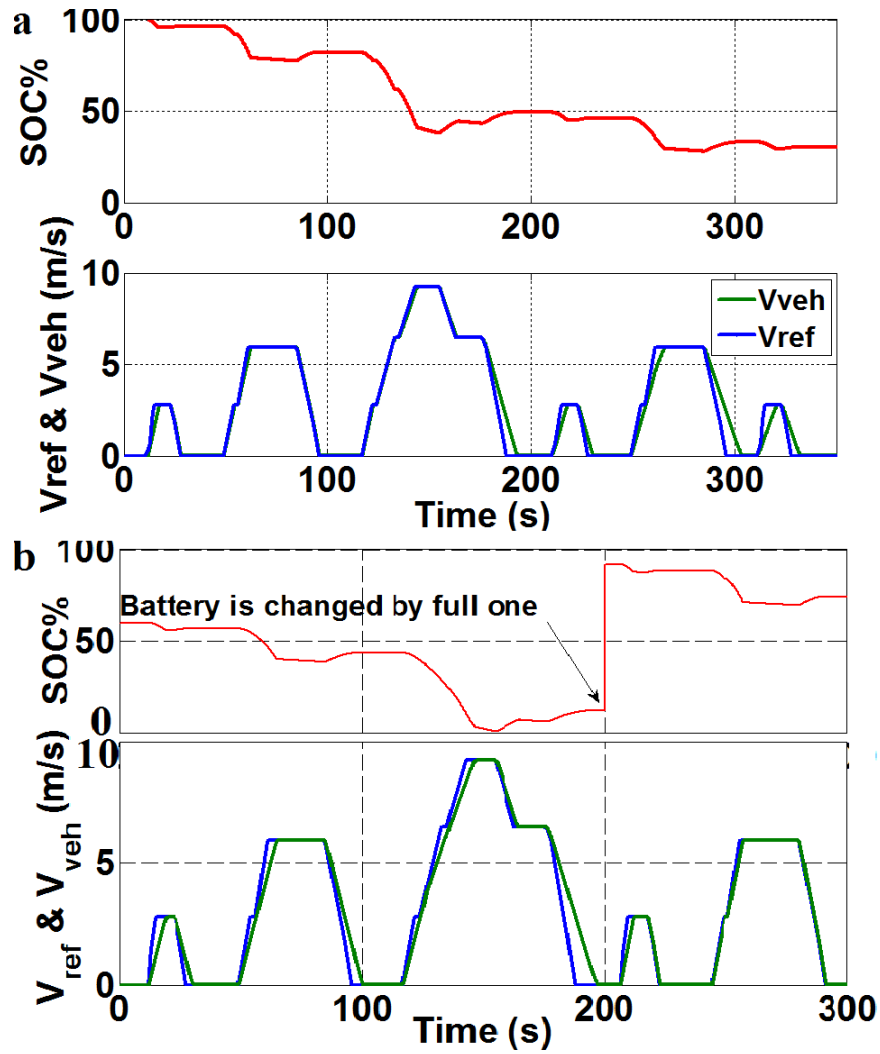


Figure 4.10: EV speeds with the AOM (a)SOC(0)=100% (b)SOC(0)=60%.

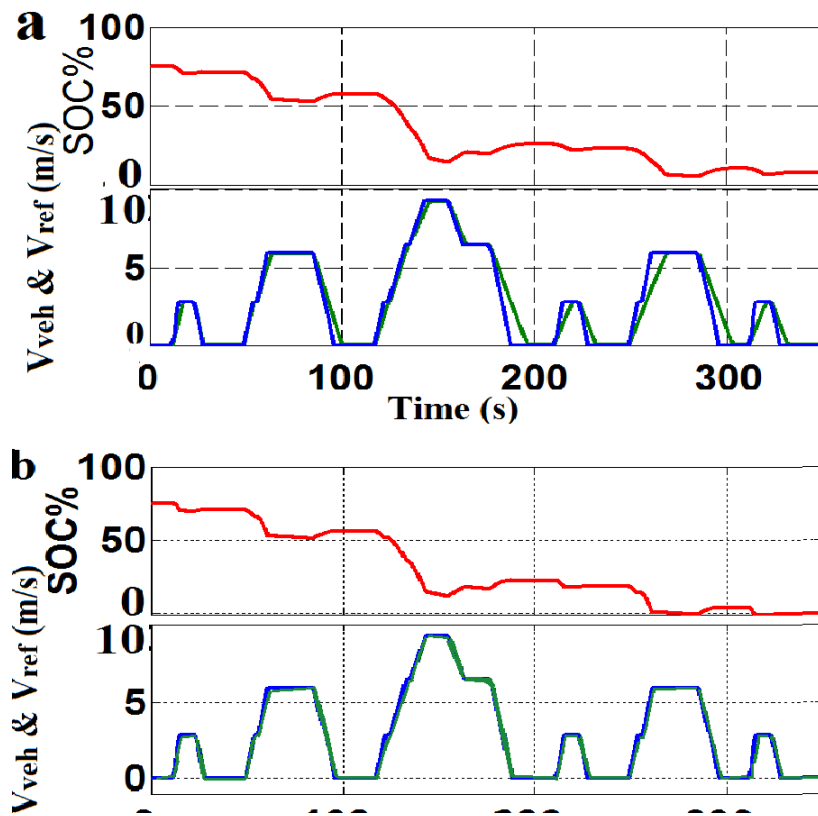


Figure 4.11: SOC_s (SOC(0)=100%), Comparison of EV with AOM and classic DOM.

a

4.7 State-space model of the electric vehicle

From the bloc diagram of the EV (Fig. 4.12), the e_{em} and F_t are written by the following expressions:

$$\begin{cases} F_t = \frac{2k\phi k_{gear}}{R_{wheel}} \cdot I_{arm} \\ e_{em} = \frac{k_{gear} \cdot k\phi}{2R_{wheel}} \cdot V_{veh} \end{cases} \quad (4.14)$$

So V_{veh} and I_{arm} can be written by (4.15).

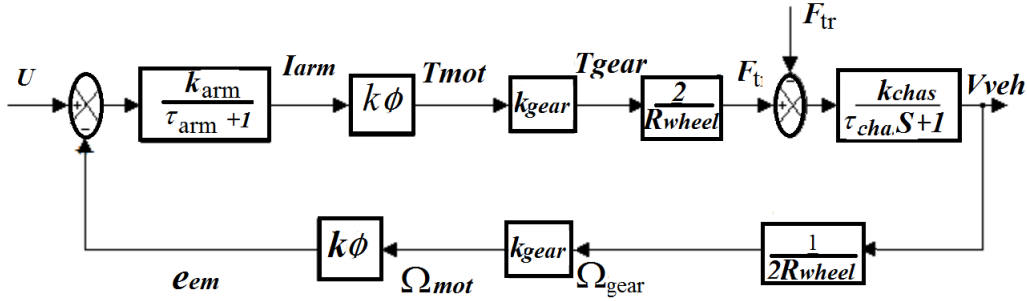


Figure 4.12: Bloc diagram of the EV.

$$\begin{cases} \dot{V}_{veh} = \frac{2k\phi k_{gear}}{M \cdot R_{wheel}} \cdot I_{arm} - \frac{f}{M} \cdot V_{veh} \\ \dot{I}_{arm} = \frac{-R_{arm}}{L_{arm}} \cdot I_{arm} - \frac{k_{gear} \cdot k\phi}{2L_{arm} R_{wheel}} \cdot V_{veh} + \frac{1}{L_{arm}} u \end{cases} \quad (4.15)$$

The general system equation can be written as:

$$\begin{cases} \dot{X} = A \cdot x + B \cdot u \\ Y = C \cdot x \end{cases} \quad (4.16)$$

Where $x \in R^2$ is the state vector, $u(t)$ the command vector and Y the output vector. A, B, C and D are matrices with appropriate dimensions and without loss of generality

information and D equals zero. $x = \begin{bmatrix} V_{veh} \\ I_{arm} \end{bmatrix}$ and

$$A = \begin{bmatrix} -\frac{f}{M} & \frac{2k\phi k_{gear}}{M \cdot R_{wheel}} \\ \frac{-k_{gear} \cdot k\phi}{2L_{arm} R_{wheel}} & -\frac{R_{arm}}{L_{arm}} \end{bmatrix}, B = \begin{bmatrix} 0 \\ \frac{1}{L_{arm}} \end{bmatrix} \text{ and } C = \begin{bmatrix} 1 & 0 \end{bmatrix}.$$

4.8 Formulation of the control problem

The desired objective is to synthesize a linear control law, such that the poles of the controlled system coincide exactly with the zeros of a polynomial:

$$P(s) = s + a_{n-1}s^{n-1} + a_{n-2}s^{n-2} \dots + a_1s^1 + a_0 \quad (4.17)$$

The control law, which satisfies the preceding objective, is called: state feedback.

4.8.1 State Feedback Controller using poles placement

State-Feedback is the most important aspect of modern control system. Using an appropriate state-feedback, unstable systems can be stabilized or damping oscillatory can be improved [Rig09]. Pole-placement design allows placing the poles to specified location. The control is achieved by feeding back the state variables through a regulator with a matrix K (control gains) and G as it is shown in the following control law [Hus10].

$$u(t) = -Kx(t) + GY_{ref}(t) \quad (4.18)$$

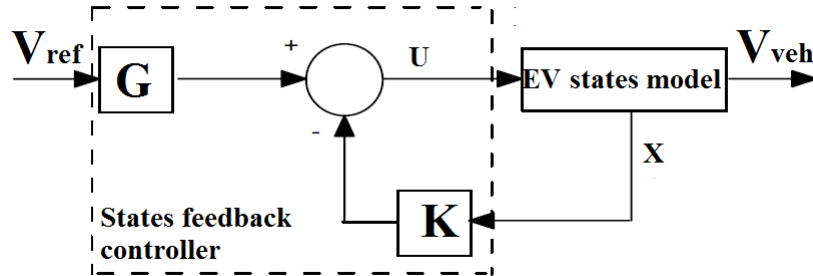


Figure 4.13: Structure of state feedback control of studied EV

4.8.2 Reconstruction of the state model

For the practical implementation problem of a state feedback control law, its solution consists of building a system, whose inputs are u and Y and whose output is a vector \tilde{x} , obtained from the state vector x of the EV process. After some simple calculations, the equilibrium states are expressed by:

$$\bar{x} = \begin{bmatrix} V_{ref} \\ f \\ \frac{M}{2k\phi k_{gear}} V_{ref} \\ M.R_{wheel} \end{bmatrix} \quad (4.19)$$

and

$$\bar{u} = \frac{V_{ref}}{L_{arm}^2} \left(\frac{R_{arm}fR_{wheel}}{2k\phi k_{gear}} + \frac{k\phi k_{gear}}{2R_{wheel}} \right) \quad (4.20)$$

where V_{ref} is the reference vehicle velocity. So the parameter G of the control law (4.18) is written by;

$$G = \frac{1}{L_{arm}^2} \left(\frac{R_{arm}fR_{wheel}}{2k\phi k_{gear}} + \frac{k\phi k_{gear}}{2R_{wheel}} \right) \quad (4.21)$$

After dynamic's error calculation where $\tilde{x} = x - \bar{x}$, the new state-space model is:

$$\dot{\tilde{X}} = \bar{A}.\tilde{x} + B.\tilde{u} \quad (4.22)$$

where the new control law $\tilde{u} = -K\tilde{x}$ and K is the same control gains vector presented in (4.18).

The state-feedback regulator is then applied to the state \tilde{x} . The new state matrix of the closed-loop system takes the following form [GRN09]:

$$\bar{A} = A - BK \quad (4.23)$$

In order to place the poles of the system, it needs to calculate the difference between the desired eigenvalues and those of the state matrix A . The desired closed-loop performances are presented by the following characteristics:

- EV speed response time $tr = 1,8s$;
- EV speed response is without overshoot ($D\% = 0\%$) and steady error equals zero;
- Then desired system Eigenvalues are $[-3; -1]$.

$$K = \begin{bmatrix} -7.7181 & -0.3262 \end{bmatrix}$$

4.9 Linear quadratic regulator

In this study, The problem of the optimal regulator at the finished horizon consists of determining the control u_{opt} of system (4.8.2), which optimizes the criterion [SSS12]:

$$J = \frac{1}{2} \int_{t_0} [x(t)^T Q x(t) + u(t) R u(t)] dt \quad (4.24)$$

Where Q and R) are a symmetric positive semi-definite and a symmetric positive definite matrices, respectively. The objective of the regulator problem is to bring back as quickly as possible the state in the vicinity of the origin, the solution sought here corresponding well with a compromise between the previous goal. The optimal control of the problem formulated above is given by [SSS12], [Hus10]:

$$u_{opt} = -R^{-1} B^T P x \quad (4.25)$$

where P is the single positive definite. The Riccati equation in steady state can be written as [Hus10]:

$$P A + A^T P + P B R^{-1} B^T P + Q = 0 \quad (4.26)$$

Then, the expression of the optimal solution is a linear control in closed loop, given by:

$$u_{opt} = -R^{-1} B^T P x = -K x \quad (4.27)$$

By using the LQR algorithm in Matlab, the obtained resulting controller gains are:

$$K = \begin{bmatrix} -5.0915 & 0.7091 \end{bmatrix}$$

The eigenvalues of closed loop system are then: $[-0.3868; -162.8825]$

4.10 Simulation results

The system simulation under Matlab/Simulink is illustrated in Fig. 4.14. In order to validate the proposed controller, the simulation was carried out to the stander FTP-75 , the American HWFET and the European NEDC driving cycles as illustrated in Fig. 4.15, Fig. 4.16 and 4.17 respectively. They are used as an imposed reference velocities of the vehicle. These results show the responses of the studied EV with control strategies, whereas the vehicle velocity controlled by the States Feedback Regulator using Pole Placement (PP) and the Linear Quadratic Regulator (LQR). The Fig. 4.18 (a) shows the reference and vehicle velocities of EV, whereas, Fig. 4.18 (b) presents the behaviour

of the armature current (a variable state I_{arm}). This simulation was carried out to part of European driving cycles. It is clearly seen that the response of system has good dynamic behaviour and tracks very well its reference without steady error or overshoot for both used methods (LQR and PP).

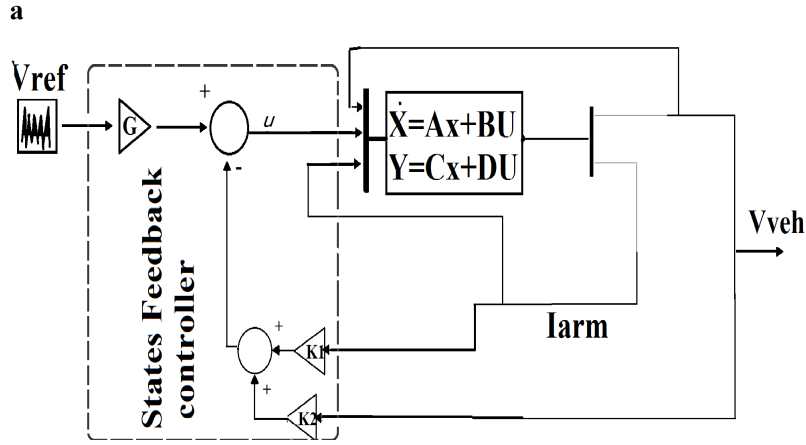


Figure 4.14: Structure of the studied control system .

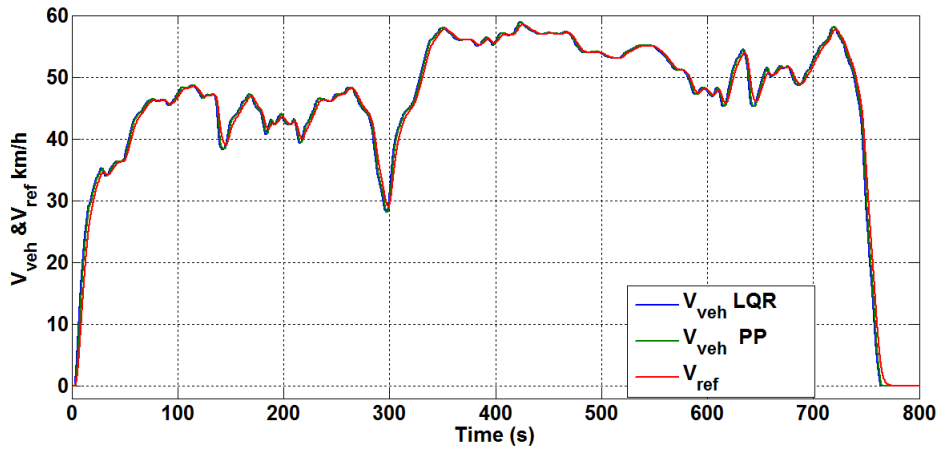


Figure 4.15: Reference and vehicle speed applying FTP-75.

At 65s the vehicle makes a turn during 3.46 s but it does not effect on the vehicle speed as illustrated in the Fig. 4.19

$$\begin{cases} V_{veh, left} = \frac{R_{coub} + \frac{l_{eft}}{2}}{R_{coub}} V_{veh} \\ V_{veh, right} = \frac{R_{coub} - \frac{l_{eft}}{2}}{R_{coub}} V_{veh} \end{cases} \quad (4.28)$$

Under the same driving cycles and simulation conditions, Fig. 4.20 presents a comparison between the EV energy consumption of two different control strategies. One is the developed LQR, the second is the State Feedback controller using Poles Placement (PP),

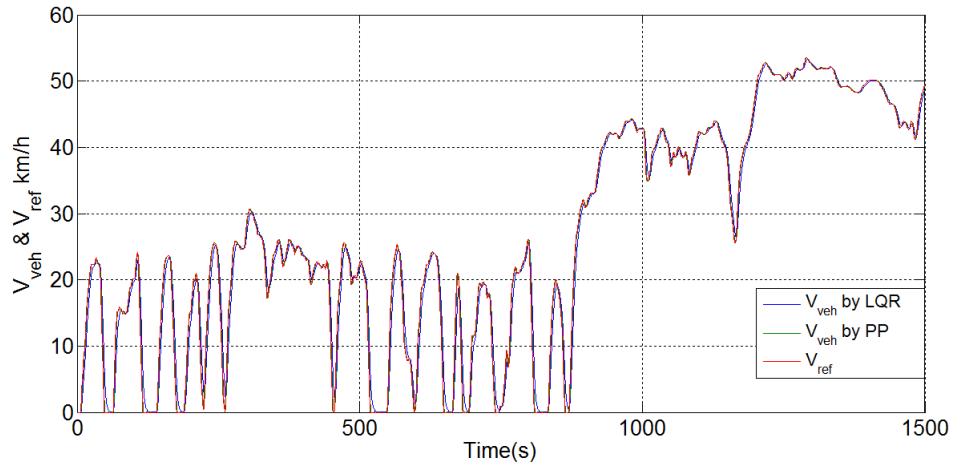


Figure 4.16: Reference and vehicle speed applying HWFET.

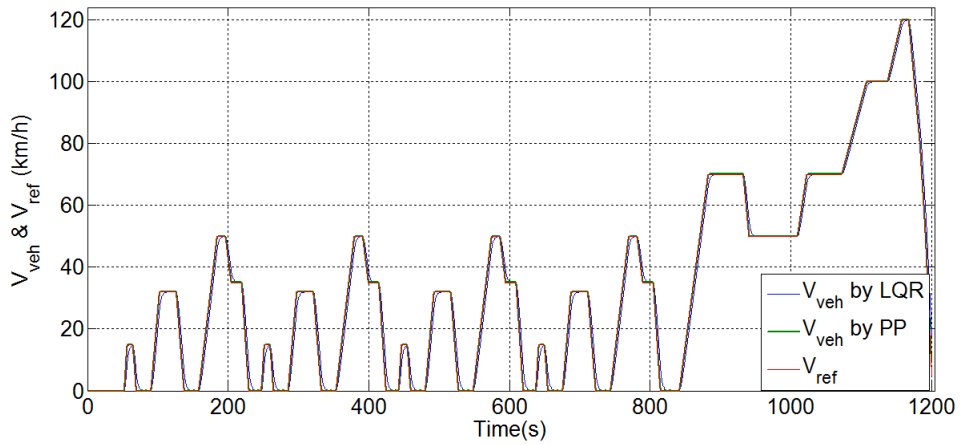


Figure 4.17: Reference and vehicle speed applying NEDC.

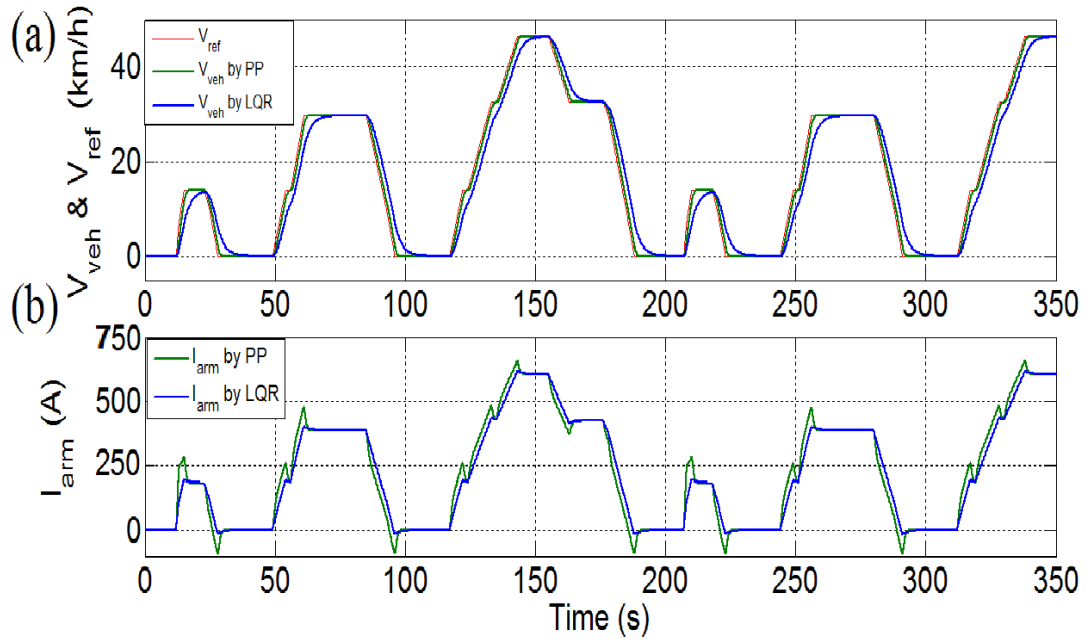


Figure 4.18: (a) Reference and vehicle's velocities; (b) Armature's current.

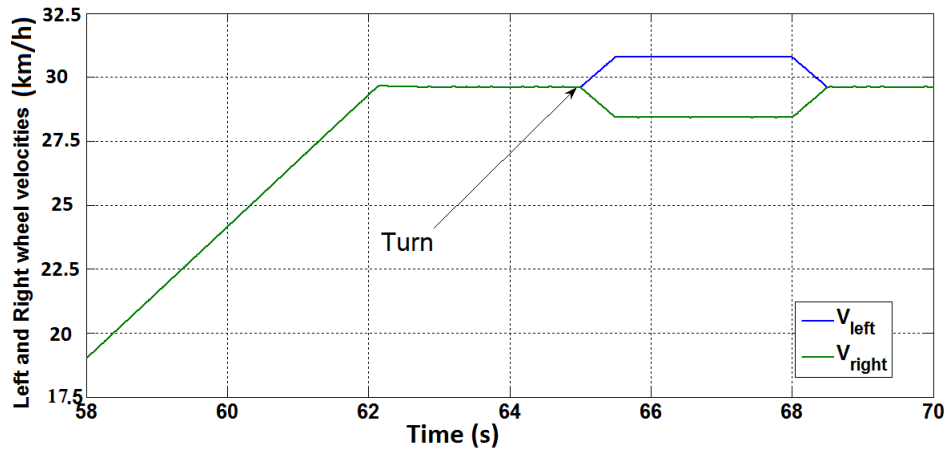


Figure 4.19: wheels's velocities while vehicle makes a turn.

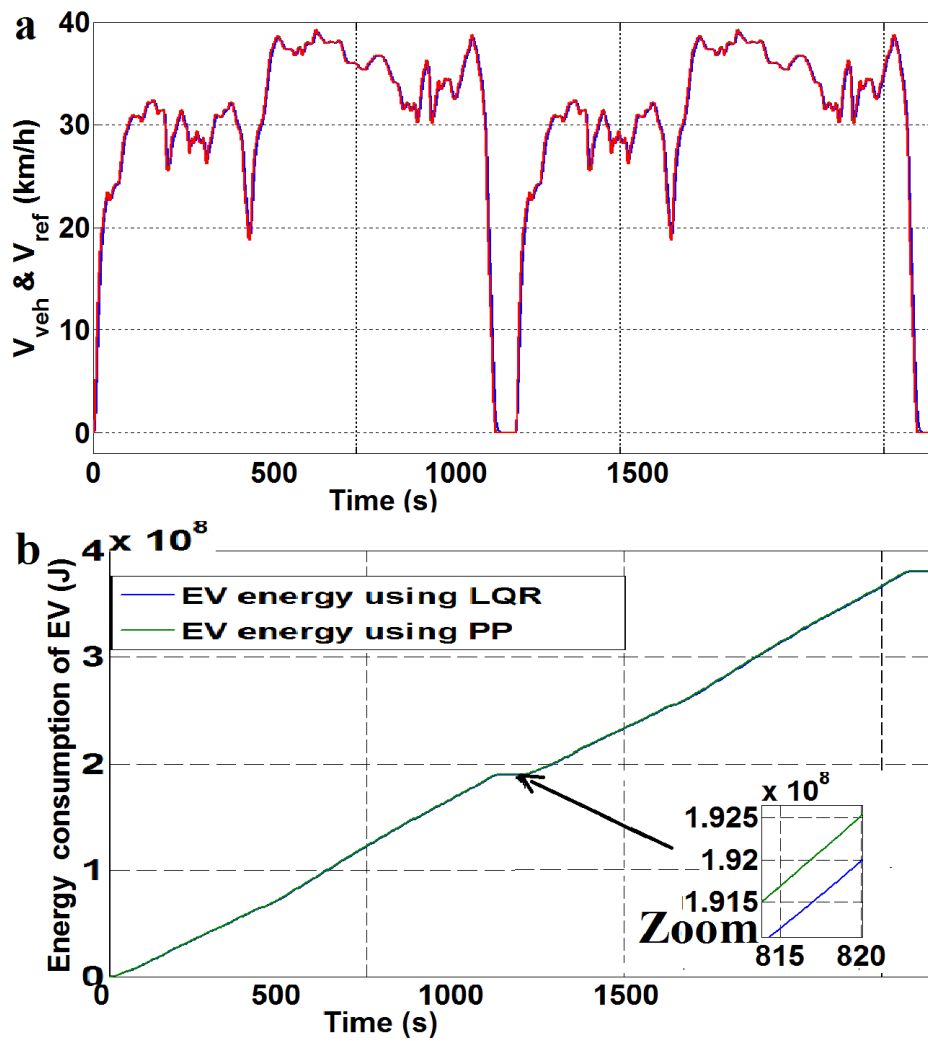


Figure 4.20: (a) Reference and vehicle speed with double FTP-75 (b) Energy consumption of EV

as it is indicated in Fig. 4.20 (b) the energy consumption of the EV using LQR is less than the energy consumption of the EV using PP and the difference between them equals $494.9kJ$. The closed loop Eigenvalues of system using Pole placement and LQR technique are real and negatives, then EV system is stable and robust in presence of perturbation on the road such as the case of the turn.

4.11 Conclusions

A new ADOM for EV has been presented in this chapter in order to reduce the energy consumption and extend the EV's travel range or to meet the required autonomy regarding to the battery SOC. It makes the EV works with an adaptive performance. It can be fast, medium or less dynamic according to the battery SOC and the distance between the EV and the nearest charging station. The SMC technique is enhanced using a specific AFLC instead of a simple PI or IP control. This drawback of the MCS can be overcome using the presented FLC to invert these kind of EMR elements. The simulation results show a good agreement between different types of the EV operation mode.

Also, the EV has been modelled by a linear dynamic model expressed by a state space representation. The states feedback controller based on linear quadratic regulator and poles placement are designed to control EV speed. The closed loop system using Pole placement and LQR control gives a stable and robust system in presence of perturbation on the road. The LQR results showed that the energy consumption of the EV is significantly minimized and the dynamic behaviour of EV can be improved according to the choice of R and Q matrices.

Conclusions and perspectives

Through this work, the control of the electric vehicle drive-train and the energy management of its power-train system have been presented. The goal of the drive-train's control was to provide an inversion base control and propose an adaptive operation mode of the studied vehicle. This model-based control was realized by means of a formalism called Energetic Macroscopic Representation (EMR). Hence, EMR gives insights into the energy operation of the EV system and allows a deep understanding of its potentialities from dynamics point. Due to features of the EMR, an inversion-based control can be deduced from the EMR. It leads to local control structure of the EV.

The EMR proved its capability by representing the complex electromechanical system of an EV. Maximum Control Structures (MCS) using fuzzy logic to invert the accumulation element allowed the development of an Adaptive Operation Mode (AOM). It allows reducing the consumption of the energy. The EV operation mode is online adapted to become economic, dynamic or eco-dynamic mode, thanks to a specific Adaptive Fuzzy Logic Control (AFLC) that is integrated in the MCS.

The kinematic and energy description of the EV power and drive trains are considered as first step to understand and model the EV system. The similarities and comparison between different pure and hybrid EV architectures and their drive-trains were discussed. Consequently, the drive-train scheme with the differential and single-level reduction gear is well suitable for electric motor drives with wide speed range and highly maximum speed in EVs.

Also, in the thesis an insightful study of the used supply sources in the EVs was presented. The fundamentals and comparison of the EV battery, SCs and FC technologies, were suggested and explained. According to this study our answer of the following question

"Which energy source is best for EV's road transport in the future?" is: «the use of FC allows fixing the problem of the limited travel range of the EV but its slowest transient dynamic performance is still a significant drawback. In the hybrid system, the SCs have better performances than the battery, where the hybrid FC-SC source has advantages of the FC plus the SCs that eliminate the drawbacks of the FC (slow transient dynamic performance) and recover quickly the regenerative braking energy».

We revealed the intention behind this research work through highlighting the main concerns and difficulties for developing an energy management strategy of a hybrid source. A new energy management method based on the flatness strategy and the sliding mode control are suggested and explained to control a hybrid system composed of a fuel cell and a supercapacitor as the main and auxiliary sources, respectively. The nonlinear flatness strategy is used to achieve a linearizing feedback control law that gives an exponential tracking of the FC and SCs power trajectories. The proposed flatness control allows decoupling the hybrid system into two decoupled sources as each subsystem has a separate control target. The role of sliding mode controllers is to ensure instantaneously the power sharing between the DC-link inverters by controlling the FC and SC currents.

For future work, the energy management based flatness-sliding should be extended to control different hybrid sources like : fuel cell-battery, battery-supercapacitor or fuel cell-battery and supercapacitor. The developed flatness-sliding control is not validated experimentally and it would be of great interest to see the actual performance of the strategy implemented in the studied hybrid source. Also, extending the simulation and the experimental validation presented in the thesis with the fuel cell-battery and supercapacitor would be one of the main goals for future work.

For long term gains, this research can be extended to implement the same control strategies to hybrid EV types such as series, parallel, double parallel,..etc. Also, not limited to EVs, the energetic macroscopic representation can be extended to other engineering applications. The relevance of this EMR is significant at a time when energy optimization and reduction of oil consumption make headlines almost every day.

Bibliography

- [ABH⁺10] MY Ayad, M Becherif, A Henni, A Aboubou, M Wack, and S Laghrouche. Passivity-based control applied to dc hybrid power source using fuel cell and supercapacitors. *Energy Conversion and Management*, 51(7):1468–1475, 2010.
- [ABH11] MY Ayad, M Becherif, and A Henni. Vehicle hybridization with fuel cell, supercapacitors and batteries by sliding mode control. *Elsevier Renewable Energy*, 36(10):pages 2627–2634, 2011.
- [Bar11] Ph Barrade. Supercapacitors: Principles, sizing, power interfaces and applications. *Energy Storage*, pages 217–241, 2011.
- [Bar13] F Barbir. *PEM fuel cells: theory and practice*. Academic Press, 2013.
- [BCLM08] V Boscaino, G Capponi, P Livreri, and F Marino. Fuel cell modelling for power supply systems design. *Control and Modeling for Power Electronics, Workshop on Digital Object Identifier*, pages pages 1–4, 2008.
- [Ber05] J Beretta. *Le génie électrique automobile: la traction électrique*. Lavoisier, 2005.
- [CBC10] Ch Chan, A Bouscayrol, and K Chen. Electric, hybrid, and fuel-cell vehicles: Architectures and modeling. *Vehicular Technology, IEEE Transactions on*, 59(2):pages 589–598, 2010.
- [CBLM09] M Ceraolo, S Barsali, G Lutzemberger, and M Marracci. Comparison of sc and high-power batteries for use in hybrid vehicles. Technical report, SAE Technical Paper, 2009.

- [Cha00] HL Chan. A new battery model for use with battery energy storage systems and electric vehicles power systems. In *Power Engineering Society Winter Meeting, 2000. IEEE*, volume 1, pages 470–475. IEEE, 2000.
- [Cor10] J.J Cornaert. *L’avenir de l’automobile*. Armand Colin, 2010.
- [CY13] Ch Chiang and W Yang, Jand Cheng. Temperature and state-of-charge estimation in ultracapacitors based on extended kalman filter. *Journal of Power Sources, Elsevier*, 234:pages 234–243, 2013.
- [EGE09] M Ehsani, Y Gao, and A Emadi. *Modern electric, hybrid electric, and fuel cell vehicles: fundamentals, theory, and design*. CRC press, 2009.
- [Fra05] L2EP Lille 2005. France. Summer school on Modelling and Control of electromechanical system using Energetic Macroscopic Representation Formalism, 2005.
- [GJL08] D Gao, Z Jin, and Q Lu. Energy management strategy based on fuzzy logic for a fuel cell hybrid bus. *Journal of Power Sources*, 185(1):311–317, 2008.
- [Gop08] M Gopal. *Control systems: principles and design*. Tata McGraw-Hill Education, 2008.
- [GRN09] LV Gopala Rao and S Narayanan. Sky-hook control of nonlinear quarter car model traversing rough road matching performance of lqr control. *Journal of Sound and Vibration*, 323(3):pages 515–529, 2009.
- [Hir05] E.H Hirschel. *Basics of aerothermodynamics*, volume 206. Springer, 2005.
- [Hus10] R Husson. *Control methods for electrical machines*, volume 125. John Wiley & Sons, 2010.
- [Hus11] I Husain. *Electric and hybrid vehicles: design fundamentals*. CRC press, 2011.
- [IT11] D Iannuzzi and P Tricoli. Supercapacitor state of charge control based on changeover finite state controller for metro-train applications. In *Clean Electrical Power (ICCEP), 2011 International Conference on*, pages 550–556. IEEE, 2011.

- [Jar12] E Jarzebowska. *Model-based tracking control of nonlinear systems*. 2012.
- [KBA⁺13] O Kraa, M Becherif, A Aboubou, MY Ayad, I Tegani, and A Haddi. Modeling and fuzzy logic control of electrical vehicle with an adaptive operation mode. In *Power Engineering, Energy and Electrical Drives (POWERENG), 2013 Fourth International Conference*, pages 120–127. IEEE, 2013.
- [KCC⁺12] R Klein, N Chaturvedi, J Christensen, J Ahmed, R Findeisen, and A Kojic. Electrochemical model based observer design for a lithium-ion battery. 2012.
- [KT05] W Kempton and J Tomić. Vehicle-to-grid power fundamentals: calculating capacity and net revenue. *Journal of Power Sources, Elsevier*, 144(1):pages 268–279, 2005.
- [LDBB05] W Lhomme, Ph Delarue, Ph Barrade, and A Bouscayrol. Maximum control structure of a series hybrid electric vehicle using supercapacitor. In *EVS" 21: The 21st Worldwide Battery, Hybrid and Fuel Cell Electric Vehicle Symposium Exhibition*, number LEI-CONF-2006-027, 2005.
- [LSL61] JP La Salle and S Lefschetz. *Stability by Liapunov's direct method: with applications*, volume 4. Academic Press New York, 1961.
- [Mat] Matchwork kernel description. <http://www.mathworks.com/help/physmod/sps/powersys/ref/fuelcellstack.html>. Accessed: 2014.
- [MH94] B Multon and L Hirsinger. Problème de la motorisation d'un véhicule électrique. *Journées de la section électrotechnique du club EEA 1994*, 1994.
- [MHPA11] Javier Solano Martínez, Daniel Hissel, M-C Pera, and Michel Amiet. Practical control structure and energy management of a testbed hybrid electric vehicle. *Vehicular Technology, IEEE Transactions on*, 60(9):4139–4152, 2011.
- [MKB⁺14] M Mohammedi, O Kraa, M Becherif, A Aboubou, MY Ayad, and M Bahri. Fuzzy logic and passivity-based controller applied to electric vehicle using fuel cell and supercapacitors hybrid source. *Energy Procedia*, 50:619–626, 2014.

- [MT10] V Musolino and E Tironi. A comparison of supercapacitor and high-power lithium batteries. In *Electrical Systems for Aircraft, Railway and Ship Propulsion (ESARS), 2010*, pages 1–6. IEEE, 2010.
- [MTD12] S Motapon, O Tremblay, and L Dessaint. Development of a generic fuel cell model: application to a fuel cell vehicle simulation. *International Journal of Power Electronics*, 4(6):pages 505–522, 2012.
- [Mul13] B Multon. Motorisation des véhicules électriques. *Techniques de l'ingénieur, Base documentaire: E*, page page 996, 2013.
- [NBDEB07] A Nouh, M Becherif, A Djerdir, and M El-Bagdouri. Traction control of an electric vehicle with two separate wheel drive. In *International Conference on Ecologic Vehicle and Renewable Energies, EVER07, Monaco, 2007*.
- [PH11] R.E Precup and H Hellendoorn. A survey on industrial applications of fuzzy control. *Computers in Industry*, 62(3):pages 213–226, 2011.
- [PPMTD11] A Payman, S Pierfederici, F Meibody-Tabar, and B Davat. An adapted control strategy to minimize dc-bus capacitors of a parallel fuel cell/ultracapacitor hybrid system. *Power Electronics, IEEE Transactions on*, 26(12):pages 3843–3852, 2011.
- [PSP04] JT Pukrushpan, A Stefanopoulou, and H Peng. *Control of fuel cell power systems: principles, modeling, analysis and feedback design*. Springer, 2004.
- [Puk03] J.T Pukrushpan. *Modeling and control of fuel cell systems and fuel processors*. PHD thesis, University of Michigan, 2003.
- [Put12] U Putnieks. Electric vehicle history. *Students on their way to science*, page 7, 2012.
- [Ram03] M.BE Ramachandra. *Modeling of hybrid electric vehicle batteries*. PhD thesis, Texas Tech University, 2003.
- [RBE00] Z Rahman, K.L Butler, and M Ehsani. Effect of extended-speed, constant-power operation of electric drives on the design and performance of ev-hev propulsion system. Technical report, SAE Technical Paper, 2000.

- [Red11] Th.B Reddy. *Linden's Handbook of Batteries*, volume 4. McGraw-Hill New York, 2011.
- [Rig09] G Rigatos. Adaptive fuzzy control of dc motors using state and output feedback. *Electric Power Systems Research*, 79(11):1579–1592, 2009.
- [Ros13] T.J Ross. *Fuzzy logic with engineering applications*, volume 686. Wiley, 2013.
- [RX01] A Rowe and Li Xianguo. Mathematical modeling of proton exchange membrane fuel cells. *Journal of power sources*, 102(1):pages 82–96, 2001.
- [SA10] S Soyguder and H Alli. Fuzzy adaptive control for the actuators position control and modeling of an expert system. *Expert Systems with Applications*, 37(3):2072–2080, 2010.
- [SB10] P Sharma and TS Bhatti. A review on electrochemical double-layer capacitors. *Energy Conversion and Management, Elsevier*, 51(12):page2901–2912, 2010.
- [SBA⁺14] R Saadi, M Bahri, MY Ayad, M Becherif, O Kraa, and A Aboubou. Dual loop control of fuel cell source using non-isolated ibc-iddb converter for hybrid vehicle applications. *Energy Procedia*, 50:155–162, 2014.
- [SBAA13] A Saadi, M Becherif, A Aboubou, and MY Ayad. Comparison of proton exchange membrane fuel cell static models. *Renewable Energy, Elsevier*, 56:pages 64–71, 2013.
- [SBK⁺13] R Saadi, M Benaouadj, O Kraa, M Becherif, MY Ayad, A Aboubou, M Bahri, and A Haddi. Energy management of fuel cell/supercapacitor hybrid power sources based on the flatness control. In *Power Engineering, Energy and Electrical Drives (POWERENG), 2013 Fourth International Conference on*, pages 128–133. IEEE, 2013.
- [SFP⁺13] S Sikkabut, N.H Fuengwarodsakul, M Phattanasak, Ph Thounthong, A Houari, S Pierfederici, and B Davat. Differential flatness based control of hybrid power plant based on supercapacitor storage energy for ac distributed

- system. In *Power Electronics and Drive Systems (PEDS), 2013 IEEE 10th International Conference on*, pages 818–823. IEEE, 2013.
- [SFS⁺13] S Sikkabut, N Fuengwarodsakul, P Sethakul, Ph Thounthong, S Pierfederici, M Hinaje, B Nahid-Mobarakeh, and B Davat. Control strategy of solar/wind energy power plant with supercapacitor energy storage for smart dc microgrid. In *Power Electronics and Drive Systems (PEDS), 2013 IEEE 10th International Conference on*, pages 1213–1218. IEEE, 2013.
- [SJS⁺10] H.S Song, J.B Jeong, D.H Shin, B.H Lee, H.J Kim, and H Heo. Dynamic soc compensation of an ultracapacitor module for a hybrid energy storage system. *Journal of Power Electronics*, 10(6):pages 769–776, 2010.
- [SSS12] S Saini, M Sharma, Yand Bhandari, and U Satija. Comparison of pole placement and lqr applied to single link flexible manipulator. In *Communication Systems and Network Technologies (CSNT), 2012 International Conference on*, pages 843–847. IEEE, 2012.
- [Sye12] S.A Syed. *Energetic macroscopic representation and multi-level energy management for heavy-duty hybrid vehicles using double planetary geartrain*. PhD thesis, Lille 1, 2012.
- [TCDH09] Ph Thounthong, P Chunkag, Vand Sethakul, B Davat, and M Hinaje. Comparative study of fuel-cell vehicle hybridization with battery or supercapacitor storage device. *Vehicular Technology, IEEE Transactions on*, 58(8):pages 3892–3904, 2009.
- [TRD07] Phatiphat Thounthong, Stéphane Raël, and Bernard Davat. Control strategy of fuel cell and supercapacitors association for a distributed generation system. *Industrial Electronics, IEEE Transactions on*, 54(6):3225–3233, 2007.
- [TRD09] Ph Thounthong, S Rael, and B Davat. Energy management of fuel cell/battery/supercapacitor hybrid power source for vehicle applications. *Journal of Power Sources*, 193(1):376–385, 2009.

- [TS07] P Thounthong and P Sethakul. Analysis of a fuel starvation phenomenon of a pem fuel cell. In *Proc. Power Conversion Conference-Nagoya PCC*, volume 7, pages 2–5, 2007.
- [TT13] S.F Tie and Ch.W Tan. A review of energy sources and energy management system in electric vehicles. *Renewable and Sustainable Energy Reviews*, 20:pages 82–102, 2013.
- [TTD14] Ph Thounthong, P Tricoli, and B Davat. Performance investigation of linear and nonlinear controls for a fuel cell/supercapacitor hybrid power plant. *International Journal of Electrical Power & Energy Systems*, 54:pages 454–464, 2014.
- [VMML06] J Van Mierlo, G Maggetto, and Ph Lataire. Which energy source for road transport in the future? a comparison of battery, hybrid and fuel cell vehicles. *Energy Conversion and Management*, 47(17):pages 2748–2760, 2006.
- [XCC08] XD Xue, KWE Cheng, and NC Cheung. Selection of electric motor drives for electric vehicles. In *Power Engineering Conference, 2008. AUPEC'08. Australasian Universities*, pages 1–6. IEEE, 2008.
- [YWWS13] K Young, C Wang, L.Yi Wang, and K Strunz. Electric vehicle battery technologies. In *Electric Vehicle Integration into Modern Power Networks*, pages 15–56. Springer, 2013.
- [Zac] World electrified vehicle sales (2013 report). <http://evobsession.com/world-electrified-vehicle-sales-2013/>. Accessed: 2014.
- [ZWZ12] Y Zhan, H Wang, and J Zhu. Modelling and control of hybrid ups system with backup pem fuel cell/battery. *International Journal of Electrical Power and Energy Systems*, 43(1):pages 1322–1331, 2012.